Lehigh University
Lehigh Preserve

Fritz Laboratory Reports | Civil and Environmental Engineering

1966

Plastic design in high strength steel. Thesis (Ph.D.)--Lehigh University, 1966.

P. F. Adams

Follow this and additional works at: http://preserve.lehigh.edu/engr-civil-environmental-fritz-lab-reports

Recommended Citation
Adams, P. F., "Plastic design in high strength steel. Thesis (Ph.D.)--Lehigh University, 1966. " (1966). *Fritz Laboratory Reports.* Paper 1849.
http://preserve.lehigh.edu/engr-civil-environmental-fritz-lab-reports/1849

This Technical Report is brought to you for free and open access by the Civil and Environmental Engineering at Lehigh Preserve. It has been accepted for inclusion in Fritz Laboratory Reports by an authorized administrator of Lehigh Preserve. For more information, please contact preserve@lehigh.edu.

PLASTIC DESIGN IN HIGH STRENGTH STEEL

by

Peter F. Adams

This work has been carried out as part of an investigation sponsored jointly by the Welding Research Council and the Department of the Navy with funds furnished by the following:

American Insitute of Steel Construction
American Iron and Steel Institute
Institute of Research, Lehigh University
Column Research Council (Advisory)
Office of Naval Research (Contract No. 610(03))
Bureau of Ships
Bureau of Yards and Docks

Reproduction of this report in whole or in part is permitted for any purpose of the United States Government.

May 1966

Fritz Engineering Laboratory
Department of Civil Engineering
Lehigh University
Bethlehem, Pennsylvania

Fritz Engineering Laboratory Report No. 297.19

TABLE OF CONTENTS

		Page
	ABSTRACT	1
1.	INTRODUCTION	3
	1.1 Scope	3
	1.2 Assumptions of the Analysis	4
	1.3 The Analysis of Plane Frames	5
	1.4 High Strength Steel	6
	1.5 Summary	8
2.	HIGH STRENGTH STEEL - THE MATERIAL	10
	2.1 The Moment Redistribution Process	10
	2.2 The Influence of Strain Hardening	14
	2.3 Experimental Verification	16
	2.4 Influence of Material Characteristics on Inelastic Behavior	22
	2.5 The Influence of Cold Bending on Material Characteristics	35
	2.6 Metallurgical Factors in Strain Hardening	46
3.	PLATE ELEMENTS IN PLASTICALLY DESIGNED MEMBERS	52
	3.1 Stub Column Behavior	52
	3.2 Review of Previous Work	57
	3.3 Flange Buckling - Web Under Strain Gradient	63
	3.4 Web Buckling	67
	3.5 Proposed Test Program	70
	3.6 Flange Buckling - Short Yielded Lengths	75

		Page
4.	MEMBERS IN PLASTICALLY DESIGNED STRUCTURES	83
	4.1 Beams Under Uniform Moment	84
	4.2 Beams Under Moment Gradient	90
	4.3 In-Plane Behavior of Beam-Columns	92
	4.4 Limitations on the In-Plane Behavior of Beam-Columns	97
	4.5 Axially Loaded Columns	101
	4.6 Connections	102
	4.7 Other Considerations	103
	4.8 Summary	103
5.	BEHAVIOR OF STRUCTURAL SUBASSEMBLAGES	104
	5.1 Structural Action	104
	5.2 Behavior of a Braced Hybrid Subassemblage	105
	5.2.1 Test Subassemblage	105
	5.2.2 Test Procedure	107
	5.2.3 Test Results	110
	5.2.4 Summary of Test	114
	5.2.5 Previous Subassemblage Tests	115
	5.3 Behavior of an Unbraced Hybrid Subassemblage	117
	5.4 Frame Buckling	123
	5.5 Summary	124
6.	SUMMARY AND CONCLUSIONS	125
7.	TABLES	129
8.	APPENDIX A - EFFECT OF LARGE STRAINS	138

		Page
9.	SYMBOLS	143
10.	FIGURES	145
11.	REFERENCES	189
12.	ACKNOWLEDGEMENTS	197

ABSTRACT

This dissertation attempts to summarize the present state of knowledge relating to the plastic design of structures fabricated from high strength low alloy steels having yield stress levels up to 50 ksi. The areas in need of additional research are outlined.

The stress-strain relationship is discussed and the effect of changes in this relationship on the progress of moment redistribution is shown. It is concluded that for materials possessing a significant strain hardening modulus moment redistribution will be successful in a statically indeterminate structure.

The effect of rotary straightening on the material properties is illustrated. It is concluded that more research is necessary before this influence can be fully evaluated.

The various situations under which flange or web local buckling can occur are outlined. Previous web buckling solutions are discussed and a test program to investigate web buckling under bending and axial load is presented.

The present state of knowledge relating to the plastic design of beams and beam columns is summarized. Where practicable design rules are presented and their limitations outlined.

The behavior of hybrid subassemblages consisting of low carbon beams rigidly connected to low alloy columns is discussed. For both the braced and unbraced subassemblages, the behavior can be

predicted by theories previously tested on low-carbon steel subassemblages. For the unbraced subassemblage, a method is presented for including the strengthening influence of strain hardening in the prediction of the response. It is concluded that the prediction of the behavior of hybrid subassemblages or subassemblages of low alloy steel members presents no unusual difficulties.

It is concluded that plastic design of low alloy steel structures is feasible and presents no unusual complications. The problems which remain to be solved are those for which no complete solution exists for the low carbon steels.

1. INTRODUCTION

1.1 SCOPE

The purpose of this investigation is to investigate the behavior of low alloy steel members and to obtain sufficient information to extend plastic design procedures to include these steels. The major portion of the previous research on plastic design has been restricted almost entirely to low carbon structural steels.[1] Much of this work can be applied with very little change to low alloy steels provided that the properties of the two types of steels are similar. On the other hand, there are problems encountered in plastic design which have been solved in an empirical or semi-empirical manner for the low carbon steels. Before these solutions can be applied to low alloy steels, they must be re-examined, and confirming test results provided where necessary.

This dissertation will examine the material characteristics of low carbon and low alloy steels, determine which of these characteristics significantly affect moment redistribution and how changes in specific characteristics will influence member and frame behavior. The dissertation will summarize the present state of knowledge relating to the plastic design of high strength steel members and frames and finally will attempt to delineate the regions in which more research is necessary.

1.2 ASSUMPTIONS IN THE ANALYSIS

In order to base the selection of structural members on a plastic analysis, this analysis must not only give a reasonable indication of the maximum strength of the structure, but in addition, the maximum strength must be indicative of the limit of usefulness of the structure.[2,3]

The use of the maximum plastic strength as a design criterion implies that independent checks have been made to ensure that factors such as brittle fracture, fatigue, working load deflection, deflection instability and alternating plasticity will not be critical.

It will be assumed that all loads are gradually applied so that dynamic effects may be neglected. It has been usual in plastic design to assume that the loads are applied proportionally.[3] However, in some cases it is more realistic to load the structure (either theoretically or experimentally) in a manner that is not proportional. When this is done, allowance is made to account for the strain history of the material.

Additional assumptions usual in simple plastic theory are missing from those listed above. These are: (1) the axial load in the column does not reduce the moment capacity of the member; (2) equilibrium may be formulated on the undeformed structure; (3) local or lateral instability do not reduce the strength of the member before the maximum load has been attained. These conditions will be considered in the sections that follow.

1.3 THE ANALYSIS OF PLANE FRAMES

In attempting to assess the load deformation behavior of plane frames several concepts are relevant. Figure 1.1, which contains a plot of load versus deflection for the simple frame shown in the inset illustrates these concepts.[4] The frame is subjected to proportional loading and the effect of the axial force in the beam is neglected. For low values of W, before the stress reaches the yield point, the load deformation relationship may be obtained by conventional elastic analysis procedures (first order elastic curve). If the reduction in stiffness due to axial load is considered and equilibrium formulated on the deformed structure, a modified elastic curve is obtained.[5] This type of analysis is usually called second-order because it accounts for the above factors, which are normally considered to be of secondary importance. Under conditions of high axial load on relatively slender structures these "secondary" factors have a dominant influence on the structural behavior. The second order elastic curve is asymptotic to the value of W which represents the elastic buckling load of the frame.[6,7]

If the material were perfectly elastic, the true load-deformation relationship would be that given by the second order elastic curve. However, as the structure deforms, the applied strains are superimposed on the residual strains and at a load, W_y, the strains in some portions of the frame reach the yield strain. As the structure continues to deform, the yielded zone penetrates into the cross section of the member thus forming a plastic hinge.

An analysis can be performed which accounts for this gradual progression of yielding.[8,9] Such an analysis is tedious, and it has only been performed for very simple structures. The load deflection curve resulting from this "exact analysis" is shown in Fig. 1.1 as the dashed curve.

For these simple structures a very close approximation to the true behavior has been obtained by assuming the plastic hinges to be concentrated at the peak moment points.[10] This analysis is termed elastic-plastic. Because equilibrium is formulated on the deformed structure, it is more completely termed a second order elastic-plastic analysis. The load-deformation curve is shown in Fig. 1.1. The load at which each plastic hinge forms is marked with a solid circle. When sufficient hinges have formed so that the structure deforms as a mechanism, the response merges into that resulting from a rigid plastic analysis. This rigid plastic analysis assumes that no movement takes place until after the formation of a mechanism. The equilibrium equations which describe the response of the structure are identical once a mechanism has formed in both cases.

In the analyses described above, the effect of strain hardening has been neglected. Experiments have shown that this effect increases the strength of a simple frame.[11] This is shown in Fig. 1.1 as the curve above that representing the rigid plastic response.

1.4 HIGH STRENGTH STEEL

From a strength consideration the most economical material is

that which has the lowest ratio of unit price to design stress.[12] Recent figures show that the low alloy steels have indeed a lower price-to-strength ratio.[13] These figures equate weight to economy, which may not always be true.

The above reasoning must be tempered by consideration of the stability and deflection influences. These are basically functions of the stiffness of the member. In a given design situation the use of higher strength steel will lead to a lighter and more slender member. This increase in material strength is not accompanied by an increase in the Modulus of Elasticity.[14] Thus the smaller, more slender member, must of necessity, be less stiff than its lower strength counterpart. This in turn means that in cases where stability considerations are significant the higher strength member may be penalized to such a degree that its apparent lower cost, based on the price-strength ratio, becomes higher than that of the equivalent low strength member. A similar situation exists where deflections must be held below certain specified limits.

Thus, as a general rule, high strength steels will be economical where strength rather than stiffness considerations are of major consequence.

In structures designed according to elastic design procedures, higher strength steels have found application in the highly stressed portions of the bridge trusses, as columns in building frames where deflection is not a problem and as bending members where lateral instability is prevented by suitable bracing.

At the present time the most suitable application of low alloy steel members in plastically designed structures appears to be as beam columns in braced frames, where a stocky member is used and drift is prevented by suitable bracing. In slender structures where bracing must be provided as a part of the structural system, high strength members may lose their appeal.

1.5 SUMMARY

As an initial step the process of moment redistribution will be reviewed and the requirements that this process imposes on the material stress-strain curve will be outlined. The significant features of various stress-strain relationships will be examined and recommendations made in Chapter 2 for those materials that would be suitable for plastic design procedures.

Chapter 3 will discuss the behavior of the plate elements of the cross section. The various strain conditions to which these plates may be subjected are reviewed and solutions which have been advanced are discussed. The results of tests conducted to study the plate buckling problem are presented. Finally, test programs are proposed to investigate the problem of web buckling. These tests will relate the web buckling strength directly to the rotation capacity of the member.

Chapter 4 reviews the present state of knowledge relating to the plastic design of members. The behavior of beams under uniform moment and moment gradient is discussed as well as that of beam columns.

In all cases the limitations of the solutions are outlined and areas are pointed out in which additional research is required.

In Chapter 5 the behavior of hybrid subassemblages is discussed. These subassemblages consist of low alloy steel columns rigidly connected to low carbon steel beams and designed to simulate both braced and unbraced frames. The methods of analysis are discussed and a process for including the influence of strain hardening in the response of unbraced frames is presented.

In this dissertation the significance of the shape of the stress-strain relationship in plastic design is presented for the first time. The relative importance of failure by fracture versus failure due to local and lateral instability is investigated. The influence of the rotarizing process on the effective material properties is illustrated. The method of relating the geometry of the flange plate to the rotation capacity requirement is original; as is the testing program which is designed to investigate the influence of web slenderness on rotation capacity of beam columns. The inclusion of the strain hardening influence on the structural response is approached from a different viewpoint. However, the importance of the work lies not only in the number of solutions to detailed problems but in the collection and evaluation of a large amount of information into a form suitable for design use. Where this is not possible, the additional investigations necessary are clearly indicated.

2. HIGH STRENGTH STEEL - THE MATERIAL

The purpose of the following chapter is to show how the stress-strain relationship of the material influences the ability of the structure to redistribute bending moments in the inelastic range. The influence of the strain-hardening portion of the relationship is examined in particular detail and its effect documented by experimental evidence. In the latter portion of the chapter the influence of the straightening process on the measured values of the material properties is discussed and the metallurgical factors which influence the stress-strain relationship are delineated.

2.1 THE MOMENT REDISTRIBUTION PROCESS

The backbone of the limit design procedure is the process of moment redistribution.[3] By this process an indeterminate structure continues to accept increasing load even after the full plastic moment has been reached at one or more sections.

Consider the simple example shown in Fig. 2.1(a). The beam is a propped cantilever of length, L, loaded with a central concentrated load, P. The beam has a moment of inertia, I, and a plastic modulus, Z. The material from which the beam is constructed has a modulus of elasticity, E, a yield point, σ_y, and the stress-strain (σ - ϵ) relationship of the material is assumed to be that shown

in Fig. 2.2.

For simplicity it will be assumed that the beam cross section has a shape factor of unity -- that is, the cross section is composed of two infinitely thin flanges separated by the depth of the beam, d. Under this assumption all elements of the cross section are subjected to the same bending strain, thus all elements are assumed to yield when the strain reaches the yield strain, ϵ_y ($\epsilon_y = \sigma_y/E$). Thus the moment-curvature (M-ϕ) relationship is that shown in Fig. 2.3. In this figure, M_p, is the full plastic moment ($M_p = \sigma_y Z$) and ϕ_p is the curvature corresponding to M_p, assuming the material to be ideally elastic ($\phi_p = M_p/EI$).

The implications of these assumptions are illustrated with reference to Fig. 2.1. For low values of the load P the bending moment distribution is elastic and is shown in Fig. 2.1(b). As the load is increased the support moment reaches the full plastic value of M_p. In accordance with the moment-curvature relationship of Fig. 2.3, under further load increase the curvature at the support can now increase indefinitely while the moment remains constant at M_p. It is this action which has given rise to the term plastic hinge.

The structure to be analyzed for an additional load increment is the simple beam shown in Fig. 2.1(c). The load can be increased until the central moment reaches M_p. The change in the bending moment diagram is shown in Fig. 2.1(d) and the total bending moment diagram in Fig. 2.1(e). The mechanism is shown in Fig. 2.1(f).

The load-deformation curve for the structure is shown in Fig. 2.4. The load is given non-dimensionally as P/P_p, where P_p is the load predicted by simple plastic theory ($P_p = 6M_p/L$) and the center-line deflection, v, has been nondimensionalized as

$$\frac{v}{d} \quad \frac{1}{\sqrt{\epsilon_y}} \quad \frac{1}{(L/d)^2} .$$

The introduction of real hinges at plastic hinge locations simply substitutes discrete reductions in stiffness for the gradual deterioration that occurs during the yielding of an actual structure. This approach provides an excellent indication of the overall behavior of the structure as well as resulting in a convenient means of analysis at maximum load.[15,16] However, it cannot provide information on the local behavior in the regions near plastic hinges.

The situation in the hinge areas can be studied by means of an analysis which considers the detailed curvature distribution along the length of the member and which enforces geometrical compatibility at the load point and the fixed support. Such an analysis has been performed for the structure shown in Fig. 2.1(a). In order to perform the analysis the curvature which corresponds to a given moment must be finite. The bilinear stress-strain curve shown in Fig. 2.5 was used as the basis of the analysis. In this figure E_{st} represents the strain-hardening modulus. Assuming that the cross section has a shape factor of unity, the moment-curvature relationship is shown in Fig. 2.6.

For the elastic-plastic material, E_{st} is zero. This would render any analysis based on compatibility conditions impossible since the curvature corresponding to M_p is indefinite. To illustrate the behavior which would result if the material were elastic-plastic a compatibility analysis was performed using two low values of E_{st}; 1.5 ksi and 0.3 ksi. For a given load on the structure a bending moment distribution is assumed which satisfies the equilibrium conditions. The corresponding curvature distribution is computed and adjusted to satisfy the compatibility conditions. The process is illustrated in more detail in a succeeding section.

The load causing the moment at the support to reach M_p is $0.89P_p$. At loads above this value the strains at the fixed support increase rapidly. For example, if $E_{st} = 1.5$ the maximum strain at the support is 35 times the yield strain at $0.92P_p$ and 120 times the yield strain at P_p. If the lower value of E_{st} is used (0.3) the strains at the same loads are 90 and 480 times the yield strain.

The presence of large strains in the material may be harmful in two ways. For materials having low fracture strains, the large applied strains would cause rupture. For structural steels the fracture strain is approximately 200 ϵ_y, and fracture has never been observed.[1,3,16,17] However, Hrennikoff has made much of this possibility and has even suggested that steels possessing low values of E_{st} not be used for plastically designed structures because of the danger of fracture before complete moment redistribution.[18]

The most important consequence is the danger of premature

local buckling. The large applied strains coupled with a low strain-hardening modulus could precipitate early local buckling. This will be discussed further in later sections.

2.2 THE INFLUENCE OF STRAIN-HARDENING

The situation discussed in the previous section is to some extent artificial. Many indeterminate structures have been tested under controlled conditions, and have reached and even exceeded the loads predicted by simple plastic theory.[16,17,19]

The answer lies in the fact that the low carbon steels have a stress-strain diagram which is not elastic-perfectly plastic (Fig. 2.2). The initial portion of the stress-strain diagram for A36 steel is shown idealized in Fig. 3.7. The important feature to be noted is that the strains do not increase indefinitely when the material is stressed to the yield point. At this stress there is a strain jump from the yield strain, ϵ_y, to the strain at the initiation of strain-hardening, ϵ_{st}. To strain the material beyond ϵ_{st} the stress must necessarily be increased.

Again assuming a shape factor of unity and the absence of residual stress, the M-ϕ relationship corresponding to the stress-strain curve of Fig. 2.7 is shown in Fig. 2.8. Using this relationship it is profitable to re-examine the behavior of the beam shown in Fig. 2.1(a).

The beam is the propped cantilever which is redrawn as Fig. 2.9(a) for convenience. For small values of P the behavior is elastic and the curvatures along the length of the beam are shown in Fig. 2.9(b). If the load is now increased on the beam the elastic portions offer the resistance characterized by the initial slope of the M-ϕ diagram. The area adjacent to the support section however is at ϕ_p, thus before it can offer any additional resistance the curvature at this location must jump to the curvature at the initiation of strain-hardening, $\phi_{st} = \frac{\epsilon_{st}}{\epsilon_y} \phi_p$, and then increase along the strain-hardening path. The resistance of this section is much less than that of the elastic sections. The curvature distribution along the length of the member at this stage is shown in Fig. 2.9(c).

As the load is increased the yielded zone spreads along the length of the member. When the curvature at the load point reaches ϕ_p the plastic moment value has been reached at two locations. Since the moment at the support is greater than M_p, the load exceeds P_p.

If the load is increased, the curvature distribution takes the form shown in Fig. 2.9(d). Two yielded zones are now present and will spread along the member.

The load-deformation relationship for this structure, assuming the material properties of Fig. 2.7, is shown in Fig. 2.10. This relationship is obtained by formulating the equilibrium and compatibility conditions for the structure and linking them with the idealized M-ϕ relationship. The method is discussed in Ref. 10. The significant factors shown by this figure are (1) that the simple plastic theory

underestimates by a small amount the load at which deflections tend to increase rapidly and (2) when the moments at all hinge locations are equal to or greater than M_p the load will increase with continued deformation, above P_p. In contrast to the elastic-plastic material, the strains are relatively low due to the presence of strain-hardening. At the fixed support the maximum strain is 12.0 ϵ_y at 0.92 P_p, 12.8 ϵ_y at P_p and 14.2 ϵ_y at 1.02 P_p.

2.3 EXPERIMENTAL VERIFICATION

The conclusions reached in the previous sections were based on somewhat crude assumptions concerning the distribution of stress over the cross section. It is of interest to find out if these conclusions can be supported by experimental evidence. Of the many tests reported on indeterminate structures loaded into the inelastic range, the pertinent data, which will enable the redistribution process to be traced, have been reported in relatively few cases.[16]

Yang et al reported the results of five continuous beam tests.[20] The results of Yang's Beam Test No. 4 are used for the purpose of discussion. All tests in the series behaved in a similar manner. Test No. 4 was performed on an 8WF40 section of material having a stress-strain curve similar to that shown in Fig. 2.7 and loaded as shown in Fig. 2.11(a). The loads P on the central span and the end loads, R, were adjusted at each stage of loading so that the slope over the interior reaction was equal to zero. The deflected shape of the member

is shown in Fig. 2.11(b).

The moment distribution along the length of the beam was computed at each stage of loading. Deflections, rotations and loads were also measured and recorded. The plots of load versus bending moments at mid-span and over the fixed reaction are shown as Fig. 2.12. The dashed lines represent the elastic-plastic solution which does not include the influence of strain-hardening. The experimental curves, represented by the full lines, agree reasonably well with this theory up to a load equal to about 0.80 P_p. It can be seen from the figure that beyond this load the end and center moments are not equal but that the strain-hardening properties of the steel have forced the moment at the support to rise with increasing deformation. It is this increase in moment (and thus in curvature over some finite length) which enables the center moment to increase at a higher rate than that predicted by an elastic-plastic analysis. P_p is attained when the central moment is still less than M_p but the end moment has increased above M_p. After both moments have exceeded M_p, the load increases further due to strain-hardening in the two yielded areas.

The load versus mid-span deflection for the beam is shown as the solid line in Fig. 2.13. For comparison the curve predicted by the elastic-plastic theory is shown dashed on the same graph.

The comparison of the two load-deflection curves illustrates that for a beam which has significant strain-hardening properties the load calculated by simple plastic theory can be reached and exceeded, and furthermore that the overall load-deformation relationship for

such a member may be predicted adequately by an elastic-plastic analysis. The significant point is that this is consistently true in spite of the fact that the local behavior in the hinge regions cannot be predicted by the elastic-plastic theory.

Yang's tests were performed on beams of A7 steel. An extensive series of tests on continuous beams has been performed which includes beams of low alloy steel.[19] Sixteen tests were performed in all, eight on beams of A52 steel and eight on beams of A37 steel. These steels are the Belgian equivalent of ASTM-A441 and A36 steels. The test arrangement is shown in Fig. 2.14. In this figure αL is the length of the adjacent span. Four beams were tested at each value of α for α equal to 0.5, 1.0, 2.0 and 3.0; two beams were of A37 steel and two of A52. The length of the central span was 33.5 inches. The tests were performed on a modified WF section.

The load-deflection behavior of all test beams follows the same pattern. The behavior of Test Nos. 5 and 6 and 13 and 14 have been chosen for discussion purposes. The pertinent quantities are given in Table 2.1.

Figure 2.17 shows a non-dimensionalized load-deflection curve for the four beams under discussion. In this figure P is the load at mid-span on the beam and v is the deflection at the load point. The solid curve is an averaged curve for the four test results. The solid circles are those representing the test points for the two A52 beams while the open circles represent the A37 test points. The elastic-plastic prediction is shown as the dashed line. Although the test

results do exhibit some scatter, the beams of both materials reach and exceed the load predicted by simple plastic theory. The load-deflection behavior is closely predicted by the elastic-plastic analysis. From these tests and other related information it appears that those steels which possess adequate strain-hardening characteristics will successfully redistribute moments in an indeterminate structure.(19)

The load versus bending moment relationships for these four tests are shown in Fig. 2.16. At P_p, the support moment is greater than the full plastic value while the moment at the load point is less. However, both moments exceed M_p after a small increment of deformation, and continue to increase with additional deformation.

In summary the tests performed by Yang and Massonnet have shown that, for the low carbon and low alloy steels tested, if an adequate strain-hardening modulus is present in the material, the load predicted by simple plastic theory can be reached and exceeded.(19,20) The overall behavior of the structure can be satisfactorily predicted by the elastic-plastic theory even though the behavior of the sections in the yielded areas can only be predicted by a theory that accounts for the distribution of curvature over the structure.

It has been shown above that if a material does not possess a relatively large strain-hardening modulus the inelastic rotations required to reach P_p will introduce large strains in the material. The influence of these large strains must be documented experimentally.

It is difficult to find a material that possesses a very low strain-hardening modulus. Hrennikoff has performed tests on an

aluminum alloy which possessed a low modulus combined with a low fracture strain.[21] The purpose of these tests was to attempt to show that a material possessing a sufficiently low strain-hardening modulus will fail by fracture of the tension flange before complete moment redistribution can occur. It will be shown instead that these tests represent a completely artificial situation and that the true mode of failure would be by local buckling of the compression flange.

Tests were performed on continuous beams of aluminum alloy 6061-T6. A typical stress-strain curve for this material plotted from values used in Ref. 21 is shown in Fig. 2.17. The solid dots in this figure represent values given in Ref. 21.

The tests were designed so that critical sections of the test beams would have to undergo relatively large rotations in order to redistribute moments and form a mechanism. The arrangement for one series of tests is shown in Fig. 2.18(a). In this series of tests the left end of the specimen was deflected upward, due to the action of the load P, a distance of 1.82 inches before the support was allowed to exert any reaction. At this stage the deflected shape is shown by the dashed lines in Fig. 2.18(b). For further increments of load the member behaves as a continuous beam and the resulting shape is given by the full line in Fig. 2.18(b). This situation is intended to represent a continuous beam subjected to a concentrated load on one span and having the center support settle.

Figure 2.19 contains a plot of load, P, versus the bending moments under the load and at the interior support. In this figure the

solid lines joining the open circles represent the experimental behavior, while the elastic-plastic prediction is shown by the dashed lines.

The behavior of the member as a simply supported beam was almost completely elastic. When the exterior support began to exert a reaction the moment under the load was 188 in. kips. This moment increased rapidly and under further loading reached and exceeded M_p (236 in. kips). While this was occurring the moment at the reaction also increased. However, before this moment could reach M_p, failure occurred by fracture of the tension flange under the load. At this point the moment under the load had reached 253 in. kips or 1.07 M_p. The support moment had only increased to 226 in. kips or 0.96 M_p. The load at failure was above that predicted by simple plastic theory, 1.04 P_p.

Hrennikoff performed a second series of tests for which the arrangement is that shown in Fig. 2.20. The progress of the bending moments at sections B, C, and D (see Fig. 2.20) is shown in Fig. 2.21. The bending moments at sections B and C are almost equal at every stage of loading. These moments increased linearly to approximately M_p (298 in.kips) then at a decreasing rate to the point of failure. The moment at D also increased. When hinges had formed at B and C the moment at D then increased at a faster rate. However, fracture occurred in the tension flange at C before complete redistribution could occur. At fracture, the moments at B and C were above M_p (218 and 312 in. kips) while the moment at D was significantly below M_p (178 in. kips). The load at fracture was 33.25 kips, or 1.10 P_p.

This increase is due to the increase in moment at points B and C over the value of M_p. The redistribution of moments was incomplete and failure occurred by sudden fracture rather than by the more ductile mode associated with out-of-plane phenomena.

In both series of tests lateral buckling was prevented by suitable bracing spacing. In addition, local buckling was inhibited by collar arrangements placed on the member after local deformations were observed. Thus the collars were used to oppose the incipient flange motion. Although the test members did fail by fracture, there is every reason to believe that under less artificial conditions local buckling would have been the failure mode.[22]

In summary, the tests performed on low carbon or low alloy steel members, which possess adequate strain-hardening properties were satisfactory from a plastic design standpoint.[19,20] Those tests performed on members of a material which possesses a relatively small strain-hardening capacity were not successful.[21] There is no doubt as to the reason for this lack of success, however, and this will be discussed in the next section. It may be concluded that materials which possess little strain-hardening capacity are not suited for plastic design, particularly when applied to wide-flange members.

2.4 INFLUENCE OF MATERIAL CHARACTERISTICS ON INELASTIC BEHAVIOR

In the previous sections evidence has been presented to show

that: (1) if a material possesses strain-hardening characteristics typical of the low carbon or low alloy steel groups, moment redistribution will take place in a statically indeterminate structure and the load predicted by simple plastic theory will be reached and exceeded; (2) if a material does not possess adequate strain-hardening capability, successful redistribution of moments will not be possible.

The following section will investigate the influence of the stress-strain characteristics on the moment redistribution process. The problem can be stated as follows: In a structure having one hinge formed, it is desired to increase the moment at adjacent hinge locations while at the same time holding the strains at the original hinge location to reasonable values and, in addition, ensuring that the yielded length at any hinge location does not reach the length required to precipitate local buckling.

An analysis of a similar type was performed by Horne with a more restricted object in mind.[15] Horne analyzed two different types of structures, the material of one having a stress-strain diagram similar in shape to that of the low carbon steels while that of the second had an abbreviated plastic plateau and a very large strain-hardening modulus. The object of this investigation was to see how the load predicted by simple plastic theory compared with the load predicted by a more exact analysis. Although the methods of investigation were similar, Horne did not study the effect of the shape of the stress-strain curves on the response of the structure.

The propped cantilever of Section 2.1 will again be used as

an example. The behavior of this member has been investigated in a previous section by assuming that the material follows the behavior characteristic of low carbon steels.

The beam will now be analyzed assuming the member to have a shape factor of unity and that the material follows the various stress-strain relationships shown in Fig. 2.22(a) to (f). The results will be presented as much as possible in a non-dimensionalized form so that the only numerical data necessary are the strain-hardening modulus, E_{st}, and the strain-hardening strain, ϵ_{st}.

The values of E_{st} and ϵ_{st} for the curves of Fig. 2.22 were selected to show the influence of these factors. The values chosen bracket those which have been observed for the structural steels. The results will be presented in the following manner:

(a) The results for $\epsilon_{st} = \epsilon_y$; $E_{st} = E/45$ and $E/450$ are compared.

(b) The results for $\epsilon_{st} = 12\epsilon_y$; $E_{st} = E/45$ and $E/450$ are compared.

(c) The results for $E_{st} = E/45$; $\epsilon_{st} = \epsilon_y$, $12\epsilon_y$ and $20\epsilon_y$ are compared.

In this manner the influence of the strain-hardening modulus may be observed both on a bilinear material and on a material having a definite strain jump at the yield stress. The influence of the length of the plastic plateau may then be observed for a material having a fairly typical strain-hardening modulus. Throughout the studies in this section the strain-hardening modulus is assumed to

remain constant up to the fracture strain. This is done in the interest of simplicity; however, the implications of this assumption will be discussed in more detail later.

The magnitudes of the inelastic strains are shown graphically in Figs. 2.23, 2.24 and 2.25. These figures plot the load, P, nondimensionalized as P/P_y, versus the maximum strain adjacent to the fixed support, nondimensionalized as $\epsilon_{max}/\epsilon_y$.

Considering the relationship between the maximum strain and the stress-strain characteristics, Figs. 2.23 and 2.24 show that at a given load, the material with the smaller E_{st} is subjected to greater strains. Figure 2.23 presents the results for $\epsilon_{st} = \epsilon_y$ and Fig. 2.24 for $\epsilon_{st} = 12\ \epsilon_y$. The difference is not too great at loads below P_p but increases rapidly with further load increase. Figure 2.25 shows that the difference in maximum strains for materials having different values of ϵ_{st} but the same E_{st}, is almost equal to the length of the plastic plateau. In summary, that material having the highest value of E_{st} and the lowest ϵ_{st} produce the lowest strains at P_p and for loads above this value. Table 2.2 shows the values of the maximum strains at $P = P_p$ for the various values of ϵ_{st} and E_{st} considered in this chapter.

Figure 2.26 shows graphically the moment redistribution process. More detailed plots are shown in Figs. 2.27, 2.28 and 2.29. In these figures the support and load point moments, nondimensionalized as M/M_p, are plotted against P/P_p. In these figures and those that follow, the response predicted by elastic-plastic theory is

shown by the dashed lines. In all cases the moments reach and exceed their M_p values as the load is increased. For the bilinear material shown in Fig. 2.27 a decrease in the value of E_{st} leads to a decrease in the support moment at the simple plastic theory load. This is simply explained as a small increase in the support bending moment will cause a larger increase in the area of the curvature diagram at the support, for the more flexible material. This in turn will rotate the member to a greater extent than for the stiff material, thus resulting in a greater increase in the load point moment.

The influence is the same in the material containing a strain jump as shown in Fig. 2.28. However, in this case, the variation of E_{st} is masked by the influence of the strain jump itself which also contributes significantly to the area of the curvature diagram. This latter influence is shown clearly in Fig. 2.29. The bilinear material has the largest support moment at $P = P_p$; the plateau lengths in the flexible materials(ϵ_{st} = 12 ϵ_y, 20 ϵ_y) enable these materials to deform and redistribute moments to a much greater extent (for the same load increase) than is possible for the stiffer materials. There appears to be no significant difference in the rate at which the moments increase with increase in load above P_p.

Figures 2.30 to 2.32 plot the deflection at the load point, v, nondimensionalized as $\frac{v}{d}\frac{1}{\sqrt{\epsilon_y}}\frac{1}{(L/d)^2}$ against P/P_p. For the materials considered the deflections below P_p were essentially equal. Once this load had been exceeded the flexible materials exhibited considerably increased deflections. The contribution of the change in E_{st} is illustrated in Fig. 2.30 for the bilinear material and in Fig. 2.31 for the

material having $\epsilon_{st} = 12\ \epsilon_y$.

The influence of the strain jump can be clearly seen in Fig. 2.32. The increase in deflection at any load above the simple plastic theory load is almost directly proportional to the plateau length.

The inset of Fig. 2.32 shows, to an enlarged scale, the deflections of two of the materials up to P_p. The responses plotted in the inset represent the stiffest and the most flexible materials considered. The responses for the other materials are bounded by these two. The material properties do not influence the deflection in this range to any great extent but again those materials having smaller values of E_{st} and larger values of ϵ_{st} deflect more. The strain jump masks the influence of any decrease in E_{st}. Thus for materials having a significant plateau length, the deflections below the simple plastic theory load will not be influenced by any decrease in E_{st}.

Figures 2.33, 2.34 and 2.35 plot the nondimensionalized load, P/P_p, versus the inelastic rotation at the support section, θ_H, nondimensionalized as $\theta_H/\phi_p L$. The moment and curvature distributions in this region are shown in Fig. 2.36(a) and (b). The inelastic rotation plotted in Figs. 2.33, 2.34 and 2.35 is the rotation (from the horizontal) of the tangent to the deflected shape at a distance τL from the face of the support; minus that rotation which occurred over this same length while the beam remained completely elastic. The final curvature distribution is that bounded by the full lines in Fig. 2.36(b) while the curvature distribution at the limit of elastic behavior is shown by the dashed line in the same figure.

The total rotation is given by

$$\theta_{TOTAL} = \tau L \phi_{st} + \frac{\tau L}{2} \frac{E}{E_{st}} \phi_p \left(\frac{M_s}{M_p} - 1 \right) \qquad (2.1)$$

Since the moment gradient is known at the elastic limit, the elastic rotation of this length is given by

$$\theta_{ELASTIC} = \phi_p \tau L \left(1 - \frac{11}{6} \tau \right) \qquad (2.2)$$

Thus the inelastic rotation is

$$\frac{\theta_H}{\theta_p L} = \tau \left\{ \frac{\epsilon_{st}}{\epsilon_y} - 1 + \frac{E}{2E_{st}} \left(\frac{M_s}{M_p} - 1 \right) + \frac{11}{6} \tau \right\} \qquad (2.3)$$

The plots in Fig. 2.33 show that for the bilinear material the rotation required to reach P_p is greater for the more flexible material. For loads above P_p the decreased value of E_{st} requires that much greater inelastic rotations be endured by the more flexible material. The same tendency is shown in Fig. 2.34 for the materials having $\epsilon_{st} = 12\epsilon_y$. However in this case the differences in E_{st} are masked by the strain jump, up to P_p.

Figure 2.35 shows the influence of the inelastic plateau length. Once again the more flexible materials require a greater inelastic rotation to reach a given load level.

The point that should be emphasized from this data is the close agreement obtained between the rotation required to reach P_p as obtained

from the exact analysis and that obtained from an elastic-plastic analysis. For the materials considered the required hinge rotations are listed in Table 2.2. As expected, those materials having larger values of ϵ_{st} and smaller values of E_{st} exhibit the smallest differences between the values obtained by the exact and the elastic-plastic analyses.

As compared with the values obtained from an elastic-plastic analysis, the exact values are conservative, that is, the approximate analysis requires the member to deliver a rotation greater than actually required. Computations have been presented which equate the required rotations (from an elastic-plastic analysis) to those which can be delivered (considering the strain-hardening properties of the material).[23] On this basis limits have been placed on the structural geometry which will be satisfactory for plastically designed structures. These limitations will be conservative but not unduly so.

Lay and Smith have shown that for other structural configurations the elastic-plastic analysis will underestimate the required rotations.[24] The amount of this underestimation is small, however, and in general the elastic-plastic analysis satisfactorily predicts the rotation requirement.

The preceeding discussion has been concerned with the satisfactory performance of the structure, considering only its in-plane behavior. For practical structures the mode of failure has been shown to be either lateral or local instability.[25,26] Lay has developed criteria for predicting the rotation capacity of beams under moment

gradient by equating the length of the member which is fully yielded, τL in Fig. 2.36, to that length required to form a local buckle.[25]

Local buckling may reduce the member strength before the load predicted by the simple plastic theory is attained, if the yielded length at the support is large; or at loads above that predicted by simple plastic theory. In this latter case local buckling could occur either at the support or under the load. Since the attainment of the load predicted by simple plastic theory is the prime objective, only the situation at the support will be discussed. The progression of the yielded area under the load point would be similar. In Figs. 2.37, 2.38 and 2.39 the yielded length, τL nondimensionalized as $\tau L/L$, is plotted against the parameter P/P_p.

Figures 2.37 and 2.38 show the influence of E_{st}. In both cases the more flexible material has the shorter yielded length at P_p. Figure 2.39 shows the influence of the plateau length, again the yielded length at the support is shorter for the more flexible material. After the structure has exceeded P_p the increase in the length of the yielded portion is affected by the increase in moment in the yielded area as well as the more subtle changes in moment gradient over the various portions of the structure. This in turn is influenced by the material characteristics. The main conclusion to be gained from these relationships is that the more flexible materials require smaller yielded lengths to redistribute bending moments and reach P_p.

If the discussion is restricted to beams subjected to moment gradient, some general conclusions may be drawn from the discussion above:

(a) For the stiff bilinear material ($\epsilon_{st} = \epsilon_y$, $E_{st} = E/45$):

(1) The maximum strains were smallest throughout the loading history.

(2) The maximum moment was greatest at P_p.

(3) The deflections were minimum.

(4) The required inelastic rotation was a minimum.

(5) The yielded length at the support required to reach P_p was a maximum.

(b) Using this material as a base, the influence of a decrease in E_{st} is to:

(1) Increase the maximum strains at any given load.

(2) Decrease the maximum moment required to attain P_p.

(3) Increase the deflections by a small amount below P_p and by a very significant amount above this load.

(4) The inelastic hinge rotation required to reach P_p is increased.

(5) The yielded length at the support required to reach P_p is decreased.

(c) From the same base ($\epsilon_{st} = \epsilon_y$, $E_{st} = E/45$)the influence of an increase in the plateau length is to:

(1) Increase the maximum strains at any given load.

(2) Decrease the maximum moment required to reach P_p.

(3) Increase the deflections by a relatively small amount up to P_p and by larger amounts for loads beyond this stage.

(4) Increase the hinge rotation required to reach P_p.

(5) Decrease the yielded length at the support required to reach P_p.

From the point of view of plastic design of real structures the mode of failure is that of local buckling followed by lateral buckling. The present solutions assume that local flange buckling will not occur before the development of a critical yielded length.[27] The capacity to resist local buckling depends on the value of E_{st} and also on the maximum moment (stress) acting over the area considered.

The stress-strain curve of both the low carbon and low alloy steels seem ideally suited for this role in plastic design. These steel groups have plateau lengths of from 10 ϵ_y to 16 ϵ_y and E_{st} values which range from 600 to 900 ksi for the virgin material.[28,29]

Comparing the structural steels with the stiff bilinear material ($\epsilon_{st} = \epsilon_y$, $E_{st} = E/45$) as a base, the former would provide a decreased support moment and a shorter yielded length at the load predicted by simple plastic theory. These, combined with a relatively high value of E_{st} would provide a large resistance to local buckling and consequently the restrictions on plate geometry which are designed to inhibit the formation of a local buckle could be relatively liberal.

The fact that a significant plateau does exist will increase slightly the deflections of the structure at the simple plastic theory load and likewise the maximum strain. Neither of these factors are considered to be significant when weighed against the more obvious advantages of these material characteristics.

An assumption implicit in the foregoing analysis was that the fracture strain of the material was many times its yield strain. The structural steels have a ratio of fracture strain to yield strain which is in the order of 200. It is obvious that for any material there will be an inelastic rotation which will lead to the attainment of the fracture strain. This situation will be most critical in those materials having a low fracture strain coupled with a high value of ϵ_{st} and a low E_{st}. However, in the case of a low E_{st} value, it appears that the local buckling situation becomes critical far in advance of the attainment of the fracture strain. The background for this point of view is given as Appendix A.

It is obvious from the graphs plotted in this section that for a material which has a plastic plateau, a change in the length of this plateau makes very little difference in the results. The plots of Figs. 2.25, 2.29, 2.32, 2.35 and 2.39 show only small differences between the results for $\epsilon_{st} = 12\ \epsilon_y$ and those for the material having $\epsilon_{st} = 20\ \epsilon_y$.

It is also obvious that the deformation capacity of a member as used in the plastic theory is not a function of the plateau length or material ductility. Rather a truly ductile material in the plastic design sense must have a significant strain-hardening modulus over the initial portion of the strain-hardening range. For braced structural steel members the deformation capacity is dependent on the local buckling characteristics only.

Since the local buckling characteristics of the section do not

depend on the length of the plastic plateau but rather on the strain-hardening modulus, a material having a significant strain-hardening modulus may be expected to be satisfactory for plastic design purposes. The shape of the initial portion of the stress-strain curve is not of great importance in practical situations. This is significant as in the following section it will be shown that recent changes in straightening procedures used in the production of rolled shapes may drastically influence the shape of the stress-strain curve.

In summary, this section has shown the following.

1. An elastic-plastic analysis satisfactorily predicts the behavior of an inelastic member with respect to strength, deformation and rotation requirements. The propped cantilever used as an example can be more generally thought of as an inelastic member having known boundary conditions at the point of maximum moment.

2. The significant material property with respect to in-plane moment redistribution and local buckling capacity is, E_{st}, the strain-hardening modulus. It is fortunate that the structural steels considered have relatively high values of E_{st}.

3. The length of the inelastic plateau is not significant. For materials possessing plateau lengths of 12 ϵ_y to 20 ϵ_y any difference in length results in no appreciable change in behavior. Both bilinear materials and those possessing large strain jumps at the yield stress (up to 20 ϵ_y) are satisfactory for plastic design.

4. The low carbon and low alloy steels have stress-strain characteristics that make them ideal for use in plastically designed structures.

2.5 THE INFLUENCE OF COLD BENDING ON THE MATERIAL CHARACTERISTICS

The purpose of this section is to show how the effective material properties of a member may be changed as a consequence of the method used to straighten the member. This is particularly important with the increased use of the rotary straightening process, which subjects the member to several severe reversals of curvature throughout its entire length. It will be shown that the deleterious effects of this process, especially with regard to the effective properties of the material in the strain-hardening range, can explain the results of recent tests on structures fabricated from members which had been rotarized.(30)

To discuss production effects on the properties of structural steel members the starting point will be taken as the rolling process.(31) This process forms the structural shape from the ingot and is performed above the recrystallization temperature of the steel. The shape is air cooled before any further processing is carried out. Of necessity, the thinner parts of the section will have a higher rate of cooling. The effect of this high cooling rate is to produce a fine grained structure with its resulting higher strength. This has been observed in structural practice as the relatively thin webs consistently show higher yield strengths than do the thicker flange specimens in tensile tests.(32) This difference in cooling rates coupled with the plastic strains induced is responsible for residual strains which are locked into the section as a result of the cooling process. The distribution of these strains over the cross section has been carefully documented and that measured for a 14WF78 section of A441 steel is shown in Fig. 2.40.(29)

These residual strains are normally well below the yield strain of the material and do not significantly affect the behavior of the material as characterized by the results of a tension test performed on a specimen cut from the cross section.

However, after the rolling process has been completed and the material has been allowed to cool it must be cold-bent before use to remove the deformations caused by disturbances during the cooling process. In order to remove any initial deformation, the member must be deformed plastically and given a permanent set in a sense opposite to that of the initial deformation. In the past the conventional straightening method has been to place the member in a gag and plastically deform the initially curved part in a direction opposite to the initial curvature.[33] Such a situation is illustrated in Fig. 2.41(a) with the member being bent about its weak axis.

The bending moment distribution for the gagging operation is shown in Fig. 2.41(b) where M_o is the bending moment directly under the load. The corresponding curvature distribution is shown in Fig. 2.41(c). In this figure ϕ_o is the curvature corresponding to M_o. The moment-curvature history for the section directly under the load is shown in Fig. 2.41(d). In the gagging process the section is deformed plastically to a curvature ϕ_o and then unloaded elastically as shown. The integrated effect of the residual curvatures produced in the process is enough to approximately overcome any initial out-of-straightness. If the material at this section were again subjected to a load causing a moment in the same sense as the gagging moment, the material would

act elastically up to an applied moment M_o, then deform further as shown by the dashed lines in Fig. 2.41(d).

Although these effects have been observed previously, due to the local nature of the gagging process, it has been common practice to neglect any influence of cold bending on the behavior of members.[33,34] However, in cases where the straightening process is continuous, the resulting residual strains must be accounted for to obtain a rational prediction of the member behavior.[35]

In recent years the use of the rotary straightening process has become increasingly popular. This process is limited at present to relatively small wide-flange sections (One approximate "rule of thumb" is that the weak axis section modulus must be less than 17.0).

The rotary straightener consists of a series of heavy rolls placed as shown in Fig. 2.42 and used to bend the section about the weak axis. In this figure the rolls are numbered for convenience. The rolls are arranged so that they bear directly on the flange-to-web junctions of the member and subject it to two complete cycles of curvature reversal; rolls No. 4 to 7 being the active, or load producing rollers. The member is fed continuously into the roller arrangement, guided by rollers Nol. 1, 2 and 3. Roller No. 4 is placed in a lowered position relative to the first three. The difference in elevation may vary from a fraction of an inch to several inches depending on the size of the member, but is enough to produce a significant permanent set. Roller No. 5 then picks up the end of the member and reverses the direction of the applied curvature. The permanent set produced by this

roller is approximately one-half of that produced by roller No. 4. Rollers 6 and 7 repeat the process with correspondingly reduced magnitudes of the applied curvature, and the remainder of the rollers act primarily as guides. The entire process is one of trial and error. The first lengths of a given cross section are rotarized with trial settings of the rollers. If the member is straightened in a satisfactory manner the remainder of the lengths are processed in the same way; if not, new settings are tried and the process repeated. During the process any initial curvatures virtually disappear and the final product is almost uniformly straight.

The loading situation at the time roller No. 4 is active on the member is shown (approximately) in Fig. 2.43(a). The corresponding bending moment distribution is shown in Fig. 2.43(b) and the curvature distribution in Fig. 2.43(c). The complete length of the beam is subjected to the applied curvature ϕ_o as it is guided over roller No. 2 and is then unloaded elastically after passing roller No.4. A smaller curvature, applied in the reverse sense, is then induced by the action of roller No. 5 and so on. In order to compute the influence of this process on the member, the material behavior under reversed loading must first be evaluated.

The material behavior of structural steel under these conditions is not well known, particularly when the strains are those encountered in the strain-hardening range. The most extensive investigation into the behavior of low alloy steels subjected to reversed loading did not consider the behavior of specimens deformed beyond the plastic plateau.[36] Several authors have postulated the behavior

of a general non-linear material under a single reversal of load but none of these consider the effect of repeated reversals of load.[14,31,37]

In order to provide a simple model, yet one which contains the significant features, the behavior postulated by Chajes et al[38] and used in a modified form by Lay will be adopted.[39] This behavior is illustrated in Fig. 2.44 and accounts for the unique stress-strain characteristics of the structural steels as well as the Bauschinger effect. Since the object herein is to gain some insight into the influence of the reversed strains on the material properties, the linear strain-hardening range used by Lay has been replaced with a parabolic curve fitted to the initial modulus E_{st} at the initiation of strain-hardening and to the ultimate stress and strain. The expression for the stress, σ, at a given strain, ϵ, is then:

$$\sigma = \sigma_y + E_{st}\,(\epsilon - \epsilon_{st}) - 2E_{st}\frac{(\epsilon - \epsilon_{st})^2}{(\epsilon_{ult} - \epsilon_{st})} + E_{st}\,\frac{(\epsilon - \epsilon_{st})^3}{(\epsilon_{ult} - \epsilon_{st})^2}$$

$$+ 3\,(\sigma_{ult} - \sigma_y)\left(\frac{\epsilon - \epsilon_{st}}{\epsilon_{ult} - \epsilon_{st}}\right)^2$$

$$- 2\,(\sigma_{ult} - \sigma_y)\left(\frac{\epsilon - \epsilon_{st}}{\epsilon_{ult} - \epsilon_{st}}\right)^3 \qquad (2.12)$$

In Eq. 2.12 ϵ_{ult} is the strain at the ultimate stress. The reduced strain-hardening modulus, $\overline{E_{st}}$, at the strain, ϵ, is then given by:

$$\overline{E_{st}} = E_{st} - 4E_{st}\left(\frac{\epsilon - \epsilon_{st}}{\epsilon_{ult} - \epsilon_{st}}\right) + 3E_{st}\left(\frac{\epsilon - \epsilon_{st}}{\epsilon_{ult} - \epsilon_{st}}\right)^2$$

$$+ 6\,(\sigma_{ult} - \sigma_y)\,\frac{(\epsilon - \epsilon_{st})}{(\epsilon_{ult} - \epsilon_{st})^2} - 6(\sigma_{ult} - \sigma_y)\,\frac{(\epsilon - \epsilon_{st})^2}{(\epsilon_{ult} - \epsilon_{st})^3} \qquad (2.13)$$

Using Eq. 2.12 combined with the model postulated by Fig. 2.44, it is possible to trace the behavior of the material through the strain reversals involved in the rotarizing process. In order to do this a sequence of applied curvatures has been selected as shown in Fig. 2.45(a). The initial curvature, ϕ_1, is 20 ϕ_y, where ϕ_y is the curvature corresponding to the attainment of the yield strain in the flange tips. This is not completely arbitrary as it results in an approximate value for the deflection under the roller of 1 inch, which has been suggested as reasonable. The curvature is then reversed twice; ϕ_2 being equal to 10 ϕ_y and ϕ_3 equal to 5 ϕ_y. The final applied curvature ϕ_4 is taken as 1.7 ϕ_y from a trial and error process which will be described below. This value is required to ensure that the final configuration results in no residual curvature on the final release of moment. The above procedure has been taken as a reasonable approximation to the actual process. Only the flange plate is considered in the analysis, the web is relatively unaffected.

To determine the influence of this process on the material an approximate analysis was used. The flange plate was divided into ten

elements as shown in Fig. 2.45(b) and the strains induced by the applied curvatures computed at the centroid of each element. For the first applied curvature, ϕ_1, the strains in each element are shown in Fig. 2.45(c) along with the corresponding stresses in Fig. 2.45(d). The stresses were calculated on the basis of a flange width of 6 inches and thickness of 0.44 inches and for material having the characteristics of A441 steel.

By integrating the stresses over the cross section, the applied moment required to produce a curvature of 20 ϕ_y can be computed. This process is repeated for the reversals of curvature specified in Fig. 2.45(a) and for the final elastic unloading. This final unloading should produce a zero net curvature for zero applied moment. The final applied curvature, ϕ_4, was adjusted to achieve this end.

The strain history for element No. 1 (Fig. 2.45(b)) is shown in Fig. 2.46(a) and (b). Figure 2.46(a) shows the strains induced for positive curvatures (ϕ_1 and ϕ_3) and Fig. 2.46(b) shows those induced by the applied curvatures ϕ_2 and ϕ_4. The final set of dashed lines in both figures mark the path which the material would follow on additional loading either in tension (Fig. 2.46(a)) or compression (Fig. 2.46(b)). For the process used in this example the behavior for either type of loading would be similar. For other sequences of curvature reversal this might not be the case.

On the final unloading cycle, the residual curvature is approximately zero. However, the strain distribution across the plate is that which is required to maintain compatibility. For the example considered

this distribution is shown in Fig. 2.47(b). In this figure the residual strains, ϵ_r, have been nondimensionalized as ϵ_r/ϵ_y and tensile strains are considered positive.

The residual strain distribution assumed to be present due to the rolling process is shown in Fig. 2.47(a). This must be superimposed on the strains due to rotarizing to obtain the final residual strain distribution for a rotarized section. This has been done and the final distribution plotted as Fig. 2.47(c).

This final distribution is typical only for the rotarizing sequence assumed in the example. Any significant variation in this process could change the final strain distribution, perhaps drastically. In addition, the coarse mesh used for the numerical integration process and the neglect of the web action could introduce errors. Nevertheless, the shape of the final strain distribution is fairly characteristic of results on rotarized sections in recent investigations.[29,30,40] One such distribution, taken from measurements on an 8WF31 section of A441 steel is shown for illustration in Fig.2.47(d).[29] Figure 2.47(e) shows the residual strain distribution on the flange of the 14WF78 section taken from Fig. 2.40. This section was not rotarized.

A consideration of the residual strains which result from the rotarizing process is necessary to document the process. Of much greater importance is the effect on the stiffness of the material in the strain-hardening range. Figure 2.45(e) shows the effective strain-hardening modulus, $\overline{E_{st}}$, plotted as a fraction of the initial modulus for the section used as an example. These are the values which would

result from the curvature reversals for the process shown in Fig. 2.45(a). It is obvious that the section is less stiff due to the process, but much more work remains to be done to determine fully the influence of the rotarizing process on the behavior of plastically designed members.

Further confirmation of the reasoning used in the section above is provided by the results of tension tests performed on specimens cut from rotarized members. In addition to the assumptions made in formulating the rotarizing process and the errors induced by the coarse mesh used in the numerical integration, any comparison with tension test results introduces additional difficulties. These difficulties are associated with the location of the specimen on the cross section.

For example if the flange width is small, the tension coupon may be cut from the material centered on the web. In this case the influence of rotarizing may be small. The other extreme would be the case of a very wide flange with the coupon cut from the material near the edge. In this case the maximum influence of rotarizing should be observed.

For reasons set out below, the tests used in this comparison are those performed on specimens cut from 12B16.5 members. The results of these tests are reported in Ref. 30. The flange width of this section is 4 inches and the specimens were milled from coupons located in the flange between the tip of the flange and the centerline of the web. If the rotarizing sequence described above is typical, then the material

near the flange tip has undergone a process similar to that traced for element No. 1 in Fig. 2.45(a) while the material near the web remained almost completely elastic.

To simulate this case a model is postulated as shown in the inset to Fig. 2.48 in which half of the specimen is noted as prestrained and is assumed to have been subjected to the rotarizing sequence. The other half is noted as the virgin material.

As the model is loaded in tension, the behavior will be elastic until the applied stress reaches the yield stress of the virgin material, σ_y. This occurs at point A in Fig. 2.48. At this point the virgin material will accept further strain with no increase in stress, however, the prestrained material will behave in an elastic manner up to the increased yield stress, $\alpha\sigma_y$. Thus the model deforms from A to B in Fig. 2.48 with an effective modulus of E/2. At point B the increased yield stress of the prestrained material is reached. To achieve any further deformation the prestrained material must be subjected to an increased stress. Due to the reduction in stiffness, as evidenced by Fig. 2.45(e), this increased stress will be small. At point C the strain-hardening strain of the virgin material is reached and further deformation now requires a distinct increase in stress. The effective modulus is approximately $0.75\ E_{st}$.

This is a very crude approximation to the actual behavior. It is surprising therefore to note how well tests on actual tensile specimens agree with the behavior postulated for the model.

The tension tests reported in Ref. 30 will be compared with the behavior of the model. Reference 30 presents results for two column sections as well as the 12 inch beam section. The results of the tests on the column sections will not be discussed. These sections were rolled from the same heat and exhibited a strain-hardening modulus in the flange which was higher than usually observed for rotarized sections. In addition, the strain-hardening modulus was measured for only three flange specimens and no two were taken at the same cross section, or at cross sections where the web modulus was also measured. Thus, a comparison would not be significant.

For the 12B16.5 section, which was rolled from a different heat, the strain-hardening modulus was measured for eight flange specimens and four web specimens. The original load-strain curves taken for specimens K4-X, Y, and Z are reproduced in Fig. 2.49. At this cross section all three tensile specimens were loaded into the strain-hardening range and the measurements necessary to determine the strain-hardening characteristics were taken.

Specimen Y was cut from the web of the section and exhibits the sharp upper yield point and significant strain-hardening modulus usually associated with the structural steels. The modulus computed for this specimen was 680 ksi. On the other hand specimens X and Z exhibit a rather rounded knee and a reduced strain-hardening modulus. The areas of interest are emphasized by the arrows in Fig. 2.49. Although the rounded knee of the load-strain diagram can be caused by influences other than cold bending it is gratifying to note the close agreement between the behavior predicted by the model used for Fig.

2.48 and the flange specimens of Fig. 2.49.[32]

For the other cross sections used in the investigation of Ref. 30, the results were similar. In each case where comparison was possible the strain-hardening modulus for the web specimen was approximately 30 percent greater than the average for the flange specimens.

In summary, for sections which have been straightened by rotarizing, the effective material characteristics (assuming the flanges to exert the dominant influence) are those of a bilinear material having an effective value of E_{st} which is reduced from that normally expected in the virgin material. Tentatively it appears that the decrease will be roughly 30 percent but a more detailed investigation must be performed before definite conclusions can be drawn. The effect of this process is to reduce the lateral and local buckling capacity of the member.[27]

2.6 METALLURGICAL FACTORS IN STRAIN-HARDENING

It appears from the previous sections that a knowledge of the strain-hardening modulus, E_{st}, is fundamental in studies of members loaded into the inelastic range. This knowledge is important both for the prediction of the moment redistribution capacity of the material and the resistance to instability of the partly yielded member.

It is therefore surprising to find that very little progress

has been made in the determination of E_{st} in the past decade, even though specifications which make use of E_{st} have been proposed.[41]

Although metallurgists have investigated the strain-hardening properties by measuring the strain-hardening exponent on the true stress-strain curve, structural practice has attempted to measure the initial tangent modulus of the strain-hardening portion of the engineering stress-strain curve.[42,43]

It is questionable whether the initial modulus is the proper quantity to use in the determination of the local buckling capacity. Obviously parts of the yielded plate will be strained into the strain-hardening range while other parts are on the verge of entering this range. However, it is this initial value which has been used in the local buckling theory and which has been correlated with test results to some extent.[27,28] In addition, the neglect of the elastic unloading in the portions of the plate undergoing strain reversal offsets to some extent the non-conservative assumption that the initial modulus is relevant during the buckling process.

In the method used in Fritz Laboratory for the determination of the strain-hardening modulus, the load on the tensile specimen is measured at two selected strains.[43] These strains are greater than that at the onset of strain-hardening, ϵ_{st}, but it is presently recommended that they be within 0.002 inches per inch of the strain-hardening strain.

Seven tests were performed on specimens of A441 steel.[29] All specimens were cut from the same cross section. The values measured

for the strain-hardening modulus ranged from 605 ksi to 815 ksi with a mean value of 730 ksi. Assuming that the load on the specimen was measured at the strain-hardening strain, and again after a strain increment of 0.002; then assuming that the stress-strain curve is represented by the parabolic relationship used in the previous section, the initial strain-hardening modulus would be 740 ksi.

The scatter in the values of E_{st} quoted would lead to the belief that the strain-hardening modulus is not a characteristic of the material but rather a property which depends to a very great extent on composition and imputities.[30,42] It has been shown in the previous section that much of the confusion surrounding the measurement of this property can be explained on the basis of the large cold bending strains induced by the rotarizing process. If the variables induced by prestraining are eliminated it remains to determine what range of scatter can be reasonably expected from a group of measurements of the strain-hardening modulus.

The behavior of structural steel subjected to uniaxial stress is well known and a brief description is included only to serve as a basis for discussion of the variables involved. In the elastic range the applied stress moves the atoms from their equilibrium positions and thus develops attractive forces between the atoms; when the stress is released, the atoms move back into their original positions.[31] The relationship between the applied stress and the resulting movement is relatively unaltered by the presence of small amounts of alloying elements.

On the other hand inelastic behavior is governed by the action of line defects in the material called dislocations. These dislocations are the mechanisms by which layers of atoms are able to slip past one another by breaking their atomic bonds one row at a time, instead of requiring that the bonds between the entire adjacent layers of atoms be broken. In structural steel this slip or yielding process is discontinuous; that is, once yielding is initiated at a certain point in the material relatively large strains occur under a constant stress. In most materials slip is accompanied by an increase in stress which is referred to as strain-hardening.

The reason for this peculiar behavior of structural steel is that the interstitial impurities present in the material migrate naturally to positions adjacent to the dislocations and act as slip inhibitors.[44] Thus in order to move the dislocations a relatively high stress is required which is reduced as the dislocation is moved away from its line of foreign atoms. This accounts for the presence of the upper and lower yield points. Once the dislocations have been moved in some localized areas, these areas act as stress raisers and additional slip proceeds at a reduced stress much in the manner of crack propagation in brittle materials.

However, as these locations are moved through the material by the applied stress they come up against obstructions which prevent further movement under the same applied stress. These obstructions may be in the form of impurities, grain boundaries or simply be caused by the interaction of two or more dislocations. Once a dislocation has

been anchored by these obstructions further yielding must occur at other locations until the specimen is completely yielded.(31)

It is this point that marks the initiation of strain-hardening in structural steels. In order to strain the material beyond ϵ_{st}, which marks the fully yielded condition, the stress must be increased above that which causes the propagation of yielding over the specimen. This stress increase is necessary as now the dislocations have been anchored by one means or another and further movement means that the stress must be sufficient to bypass that obstacle. The analysis of this situation has so far not been attempted but the factors which enter the picture have been somewhat defined.(31)

The presence of a fine grained structure means that more grain boundaries are present per unit volume. Alloying elements also complicate the picture since they may either increase or decrease the rate of strain-hardening.

It should be noted that the above factors which influence the rate of strain-hardening are the same factors which influence the yield stress. In other words in a low alloy steel the alloying elements may almost double the yield point without appreciably affecting the ductility of the steel. These same alloying elements which help to anchor the dislocations in their original positions also may serve as obstacles to dislocation movement in the strain-hardening range.(31)

When structural steel is hot rolled and then cooled, the rate of cooling depends to a great extent on the thickness of the material. Very thin material will have a high rate of cooling and thick material

will have a correspondingly low rate. As the rate of cooling is increased the resulting grain structure becomes finer and the material as a consequence harder and stronger. This has been observed consistently in structural practice as tests on the webs and flanges of structural shapes have resulted in higher strength values for the somewhat thinner web material.

In summary, the same factors that influence the yield stress of a material also influence its rate of strain-hardening. For a given material the strain-hardening modulus would seem logically to be a function of the plate thickness. Since tests carried out to measure E_{st} on non-prestrained material are few, effort should be concentrated on obtaining enough data for a statistical analysis, using a consistent method and an attempt made to correlate E_{st} to the yield stress and plate thickness. In the meantime, the values recommended by Galambos are conservative to some degree and have been checked with test results over a reasonable range of variables.(41)

3. PLATE ELEMENTS IN PLASTICALLY DESIGNED MEMBERS

In the previous chapter the influence of the material characteristics on the process of moment redistribution was discussed. It was shown in Appendix A that for the majority of practical cases the capacity of the member is limited by local buckling of the compression flange.

In this chapter the problems associated with local buckling of flange and web plates are treated. To illustrate the significance of plate buckling, as related to the behavior of the member, a description is given of the behavior of a concentrically loaded stub column. With this as background, previous work on local buckling is reviewed. Material conditions existing in the member at the point of local buckling are developed and the corresponding solutions evaluated. A test program, designed to obtain information on the rotation capacity available for members having a wide range of web slenderness ratios, is outlined. Finally, a new method of approaching the local buckling problem is presented.

3.1 STUB COLUMN BEHAVIOR

The significance of plate buckling will be illustrated by the description of the behavior of a stub column. The stub column test is chosen because nominally, at least, all fibers of the cross section are subjected to a uniformly applied compressive strain which

is increased monotonically.

The test to be described was performed on a 14WF78 section of ASTM-A441 steel, which had its flanges cut down so that the b/t ratio was equal to 12.0. The pertinent dimensions of the specimen are given in Fig. 3.1 which shows a plot of the load-deformation relationship obtained during the test. In this figure the applied load, P, has been nondimensionalized as P/P_y, where P_y is the yield load ($P_y = \sigma_y A$) and the overall contraction of the column, δ, has been nondimensionalized as δ / δ_y, where δ_y is the ideal elastic contraction corresponding to P_y ($\delta_y = P_y L/AE$).

The progress of the test can be traced with reference to Fig. 3.1. The specimen is elastic up to Load No. 7 (the numbers on the plot of Fig. 3.1 and subsequent figures represent the stages during the progress of the test at which readings were taken).

The progression of the yield bands is shown in the photographs of Fig. 3.2(a) for Load No. 8 and Fig. 3.2(b) for Load No. 9. In these photographs some of the yield bands have emanated from small drilled holes which are used to measure the relative deflection of the flange tips, while other bands start at points of high residual stress. As the specimen is deformed, the yielded areas progress until the stub column is completely yielded. At this point (Load No. 13 in Fig. 3.1) further deformation can proceed only at an increased load, due to the presence of strain hardening.[45] The condition of the specimen is shown in the photographs of Fig. 3.3(a) at Load No. 12 and in Fig. 3.3(b) at Load No. 15. In this latter photograph the local deformation

of the flange plates can be seen. Although portions of the web appear to be elastic, these areas have unloaded due to the local deformations of the web plate. The concave faces of the web are fully yielded.

As the specimen is deformed beyond the load at which local deformations of the flanges are observed (Load No. 14 in Fig. 3.1), these local deformations are magnified and the load must be reduced to maintain equilibrium. This is illustrated by the path of the load-deformation curve between Load No. 14 and Load No. 20 in Fig. 3.1. After the flanges have accepted significant local deformations, the section becomes somewhat weakened and the lateral deformations of the specimen become more pronounced. The cause of unloading appears to be large local plate deformations acting together with the resulting lateral movements induced in the specimen.

The condition of the specimen at the end of the test is shown in Figs. 3.4(a), (b), and (c). Figures 3.4(a) and (b) show the large local plate deformations of the flanges while Fig. 3.4(c) shows the lateral deformation of the specimen. In the first two photographs the loading and unloading areas in the web are clearly visible.

The lateral movements of the specimen, u, measured at mid-height and non-dimensionalized as u/b are plotted in Fig. 3.5. Due to the initial imperfections in the column, lateral movements occur with the first application of load. However, it has been shown that these movements do not significantly effect the overall structural behavior until they exceed b/120 which would correspond approximately to the deformation path beyond Load No. 13.[26]

The flange movements were also measured during the test and are plotted in Fig. 3.6. These are the relative movements of the two plates and do not include any component of the overall movement of the cross section. Small movements were observed with the first application of load, however, these plate movements were of much smaller order than the lateral deflections of the cross section and were negligible up to Load No. 12. The maximum flange movements were observed at level A.A. on the cross section as shown in Fig. 3.6. This section was approximately 12 inches from the top of the specimen. The flange deformations, ΔFLG, which occurred at this section are plotted versus the average applied strains in Fig. 3.7. In this figure the applied strain has been nondimensionalized as ϵ/ϵ_y. As the average strain increases there is a larger increment in flange deformation for each change in applied strain.

The plate deflection measurements were taken only on the flange plates; the movement of the web plate was observed visually. In this test the movements of the plate elements were such that compatibility was maintained at the flange to web junction. This can be seen in the photographs of Figs. 3.4(a) and (b) and the deformed shape of the cross section conforms to that shown in Fig. 3.8.

It is evident that the actual strain is not applied uniformly over the cross section but its distribution is influenced by the initial imperfections of the specimen as a whole and by the initial imperfections of the individual plate elements. The measured compressive strains at significant Load Nos. are shown in Figs. 3.9(a) to (d). At Load No. 10 the strain distribution is relatively uniform

although there seems to be a slight gradient from west to east across the section. The same tendency exists at Load No. 12. At Load No. 14 the individual plates show evidence of bending out of the loading plane and this trend is continued in the sketch corresponding to Load No. 16. The loading and unloading faces of the individual plates correspond to those which can be seen in the photographs of Figs. 3.4(a) and (b).

In summary, the initial imperfections of the specimen produce out-of-plane motions of the member and its individual elements which are in evidence from the initiation of loading. So-called local buckling is simply a magnification of these plate movements caused at first by the reduction in stiffness of the specimen as yielding progresses over the length; then, in the later stages, by the increase in the applied load due to strain-hardening. Unloading of the specimen occurs after the local plate deformations have become relatively large and are accompanied by lateral deformation of the member as a whole.

In the concentrically loaded stub column the strain distribution along the height of the specimen is approximately uniform, so that yielding will progress in a somewhat random fashion. In contrast, for other common structural situations, the yielded portions may be confined to particular areas of the member and this must be accounted for in any analysis of local buckling.[25] In the test discussed above the flange and web plates appear to undergo out-of-plane movements at the same strain. Where, for some reason, the stiffnesses of the web and flanges differ greatly, there is a possibility that

significant local movements will occur in one plate only, without the participation of the other plate elements.

3.2 REVIEW OF PREVIOUS WORK

A great amount of research has been done on the plate buckling problem.[46] Many of these investigations deal with the buckling of elastic plates or plates having an elastic-plastic or roundhouse σ - ϵ relationship. Because of the peculiar stress-strain characteristics of the structural steels, the buckling of elements which have been deformed into the strain-hardening range presents an essentially different problem. This section will review primarily those investigations which have considered plates strained in such a manner that they are fully yielded, or strain-hardened, before buckling occurs.

The original work on the problem of plate buckling in the strain-hardening range was done by Haaijer.[47] This work assumed that the entire plate was fully yielded as a result of a compressive strain applied parallel to the longitudinal axis of the plate. Due to the yielding process, the plate is considered to be orthogonally anisotropic, that is, in two directions (in this case parallel to and perpendicular to the direction of the applied stress) the material properties are different. The differential equation expressing the equilibrium of the bent plate may be written and solved for the applied stress at which bifurcation of the equilibrium position occurs. Alternatively, the problem may be solved by an energy approach.[48] The

external work done by the applied stress during buckling must equal the internal work done by the plate. This results in the following integral equation:

$$\frac{12\ \sigma_x}{t^2}\iint\left(\frac{\partial w}{\partial x}\right)^2\ dx\ dy = \iint\left\{ D_x\ \left(\frac{\partial^2 w}{\partial x^2}\right)^2 + D_y\left(\frac{\partial^2 w}{\partial y^2}\right)^2 + (D_{xy} + D_{yx})\left(\frac{\partial^2 w}{\partial y^2}\right)\left(\frac{\partial^2 w}{\partial x^2}\right) + 4G_{st}\left(\frac{\partial^2 w}{\partial x\,\partial y}\right)^2\right\} dx\ dy \qquad (3.1)$$

In Eq. 3.1, D_x, D_y, D_{xy} and G_{st} are the stiffnesses of the material in the strain-hardening range. The thickness of the plate is t and σ_x is the stress applied parallel to the longitudinal axis of the plate (the x direction). The deflection of the plate is denoted as w, and the appropriate derivatives used in Eq. 3.1 are taken in the x direction or across the width of the plate (the y direction). The integrations are performed over the area of the plate.

Equation 3.1 may be solved by assuming a deflected shape which is reasonable for the plate considered. If the dimensions of the plate and the material properties are known the stress at which the plate will buckle can be obtained. Alternatively, if the applied stress is specified, Eq. 3.1 may be solved for the limiting geometrical proportions required for the plate to buckle at the specified stress. This latter approach was used by Haaijer to obtain limits on the flange

and web geometry so that the plate would buckle at the yield stress.[47] the material stiffness used were those deemed appropriate for the strain-hardening range.

In order to use this type of solution some relationship must be established between the width of the plate, b, and the length of the local buckle. Haaijer obtained such a relationship by requiring that the length of the local buckle be that which would produce buckling at a minimum stress. Since this stress is actually the yield stress, an indirect relationship is obtained between the b/t ratio of the plate and its material properties. The use of this length implies that the applied strain is developed uniformly along the plate so that the plate will buckle as soon as the stress reaches the yield value and the material condition is that implied by the choice of the material properties.

In order to select material properties which would result in reasonable solutions, Haaijer correlated the theoretical values with tests performed on wide flange shapes.[28] For plates supported along one edge only, as in the case for the flange, the dominant property is the torsional rigidity in the strain-hardening range. For web plates, however, the direct stiffnesses in each direction as well as the torsional rigidity and the cross-stiffnesses play important roles. Haaijer related these constants to the half wave length of the local buckle and from observations on tested specimens was able to select reasonable values of the stiffness properties.[49]

The tests performed by Haaijer were used primarily to provide

values for the material constants but, in addition, the restraint due to the adjacent plate elements had to be evaluated.[28] It is not surprising, therefore, that Haaijer's solutions are sometimes regarded as semi-empirical.[50] The web buckling solution for combined axial load and bending must be looked on with particular caution, as for this case a solution for a plate subjected to a uniform strain was adjusted in a rather arbitrary manner and applied to a plate subjected to a strain gradient.[49]

For sections having small warping rigidities the phenomena of torsional buckling and local buckling are coincident.[5] Fisher et al used the torsional buckling solution, neglecting the warping stiffness of the plate, to limit the slenderness ratio of the flange plate to be used in haunched corner connections.[51] In this investigation the material constants used were those developed by Haaijer and the restraint due to the web was neglected.

Lay carried out studies using the torsional buckling model shown in Fig. 3.10. The basic equation for this case is given by:[5]

$$\sigma\, bt = \frac{12}{b^2}\left\{G_{st}K_t + \left(\frac{n\pi}{L}\right)^2 E_{st}I_w + k\left(\frac{L}{n\pi}\right)^2\right\} \qquad (3.2)$$

In Eq. 3.2, K_t is the St. Venant torsional stiffness, $\frac{1}{3}bt^3$, and I_w is the warping stiffness given as $\frac{7}{16}\ \frac{b^3t^3}{144}$ by thick plate theory.[5] The restraint due to the web action is denoted by k, the rotational spring constant. Lay assumed the section to deform as shown in Fig.3.11 and obtained the spring constant as:

$$k = \frac{G_{st}\ w^3}{3(d - 2t)} \qquad (3.3)$$

The value of G_{st} in these expressions is not Haaijer's experimentally determined value but rather that derived by Lay from a consideration of the discontinuous yielding process of structural steel.[27] This theoretical basis makes it possible to extend Lay's work to other materials which yield in the same manner as the low carbon steels.

The only term which remains to be determined is that which contains the length of the local buckle, $n\pi/L$. It is usual in plate problems of this nature to choose the integer value of n which gives the lowest value of P.[5] However a good estimate of n may be obtained by differentiating the expression for P (Eq. 3.2) with respect to L and setting the result equal to zero.[49] This results in:

$$\frac{L}{n\pi} = \sqrt[4]{\frac{E_{st}\, I_w}{k}} \qquad (3.4)$$

Lay made two additional contributions. He first investigated the influence of the web restraint and concluded that in most cases it was negligible. Secondly he accounted for the structural behavior of the member in applying the local buckling solutions. Thus the beam subjected to uniform moment was found to local buckle as a result of prior lateral buckling while for the beam subjected to moment gradient, local buckling was the cause of lateral buckling.[25,26]

The work discussed above based the local buckling strength of the plate on the value obtained from an initial motion type of solution based on the tangent modulus. It has been shown for columns that generally the tangent modulus does provide a reasonable estimate of the strength of the member.[52] However, in some cases it has been found

that the ultimate strength of such a member is quite removed from the tangent modulus load.[53] In addition, a knowledge of the strength alone may not be sufficient. Especially for the case of members subjected to a moment gradient, the complete load-deformation path of the plate would be most useful.

Kato has provided a step in this direction by analyzing a plate using a modified yield-line approach.[54,55] Kato first assumed the location of yield lines in the buckled plate. The deformed flange plate and the corresponding mechanism are shown in Fig. 3.12. The virtual work expressions are then used to equate the external work done by the yield stress acting through the longitudinal deformations to the internal work done by the bending moments and shear forces in the plate. To express the work done by the bending moments, Kato first used the reduced value of the plastic moment, M_{pc}, to account for the axial force in the plate. The expression for the reduced plastic moment is:

$$\frac{M_{pc}}{M_p} = 1 - \left(\frac{P}{P_y}\right)^2 \qquad (3.5)$$

Since the applied strain parallel to the longitudinal axis of the plate is σ_y, the value of M_{pc} on those yield lines perpendicular to this direction is zero. Thus the internal work done along the yield lines shown as BB' and DD' in Fig. 3.12 is also zero. Under this assumption the yield line method loses one of its most important advantages -- the strength of the plate as a function of a chosen geometrical parameter never has a minimum for finite values of this geometrical parameter. Thus, the correct yield line pattern cannot be

obtained by any rational analysis. Although Kato's results are reasonable for the dimensions chosen, a small variation in these dimensions could produce entirely different results. Because of the assumptions made, the strength of the plate is not related to the strain-hardening properties of the material. There is also no attempt in this study to relate the local buckling strength to the loading and restraint conditions on the plate in question.

Although this particular study does not lead directly to a complete knowledge of the load-deformation relationship for a plate, it appears to be the logical point at which an investigation should be initiated to determine this relationship thus enabling the behavior of the plate to be followed well into the post buckling range.

In summary, the work by Lay and Haaijer has provided solutions which produce safe, although in some cases overly conservative, restrictions on flange plate geometry for sections used as beams.[27,28,47] The local buckling of web plates subject to a uniform compressive strain has also been investigated.[49] The critical portion of the work that remains is to evaluate the local buckling strength of plate elements in sections subjected to a strain gradient. At the present time (1966) there does not appear to be any rational method of accounting for the post buckling capacity of the plate elements deformed into the strain-hardening range.

3.3 FLANGE BUCKLING - WEB UNDER STRAIN GRADIENT

Both Lay and Haaijer treated local flange buckling as the buck-

ling of a plate restrained by a spring representing the influence of the web. Haaijer determined the stiffness of this spring experimentally, while Lay obtained an analytical expression for the spring constant by assuming the web to act as a propped cantilever.[27,47] This expression is given as Eq. 3.3; in the derivation Lay considered the web plate to be in the fully yielded condition.

It has been shown that, due to the discontinuous nature of the yielding process, the material must either be elastic or in the strain-hardening range, even though the measured strain over a finite gage length is between the yield strain and that at the onset of strain-hardening.[45]

In the case of a section subjected to a strain gradient (in a beam or beam-column) the non-uniform strain distribution across the web plate could introduce considerable difficulty in the buckling problem, as an evaluation of the material properties in a partially yielded plate does not appear to be practical.[56] However, it is of interest to consider the material condition in the web plate subjected to a strain gradient as the maximum strain in the plate approaches the strain-hardening strain.

The section is shown in Fig. 3.13. It has been shown that in order to initiate yielding in the plate the stress at some point must reach $i\sigma_y$ where i is slightly greater than 1.0.[45] Lay assumed i = 1.05 but for the purposes of this discussion any reasonable value will suffice. The formation of a yield plane is a dynamic process; it requires a smaller stress to advance than it does to initiate the yield plane.

Thus, once the yield plane is initiated it extends to the level at which $\sigma < \sigma_y$. If the average strain at the top of the plate is $> i\epsilon_y$, at discrete points along the top edge of the plate yield lines will form and progress dynamically to the region where the local strain is $< \epsilon_y$. This is shown as stage No. 1 in Fig. 3.13. As the average strain at the top edge of the plate is increased, more and more yield planes will be initiated at the top of the plate and will progress through the plate to a depth greater than that to which the earlier yield lines had progressed. During this second stage of loading, those yield planes which were previously formed will also extend, until finally at stage No. 2 all the yield planes present in the plate extend to the depth where $\epsilon < \epsilon_y$. If the average strain at the top edge of the plate is increased to ϵ_{st}, then the plate should be fully yielded from the top to a depth where $\epsilon < \epsilon_y$. In other words the plate yields in layers, and on a local basis plane sections before bending do not remain plane during the plastic yielding process.

It follows, that in the case discussed, the relevant material properties in the fully yielded portion of the plate will be those which characterize the strain-hardening portion of the stress-strain curve, while the remainder of the plate remains elastic.

From the above discussion the web restraint may be evaluated for the various loading conditions which may be encountered. In the case of the beam the expression for the web spring constant given by Lay may be modified slightly to account for the actual condition of the material.[27]

The web of a beam has a stiff elastic core which is $\frac{(d-2t)\epsilon_y}{\epsilon_{st}}$ in length. The tension portion of the web is acted upon by large membrane forces which tend to hold it in an undeflected position. It has been observed that when local buckling does occur only the compressed part of the web participates in the buckle. A typical photograph showing this action is given as Fig. 3.14. Since the elastic core is stiff relative to the yielded portion of the flange, it is reasonable to assume that the yielded portion of the web acts as a propped cantilever as shown in Fig. 3.15. The plate is assumed to be fixed at the junction of the elastic and fully yielded areas. The spring constant expressing the restraint offered by the web is now:

$$k = \frac{2G_{st}\,\epsilon_{st}\,w^3}{3(d\,(\epsilon_{st}-\epsilon_y) - 2t\,\epsilon_y)} \qquad (3.6)$$

The influence of this change on the strength of the flange plate is not great and may be neglected, but the use of this reasoning for other cases enables the influence of the loading condition on the web restraint to be evaluated in a rational manner.

It is obvious that to modify Eq. 3.6 for a section subjected to axial load and bending moment, it is necessary only to locate the position of the neutral axis when the flange is on the verge of local buckling.

It has been shown that for column sections subjected to relatively high axial loads (above $P/P_y = 0.30$) the neutral axis is in the flange when the cross section is subjected to M_{pc}. This is confirmed by the results of eccentric stub column tests.[56]

The restraint provided by the fully yielded web is not significant in evaluating the local buckling capacity of the flange.[27] However, it does influence the optimum length at which a local buckle will form under a uniformly applied strain. This factor will be discussed in a later section.

3.4 WEB BUCKLING

The problem of web buckling of members in plastically designed structures has not received a great deal of attention. This is partly because of the difficulties involved in the problem and partly because of its relative lack of importance for low rigid frame structures. The existing work on this problem as applied to plastic design is due almost entirely to Haaijer.[28,47,49]

Elastic solutions for web buckling under a uniformly applied strain are available in the literature.[5] For a member used in a plastically designed structure, the case of uniform strain will be relatively rare. The member will be satisfactory if it attains the yield load, P_y. ($P_y = A\sigma_y$)[49] In this situation the cross section may be subjected to small inelastic strains due to the compressive residual stresses present.[57] The buckling of the web plate under these conditions has been studied analytically and the maximum web slenderness, d/w, which will allow the web plate to reach its yield stress has been determined. Ostapenko has given this value as

$$\frac{d}{w} = \frac{8040}{\sqrt{\sigma_y}} \tag{3.7}$$

where σ_y is measured in pounds per square inch.[46]

Equation 3.7 is a compromise, as it represents an expression intermediate between that for the elastic buckling of a simply supported plate and a plate fixed at the unloaded edges. Since the flanges will be proportioned to eliminate elastic local buckling, the web plate will be forced to buckle with the unloaded edges essentially fixed against rotation. Thus Eq. 3.7 should be conservative.

The original proposal for web geometry was based on the elastic solution for a simply supported plate but modified to account for the results of the stub column tests performed on wide-flange shapes.[28] Figure 3.16 shows a plot of the critical stress, σ_{cr}, nondimensionalized as σ_{cr}/σ_y, versus the d/w of the web. The solid lines in this figure correspond to the elastic solution terminated at $\sigma_{cr}/\sigma_y = 1.0$.[46] The yield stress used was 38 ksi. This corresponds approximately to the measured yield stress for three of Haaijer's tests - D2, D4, and D6.[28] The limiting value given by Eq. 3.7 is 41.2. These three test points are plotted on Fig. 3.16. A closer examination of the test results shows that in both Test D2 and D6, flange and web movements occurred simultaneously, thus the only case in which web buckling can be said to have definitely occurred before large flange movements is in Test D4.[28] The three test results are plotted again in Fig. 3.17. In this figure the d/w ratios are plotted versus the strains at which large plate movements were observed. It can be seen that the critical

web buckling strain for Test D4 was above the yield strain. In addition, the detailed results for this test show that although the web did buckle prematurely, causing a drop in load, on further deformation the load again increased and exceeded the yield load. The cause of final unloading was the local flange buckling.

However, the present recommendations limit the d/w ratio to 43 (for A36 steel).[58] This result is based primarily on consideration of Haaijers Test D6. It can be seen from Figs. 3.16 and 3.17 that failure was due to elastic buckling. It appears, however, that the mode of failure was combined buckling of the web and flange thus the test is not a valid one on which to base specifications.

To clear up the situation a series of tests is planned for concentrically loaded stub columns. The object of these tests will be to determine, for various b/t ratios, the maximum d/w ratios which can be used and still have the stub column reach its yield load. The tests will be performed on members of A36 and A441 material.

The problem of web buckling for a section subjected to bending and axial load is less clear. Following the reasoning presented in the previous section, if the flange is required to reach the strain-hardening strain, the web material (to the boundary of the elastic core - see Fig. 3.15) should be fully yielded. However, if the material properties corresponding to the fully yielded material are used the limitations on web geometry are unduly conservative.

Haaijer concluded that the modulus of elasticity in the direction perpendicular to the applied strain, E_y, should be close to the

to the elastic value, E, instead of the value proposed by Lay, G_{st}.[28] Haaijer then justified this increase in strength on the basis of an assumed biaxial stress condition in the plate due to the imperfections present in the section. The value of E_y predicted on the basis of discontinuous yielding by Lay is close to that obtained using the incremental theory of plasticity by Handelman and Prager.[27,59]

Coupled with the difficulties in choosing material constants for this case are those involved in analyzing the restraint conditions and the necessity of accounting for the non-uniform strain distribution. Haaijer obtained reasonable limits on web geometry by using a solution for the uniformly compressed plate and then choosing the maximum strain to which the compression flange should be subjected.[49]

In view of the somewhat arbitrary adjustments involved in the solutions which pertain to the web plate subjected to a strain gradient, a series of tests has been planned to determine the limiting web geometry which will allow the compression flange to be fully yielded over its optimum length before local buckling occurs. These tests will be outlined in the next section

3.5 PROPOSED TEST PROGRAM

The test program proposed in this section has a rather broad aim, that is: to observe the influence of changes in web geometry on the rotation capacity of beam-columns. More specifically; for a given

loading condition on a "just compact" section, the d/w of the web will be determined so that the compression flange will be fully yielded over its optimum length before local buckling occurs. This would represent the optimum behavior that could be expected from a member in a plastically designed structure.

The proposed test arrangement is shown in Fig. 3.18. The member under test is placed in a horizontal position and bolted to an upright frame, which is in turn bolted to the structural floor. An axial load is applied to the member by means of two tension jacks (one is shown in Fig. 3.18, the second is hidden behind the member under test) placed to eliminate lateral bending of the specimen. The jacks are connected in series with dynamometers and deliver load to the member through a plate bearing on the end of the specimen. The jack reactions are picked up by a second plate which delivers them to the upright column of the supporting frame through a set of rollers as shown in Fig. 3.18.

Bending moment is applied to the member by means of a tension jack placed in the vertical position. The jack is erected in series with a dynamometer and acts on the member through lugs welded to the top flange.

The testing arrangement is designed to:

(1) Subject the member to axial load and bending moment in a situation which is common in both braced and unbraced multi-story frames.[60,61]

(2) Observe local buckling in a member which is subjected to axial load in addition to a moment gradient. In this

situation the strain gradient across the web plate can be varied, but more important, the influence of the restricted zone of yielding can be studied. The test situation shown in Fig. 3.18 simulates the real member to a much greater degree than does the eccentric stub column test.

(3) Eventually, to obtain information which will lead to a rational determination of the plate stiffness coefficients used by Haaijer.[28]

The test specimen should have a length to depth ratio of at least 5 to allow a sufficient length for the formation of a local buckle to occur and provide room for instrumentation. In this range the smaller beam sections (which will be used to provide slender webs) would have a strong axis slenderness ratio of 10-15. Since the column simulates to some extent one half of the column in an unbraced frame under double curvature conditions, the series of tests will provide additional important information on the behavior of beam-columns having practical slenderness ratios.

In a local buckling sense the most important information sought is that relating to the behavior of the web. This becomes important primarily in beam sections used in the lower stories of braced frames to carry the axial forces from the diagonal bracing.

The first test series will be performed on "just compact" sections under varying axial load ratios. The tests planned are shown in Table 3.1. The d/w ratios shown are tentative only and may be adjusted

if necessary. The d/w ratios for Tests WB-2 to WB-4 will be adjusted from a consideration of the results of Test WB-1, etc. In each case the object will be to determine the maximum possible ratio of d/w that will allow satisfactory behavior. In flexural action the web is relatively less important than the flanges. Since the post-buckling strength of the web will be observed it is hoped that some liberalization of the present specifications will be possible. In spite of large web slenderness ratios, in at least some situations unloading will be triggered by the local buckling of the flange.

In this type of test the axial load is applied first to the specimen and held constant during the test. The moment is then applied, using increments first of load, then of deflection. The vertical deflections of the member are measured at several points along its length together with the rotation at the "fixed-end". Thus the internal forces in the specimen can be determined. The local flange deformations are measured with a dial gage placed in pre-punched holes drilled on the inside of the flanges. The local web deformations are measured with dial gages which bear against the web plate. A most important part of the test is the observation of the flange yield pattern in the plastic hinge area.

A pilot test, WB-1, has been performed and the results are plotted in Figs. 3.19 and 3.20. The specimen was a modified 5WF18.5 section of A441 steel which was modified so that b/t = 13.5 and d/w = 60.7. Figure 3.19 plots the transverse load, H, versus the transverse deflection, Δ. The dashed lines represent the theoretically predicted behavior of the member, assuming that web and flange local buckling do

not influence the response. The initial portion of the prediction curve is based on the elastic behavior of the member. The shear deformations and the secondary moments are accounted for.

The lower descending dashed line represents the behavior after a plastic hinge has formed at the face of the connection. To maintain equilibrium, the force, H, must be decreased as the deformation is increased. To account for the increased strength of the area adjacent to the connection, the upper descending dashed line represents the response of the member assuming that the plastic hinge has formed a distance, d, from the face of the connection. This correction will be discussed in Chapter 5. The actual member behavior should be bounded by these two curves.

The experimentally observed behavior follows the upper curve up to Load No. 14, even though web buckling occurred at Load No. 10 (as shown by the arrow). The response did not fall off until after local flange buckling had occurred, between Load Nos. 13 and 14.

The present solutions assume that local flange buckling will not occur until the yielded length, τL, reaches $2.4b$.[27]

For test WB-1, local flange buckling occurred at a yielded length of approximately $1.9b$. The progression of yielding is shown in Fig. 3.20 which shows a plot of the load, H, versus the yielded length, τL. Since the section used did not meet the compact definition for the actual material properties used ($b/t = 13.5$ versus a compact $b/t = 12.8$) it appears that the behavior obtained was close to the optimum. Additional tests will be performed to further investigate the problem. A

report containing the detailed results is in preparation.

It is hoped that this series of tests will determine safe and economical solutions to the plate buckling problem as applied to members in plastically designed structures. The test arrangement is simple, yet subjects the member to a loading condition which is typical in plastically designed frames. In addition the tests will provide badly needed information on the behavior of beam-columns under high axial loads.

3.6 FLANGE BUCKLING - SHORT YIELDED LENGTHS

In the previous initial motion solutions, the member is assumed to buckle locally only after a sufficient area of the compression flange has fully yielded to enable the flange to buckle at a minimum stress.[27,47] The flange slenderness ratio (b/t) which satisfies this condition is termed "compact" and only compact sections are deemed suitable for plastically designed structures. It is assumed in this section that web buckling will not occur.

The belief that the above situation must hold for members in plastically designed structures stems from two conditions:

(a) Convenience; the use of an optimum fully yielded length leads to a considerable simplification of the plate buckling equations and the corresponding specifications.

(b) The tests on which Haaijer and Lay based this theory were

all performed on simply supported beams of compact or near compact proportions or on stub columns. Thus local buckling did occur when the optimum length was fully yielded.

However, different structures require different amounts of inelastic rotation in order to attain the simple plastic theory load. (It is assumed throughout this dissertation that attainment of this load represents satisfactory performance of the structure.) If the required rotation is known and is less than that corresponding to the optimum yielded length, a significant liberalization of the plate slenderness limitations can be achieved.

It has been shown that the fully yielded length may be related to the rotation capacity and hence to the required plate slenderness.[22]

Consider the member segment of length, L, shown in Fig. 3.21(a). It is subjected to a bending moment distribution which varies from M_o to ρM_o. The moment ratio, ρ, is positive as shown and is chosen so that $1.0 \geq \rho \geq -1.0$. If M_o exceeds M_p, the length of the segment that is fully yielded is τL. Assuming a shape factor of unity for the cross section, the curvature distribution is as shown in Fig. 3.21(b).[27]

As in Chapter 2, the inelastic rotation, θ_H, will be taken as the rotation occurring over the yielded length, τL, after the maximum moment, M_o, attains a value of M_p. From Fig. 3.21(b), the total rotation can be taken as the area under the curvature diagram for the length τL.[25]

$$\theta_{TOTAL} = \phi_{st} \tau L + \frac{E}{E_{st}} \phi_p \frac{\tau L}{2} \left(\frac{M_o}{M_p} - 1.0 \right) \quad (3.8)$$

The rotation occurring over this same length up to the attainment of M_p can also be taken from Fig. 3.21(b) as that area bounded by the dashed lines:

$$\theta_{ELASTIC} = \rho \phi_p \tau L + \tau L \frac{\phi_p}{2} (1 - \rho) \quad (3.9)$$

From the geometry of the bending moment diagram of Fig. 3.21(a)

$$\frac{M_o}{M_p} - 1.0 = \frac{\frac{\tau L}{L} (1 - \rho)}{1 - \frac{\tau L}{L} (1 - \rho)} \quad (3.10)$$

By substituting Eq. 3.10 in Eq. 3.8 and subtracting the elastic rotation from the total rotation, the inelastic hinge rotation is:

$$\frac{\theta_H}{L\phi_p} = \frac{\tau L}{L} \left\{ \frac{\epsilon_{st}}{\epsilon_y} - \frac{1}{2} (1 + \rho) + \frac{E}{2E_{st}} \left[\frac{\frac{\tau L}{L} (1 - \rho)}{1 - \frac{\tau L}{L} (1 - \rho)} \right] \right\} \quad (3.11)$$

Equation 3.11 permits the calculation of the inelastic rotation corresponding to a given yielded length. If the inelastic change in curvature is approximated by the cross-hatched area shown in Fig. 3.21(c), the inelastic rotation can be approximated by:

$$\frac{\theta_H}{L\theta_p} = \frac{\tau L}{L} \frac{\epsilon_{st}}{\epsilon_y} \quad (3.12)$$

This approach is very similar to that used by Horne in another context.[4] The significance of the approximation will be discussed in detail in Chapter 5; it is sufficient to say that the approximation is entirely satisfactory for the structural steels.

The critical stress, σ_{cr}, at which torsional buckling of a yielded flange plate will occur is given by Lay.[27] In the following expression the restraint offered by the web has been modified as in a previous section.

$$\sigma_{cr} = \frac{12}{b^3 t}\left\{\frac{G_{st}}{3} bt^3 + \left(\frac{n\pi}{\ell}\right)^2 E_{st}\ \frac{7}{16}\ \frac{b^3 t^3}{144} + \frac{2\ G_{st}\ \epsilon_{st}\ w^3}{3(d\ (\epsilon_{st}-\epsilon_y)\ -2t\epsilon_y)}\left(\frac{\ell}{n\pi}\right)^2\right\} \qquad (3.13)$$

In the usual structural situation, the yielded portion of the plate is restrained by a stiff elastic portion on one side and by a load or reaction point on the other. Thus the plate is forced to take the shape shown in Fig. 3.22. The half wave length of the local buckle, ℓ/n, is related to the yielded length, τL, by:

$$\frac{\ell}{\pi n} = \frac{\tau L}{2\pi} \qquad (3.14)$$

From Fig. 3.21(a) the maximum moment on the member, M_o, is given by:

$$M_o = \frac{M_p}{1 - \frac{\tau L}{L}(1 - \rho)} \qquad (3.15)$$

Under the assumptions of this section the maximum stress, σ_o, is then:

$$\sigma_o = \frac{\sigma_y}{1 - \frac{\tau L}{L}(1 - \rho)} \tag{3.16}$$

If, conservatively, b is replaced by $\sqrt{12}\, r_y$ and the maximum stress is assumed to act over the entire yielded length, the b/t ratio at which buckling will occur is given by:

$$\left(\frac{b}{t}\right)^2 = \frac{1 - \frac{\tau L}{L}(1 - \rho)}{\sigma_y} \left\{ 4G_{st} + \left(\frac{2\pi L}{\tau L}\right)^2 E_{st} \frac{7}{16} \frac{1}{(L/r_y)^2} + \frac{2}{3} G_{st} \frac{A_f}{A_w} \left(\frac{w}{t}\right)^4 \left(\frac{L}{r_y}\right)^2 \left(\frac{\tau L}{2\pi L}\right)^2 \right\} \tag{3.17}$$

This is essentially the same relationship used by Lay and Haaijer, however, in these previous studies the value of the yielded length, τL, was obtained by applying the rules of differential calculus to Eq. 3.13, and solving for the buckled length, ℓ, at which σ_{cr} becomes a minimum.

In this section the value of the yielded length, τL, will be taken from Eq. 3.12, which will ensure that a sufficient length has yielded so that an inelastic hinge rotation θ_H has taken place. If this hinge rotation is taken as the value required for the structure to form a collapse mechanism, then the b/t value which results from Eq. 3.17 will be such that the section will local buckle at the load producing collapse.

As an example, consider the fixed-end beam shown in the insert of Fig. 3.23(a).[41] The curve in Fig. 3.23(a) plots the load-deformation relationship for the beam based on elastic-plastic theory. The

sequence of hinge formation is A, B and C. The required hinge rotations are given in Fig. 3.23(b). Points A and B must rotate through $\theta_H = \phi_p L/6$ after hinge formation.

It will be assumed that the member is a 14WF30 section and the length is 30 ft. The material is A36 (σ_y = 36 ksi, $\epsilon_{st} = 11\epsilon_y$, $E_{st} = E/33$). The moment ratio, ρ, may be taken as -1.0. From Eq. 3.12 $\tau L/L$ = 0.0152. The 14WF30 section has a b/t value of 17.6 which would normally not be acceptable in a plastically designed structure.

If the member and material properties are substituted into Eq. 3.17, the critical b/t value is 19.3. Since the member provides a b/t of 17.6, it will provide sufficient rotation capacity before the onset of local buckling for the complete mechanism to form.

The above procedure may be considered too involved for a design procedure. However, with the use of high strength steels in multi-story frames the range of useable column sizes is drastically diminished and it may be found necessary to adopt such procedures.

The analysis of multi-story frames in the inelastic range is complex and it is only recently that a computer program has been available for such a task.[62] As yet, the computations have been performed only for unbraced frames of A36 material. However, one such frame will serve as an example.[63]

The frame is shown in Fig. 3.24(a) with the member sizes as determined by a plastic design method. The hinges which had formed in the structure at the ultimate load are shown in Fig. 3.24(b). The

hinge locations are shown by solid circles. The program used to analyze the frame determined the condition of the frame at load increments of 0.1 times the design ultimate load. The numbers adjacent to each hinge location represent the proportion of design ultimate load at which the hinge first appeared. The frame reached its actual ultimate load at an applied (computer) load between 1.0 and 1.1 times the design ultimate load. Probably close to the former.

The two column hinges are of prime significance. These formed at the design ultimate load. Thus, in theory, they require no rotation capacity and provided the b/t of the sections used was less than that required to eliminate elastic buckling ($b/t < 32$), the section would be adequate.

To be conservative, it will be assumed that the hinges formed at 0.9 times the design ultimate load. The required hinge rotations to reach the design ultimate load may then be computed from the bending moment diagram and the frame deformations. For hinge B7 the required rotation was $0.14\ \phi_p L$ and for hinge D5 the rotation was $0.22\ \phi_p L$.

The hinge rotations are substituted into Eq. 3.12 and the yielded lengths which result along with the properties of the member are substituted into Eq. 3.17. The critical values of b/t which result are 27.7 and 28.6 for the two hinges. Obviously, the extent of yielding in the member will be small below the ultimate load. This is to be expected of columns in multi-story frames designed by presently proposed methods but should not be regarded as inevitable.[60,61]

The conclusions resulting from the work of this section are firstly: that because of the manner of the progression of yielding in the structural steels, sections which are non-compact may still be expected to deliver a certain rotation capacity before local buckling of the section occurs. In many cases it appears that the delivered rotation capacity of a section will be sufficient to enable the structure to reach its ultimate load. Secondly, it may be practicable to use non-compact sections as columns in multi-story frames. This problem is most important where the use of low alloy columns would be justified to carry high axial loads. It is gratifying to note that with very little additional work on the part of the designer, the methods of analysis used for multi-story frames could be used to estimate the rotation capacity requirement.

4. MEMBERS IN PLASTICALLY DESIGNED STRUCTURES

The primary purpose of this investigation is to formulate design rules which will permit the use of low alloy steel members, with yield stress levels up to 50 ksi in plastically designed structures. Where this is not yet possible, the areas requiring additional research must be clearly defined.

In formulating design rules the member must be considered as a part of a plastically designed structure and its interaction with other parts of the structure considered. One member in a structure may unload while, in order to maintain a compatible deformation pattern, adjacent members may accept additional load. Thus the unloading portion of a particular member may be pertinent to the determination of the maximum strength of the structure.

The initial sections of this chapter will consider the behavior of beams under uniform moment and moment gradient. For these members design rules are proposed which have adequate analytical and experimental background and which are, to some extent, conservative. Later sections are devoted to the behavior of beam columns. The design of these members is presently accomplished by the use of curves which have been fitted to the results of computations of the ultimate strength of beam-columns.[58,64] The procedure used for the computation of the ultimate strength is numerical, however, it has been shown that the results which have been obtained for A36 steel may be modified to predict the ultimate strength of A441 columns.[65] This extrapola-

tion procedure is examined and found to give adequate and conservative results.

The remainder of this chapter consists of brief discussions on the design of axially loaded columns and connections and a short outline of the problems of shear and web crippling. In these areas major research efforts are in progress or are proposed.

4.1 BEAMS UNDER UNIFORM MOMENT

Beams subjected to loading conditions which produce a uniform moment over a portion of the length have been considered at great length in the literature.[66] This perhaps undue emphasis is primarily because of the feeling that the beam subjected to a uniform moment represents one of the worst lateral buckling situations. In addition, this problem is deceptively simple in the elastic range. Lay and Galambos have recently examined the inelastic behavior of such elements and have formulated expressions for computing the rotation capacity of the member.[26]

It is useful to review the behavior of beams subjected to uniform moment so that conclusions can be generated concerning the rotations which these members should be required to sustain. The nondimensionalized moment-rotation (M/M_p vs θ/θ_p) curve for Test HT-29 is shown in Fig. 4.1.[29] The beam behaves elastically up to Load No. 6; at this stage the applied strains add to the residual strains to produce yielding and resulting non-linearity in the M-θ curve. The load on

the member continues to increase and the full plastic moment is attained (and slightly exceeded) at Load No. 8. As additional rotation is applied to the member it continues to carry the full plastic moment up to Load No. 14. Beyond this stage the load drops off.

Due to the initial lateral deformations present in the member, the compression flange of the beam deflects laterally while the in-plane deformation is applied. These lateral movements are small up to Load No. 8 and are then magnified by the decrease in stiffness of the compression flange as the yielding process takes place. The strains caused by the lateral bending of the flange add to those induced by the in-plane deformations in the area surrounding the mid-span concave portion of the flange. This is shown in Fig. 4.2. Once the flange in this region has become fully yielded local buckling will occur and the beam will unload. This unloading is assumed to mark the end of the useful life of the member segment.[26]

Based on the behavior described above an expression relating the rotation capacity to the unbraced length of the member has been formulated:

$$\frac{KL}{r_y}\ \frac{\sqrt{\epsilon_y}}{\pi} = \frac{1}{\sqrt{1 + 0.7\ \frac{\sigma_y}{E_{st}(\epsilon_{st} - \epsilon_y)}}} \qquad (4.1)$$

In Eq. 4.1 K is the effective length factor for lateral buckling. K is taken as 0.54 for adjacent spans which remain essentially elastic and 0.80 for fully yielded adjacent spans. An adjacent span is considered fully yielded if the moment gradient across the span length is greater than 0.88.[26]

The other term in Eq. 4.1 that requires explanation is the rotation capacity, R, which is defined as

$$R = \frac{\theta}{\theta_p} - 1 \qquad (4.2)$$

In Eq. 4.2, θ is the rotation at the initiation of unloading and θ_p is the rotation at M_p if the beam behaved elastically. The terms are illustrated in Fig. 4.3.

The optimum rotation capacity would be obtained if the average flange strain was increased to ϵ_{st}. For a compact section this would cause local flange buckling due only to the in-plane strains. Because of the lateral bending strains in the member, local buckling will occur before the average applied strains reach ϵ_{st} and it has been shown that the optimum rotation capacity is given by:

$$R_{opT} = 0.8 \frac{(\epsilon_{st} - \epsilon_y)}{\epsilon_y} \qquad (4.3)$$

Substituting this value for R in Eq. 4.1 we obtain for the critical bracing spacing

$$\frac{L}{r_y} = \frac{\pi}{K \sqrt{\epsilon_y} \sqrt{1 + 0.56 \frac{E}{E_{st}}}} \qquad (4.4)$$

It is presently recommended that this spacing be used for all cases where the moment ratio on the span is greater than 0.7.[41] The inelastic end rotation through which the full plastic moment could be sustained would be equal to $4 \phi_p L$ for a material having $\epsilon_{st} = 11 \epsilon_y$. (This is typical for A36 and A441 steels.)[29]

The value of the required rotation capacity for simple structures has been studied by Driscoll and Kerfoot.[67,68,69] These requirements are based on an elastic-plastic analysis and are interesting from several points of view. The continuous beams studied were three span structures and required three hinges to form a mechanism.[67,68] Because of symmetry, two of the three hinges formed simultaneously. For practical span and load ratios the first hinge did not form in a region of uniform moment. In fact, this could only occur for a ratio of side span load to center span load below 0.2 for concentrated loads, or 0.3 for a uniformly distributed load.[67,69] Considering the relative values of dead and live loads it would be unlikely to have the ratio fall in this range of values. It should be noted that if this highly improbable situation did occur the inelastic rotation, θ_H, required to complete the mechanism would be in the order of $0.5\ \phi_p L$.[69] This value is based on the uniform moment span being restrained by two slender, lightly loaded adjacent spans. In general the rotation requirement decreases as the restraint offered to the span under uniform moment increases. Thus the situation studied represents the most critical case. Any change in the structural arrangement could only serve to increase the restraint on the uniform moment portion or to change the moment ratio on the span.

It follows then from the above discussion that

(1) There are no practical cases in which a hinge forming in a region of uniform moment is required to deliver rotation capacity.

(2) Even for "non-practical" cases the rotation requirement is in the order of one-eighth that which is provided for by the proposed bracing spacing requirements.[41]

(2) Item 2 above is based on results obtained for the uniform moment region of a three span continuous beam. Driscoll has investigated single story frames as well and even in this case the maximum required hinge angle is 1.03 $\phi_p L$. This value covers cases of moment gradient as well as uniform moment.

Thus it appears that it would be satisfactory to permit bracing spacing which would allow the beam under moment gradient to reach its full plastic moment value without delivering any appreciable rotation capacity.

However, before this step can be taken, its full implications must be investigated. The more stringent provisions for beams under uniform moment are intended to guard against the possibility of yielding along the entire length due to a moment gradient that is less than but approaches 1.0. Currently, it is recommended that the uniform moment rules apply to those members having a moment gradient ≥ 0.7.[41] It is possible that a span having a moment gradient between 0.7 and 1.0 might be required to deliver a rotation greater than the 0.5 $\phi_p L$ which is regarded as the limit for beams subjected to uniform moment.

Four tests have been performed under high moment ratios ($\rho > 0.7$).[27,70] The pertinent data for these tests are listed in Table 4.1. It is obvious from the results of Table 4.1 that the beams

as tested (with elastic adjacent spans) had more than adequate rotation capacity. For their respective materials, the beams were of near compact proportions.

The results of a series of tests performed on A441 beams subjected to uniform moment are shown in Fig. 4.4. It is presently recommended that such beams be limited to $L/r_y = 28$ yet even at $L/r_y = 40$ a rotation capacity of 2.9 is obtained. This would correspond to a hinge angle of $1.5\ \phi_p L$, which is greater than that required.

Equation 4.1 could be modified to yield the bracing spacing required to sustain a more reasonable amount of rotation capacity. If a rotation capacity of 3.0 was required, unbraced lengths of $59r_y$ and $43r_y$ would result for A36 and A441 members. These values are not confirmed by the results of tests which show that the bracing spacing must be approximately $45r_y$ and $40r_y$ for the two steels to obtain this rotation capacity.[29,71] This discrepancy between experimental results and theory for the slender members has been previously noted.[26] If Eq. 4.1 is adjusted to account for this discrepancy the bracing spacing can be obtained by:

$$\frac{L}{r_y} = \frac{\pi}{K\sqrt{\epsilon_y}\ \sqrt{1 + .4\,\frac{E}{E_{st}}}} \qquad (4.5)$$

The bracing spacings which would result from the use of Eq. 4.5 are listed in Table 4.2 for various cases. This table also lists the values of experimentally determined rotation capacities for all cases where results were available.

Even with the liberalization of the bracing spacing requirement, the delivered rotation capacities are in excess of those theoretically required.[67,68,69]

4.2 BEAMS UNDER MOMENT GRADIENT

In contrast to the vast amount of research performed on beams under uniform moment there has been surprisingly little work done on beams under moment gradient. The useful results primarily consist of one set of experiments on A7 beams and three tests on A441 steel members.[29,70]

The behavior of the beam under moment gradient differs from that of the beam subjected to uniform moment.[25] A typical M-θ curve taken from a test on a simply supported A441 steel member is shown in Fig. 4.5.[29] The response of the member is at first elastic, and when yielding starts the yielded zone is restricted to a relatively small area under the load point. As the member continues to deform the yielded zone spreads along the length of the beam. At the same time, the moment rises above M_p due to the presence of strain-hardening. The process described above continues until the yielded zone reaches a length sufficient to cause local buckling. This is shown as Load No. 19 in Fig. 4.5. The cross section now is no longer symmetrical and larger lateral movements of the compression flange can occur. The applied load drops off gradually.

For the beam under moment gradient the behavior described above is the best that can be expected. For exceptionally long members, lateral buckling could occur without prior local buckling. The specifications for bracing spacing in the case of a beam under moment gradient are formulated to guard against such a possibility.(41)

The optimum situation, as in the case of the beam under uniform moment, would be to space the bracing so that local buckling would occur at the same rotation as would lateral buckling of the unbraced span. This approach has been used to formulate the equation for bracing spacing which follows.(72)

$$\frac{L}{r_y} = \frac{0.7\,\pi}{\sqrt{\epsilon_y}} \qquad (4.6)$$

Equation 4.6 results in a critical bracing spacing of $65r_y$ for A36 members and $55r_y$ for A441 members. It should be noted that neither moment gradient nor effective length appear in Eq. 4.6. The neglect of these factors is conservative. In order to guard against the possibility of the member yielding along its entire length and behaving as a beam under uniform moment, the use of Eq. 4.6 is restricted to those beams having a moment ratio less than 0.7.(41)

For beams under moment gradient, the bracing spacings given by Eq. 4.6 require that the member deliver the optimum rotation capacity. No attempt has been made to match the required rotations with those delivered.

Any liberalization of the bracing spacing requirements must

wait until:

(1) Additional computations are available to determine the hinge rotations required for beams under various moment gradients.

(2) Tests are performed on slender beams under various moment gradients and restraint conditions to define experimentally the rotation at which local and lateral buckling occur simultaneously.

(3) The response of the member once unloading begins can be predicted analytically.

Until the above points have been resolved, the bracing spacing required by Eq. 4.6 will ensure that local buckling will terminate the rotation capacity. This is the best that can be expected and thus Eq. 4.6 is recommended for use.

4.3 IN-PLANE BEHAVIOR OF BEAM-COLUMNS

The determination of the in-plane response of beam-columns has been a prime objective of researchers in the field of plastic design during the past twenty years.[52] The moment-curvature-thrust (M-Ø-P) relationships for wide-flange sections are difficult to express in closed form, particularly if the influence of residual stress is included.[33] By the use of numerical integration it is presently possible to predict the ultimate load of a beam-column.[64] The procedure uses available M-Ø-P relationships which account for the residual

stress distribution and the gradual yielding of the cross section.[73]

The design procedure for beam-columns assumes that the member is subjected to either equal end moments, equal and opposite end moments, or one end moment only.[58] Curves have been fitted to the results of the ultimate strength computations described above for these three cases. For a given axial load and slenderness ratio the ultimate strength of the member may be computed.[64]

A more general graphical procedure is also available for determining the complete response of the member.[74] Charts based on these concepts are available for design use.[75] The design charts are based on the assumption of an elastic-perfectly plastic material having characteristics typical of A36 steel. The strain-hardening range is ignored, the yield stress taken as 36 ksi and the value of the maximum compressive residual stress, which occurs at the flange tips, set at $0.3\ \sigma_y$.

The design charts are entered for given values of P/P_y and L/r_x. The response of the member, as characterized by its complete end-moment versus end-rotation (M-θ) relationship, may be read off the appropriate chart. It has been shown that to use the charts for materials having a yield stress level, σ_y, other than 36 ksi, the design charts must be entered with the actual value of P/P_y on the member but with an equivalent length $(L/r_x)_{eq.}$, given by:[65]

$$\left(\frac{L}{r_x}\right)_{eq.} = \frac{L}{r_x}\sqrt{\frac{\sigma_y}{36}} \qquad (4.7)$$

For the equivalent length as computed by Eq. 4.7 the end moments, in terms of M/M_{pc}, which correspond to various end rotations of the equivalent column, θ_{eq}, may be picked off the charts. The end-moments may be used directly, however, the rotations of the actual column are given by:

$$\theta = \theta_{eq} \sqrt{\frac{\sigma_y}{36}} \tag{4.8}$$

Beam-columns of A441 steel have been tested and the response obtained for one such test (HT-39) is plotted in Fig. 4.6.[76] The curve labelled theory in Fig. 4.6 is that obtained from the extrapolation procedure for A36 members. It can be seen that the correlation between theory and experiment is satisfactory. The larger differences in the unloading portion of the curves is due primarily to the neglect of unloading in the theoretical prediction. This will be discussed in a later section.

The extrapolation procedure results in an exact solution (within the limits of the assumptions) provided that the maximum residual stress values, σ_{rc}/σ_y, are the same for both materials. It appears, however, that the residual stress level is independent of the yield stress for the structural steels.[29] On this basis the response predicted by the extrapolation procedure for higher strength steels is conservative.

Figure 4.7 shows the response of an A441 beam-column. The solid curve represents the response predicted by a direct numerical integration procedure.[8] This procedure is able to account for the

reduced level of residual stress in the column, 0.17 σ_y. The column is subjected to an axial load of 0.6 P_y and equal end moments which deform the member in a symmetrical, single curvature mode. The yield stress of the material is 50 ksi and the length is $40r_x$.

The dashed line in Fig. 4.7 represents the response predicted by the extrapolation procedure. This procedure also utilizes the properties listed above but assumes the residual stress level to be 0.3 σ_y, as would be the case for A36 steel. The larger residual stress level implies a larger curvature at any given end moment value. The integrated effect of the increase in curvature is to produce a larger end rotation for the given moment, once yielding is initiated in the member. This causes the extrapolated curve to spread relative to the true response, in the inelastic range.

These greater deformations are in turn acted upon by the axial load on the member to produce additional moments. This influence serves to reduce the maximum applied end moment which the member can support. The difference between the maximum moment predicted by direct integration and that predicted by the extrapolation procedure is approximately 8%. The extrapolation procedure results in a conservative estimate of the maximum end moment that can be supported by the member and a fairly good approximation to the response curve. It seems reasonable to apply this procedure for yield stress levels up to 50 ksi rather than producing separate sets of charts.

It should be noted that the procedures for computing the response of the member neglect the influence of the unloading of portions

of the member due to the unloading of the applied moment. It has been shown that the neglect of this influence is conservative but not unduly so.[65] However, if for a member, $P/P_y \geq 1 - \sigma_{rc}/\sigma_y$, parts of the cross section will yield under the initial application of the axial load and will then unload as the bending moment is applied. This has been accounted for by modifying the M-Ø-P relationship. The design charts for $P/P_y > 0.7$ have included this effect.[75]

It should be emphasized that the response of the beam-column under high axial loads ($P/P_y \geq 1 - \sigma_{rc}/\sigma_y$) may be completely different from that under the moderate axial loads which have been considered typical.[16] For the higher axial loads and the lower slenderness ratios which are naturally associated with them, the influence of strain-hardening should play an important part in the response. In addition, the role of unloading, both in the M-Ø-P relationship and in the beam-column action must be accounted for to obtain a rational prediction of the behavior. It is in this range of low slenderness and high axial load ratios that previous investigators have stopped; believing that to go further would be impractical. As a final point it should be emphasized that test results on these members are virtually non-existant.[16]

Although the influences discussed above are significant, the neglect of these effects is conservative in all cases. Thus it is recommended that the procedures used for beam-columns under moderate axial loads also be used for those under the higher axial loads.

4.4 LIMITATIONS ON THE IN-PLANE BEHAVIOR OF BEAM-COLUMNS

In the previous section the in-plane behavior of beam-columns was discussed. Since design rules are formulated on the premise that this behavior will indeed occur, special precautions must be taken to preclude premature local or lateral-torsional buckling.

In a plastically designed structure, the beam-column must not only attain the maximum moment predicted on an in-plane basis, but on further deformation must continue to follow the in-plane response. For an optimum condition, the member would deform along the in-plane path until a sufficient length had yielded for a local buckle to form.

Solutions have been developed which will predict the end moment at which lateral torsional buckling will occur.[77,78] This critical end moment is sensitive to variations in the cross-sectional properties and as yet the solutions are not in a form suitable for design use.[79]

However, it would be logical in a plastically designed structure to brace the beam-column to deliver its optimum rotation capacity. If this procedure were followed the attainment of the maximum end-moment would be automatically ensured. The solution to this problem (that of the determination of the rotation capacity of beam-columns) is possible but due to the tedious nature of the computations involved, no solutions have been attempted.

It is presently proposed that the rules used for spacing the bracing of beams be applied to beam-columns. This results in an

acceptable design rule although it will be conservative since the extent of yielding in a beam-column will be less than that in a properly braced beam. Since there is a possibility that the beam-column will yield under the application of axial load, it is recommended that the rules for a beam under uniform moment be applied if

$$\frac{P}{P_y} \geqslant \frac{1 - \frac{h}{r_x}\frac{\sqrt{\epsilon_y}}{\pi}}{1 + \frac{h}{r_x}\frac{\sqrt{\epsilon_y}}{\pi}} \qquad (4.9)$$

even though the beam-column may be subjected to a moment gradient.[72]

The influence of lateral torsional buckling on the response of a beam-column is shown in Fig. 4.8.[76] The member is very similar to that shown in Fig. 4.6. The only difference between the two is that the member shown in Fig. 4.8 is unbraced. The experimental response follows that predicted by an in-plane theory up to the critical end moment. At this point large lateral-torsional deformations were observed and the applied end moment drops off rapidly. The member is obviously not suitable for a plastically designed structure.

Provided that the column is properly braced, it is expected that the in-plane response will be maintained up to the point of local buckling. For a beam, local buckling is assumed to occur as soon as the strain over a sufficient area of the member has attained the strain-hardening strain.[25,26] This approach will also be valid for beam-columns. An attempt has been made to compute the termination point of the in-plane response by searching for the end rotation at which a strain

equal to that at the onset of strain-hardening will be attained over the optimum local buckling length.[80] Since the response of the beam-column is based on an elastic-perfectly plastic material the method can give, at best, only a rough approximation to the local strain condition in the areas which are prone to local buckling. Experiments on beam-columns have not confirmed the predicted results.[76] As an example on A441 column having $P/P_y = 0.6$ and $L/r_x = 40$ will be considered. The member is a 6WF25 section and was tested recently as part of a sub-assemblage. The results will be discussed in detail in the following chapter.

The experimental M-θ curve is given in Fig. 4.9. In this figure the dashed lines represent the theoretical prediction based on an elastic-plastic stress-strain diagram. The actual stress-strain curve for the column cross section would include the influence of strain-hardening. The moment-curvature-thrust relationship, allowing for the residual stress distribution, and corresponding to the actual stress-strain diagram has been computed. This has been obtained by subdividing the cross section into elements and numerically integrating the forces acting on those elements to give the thrust and moment corresponding to a given curvature. The inclusion of the influence of strain-hardening was accomplished by fitting the parabolic curve used in Chapter 2, to that portion of the σ - ϵ curve.

The consideration of strain-hardening does not influence the in-plane behavior of the column in the early stages of loading. The curve of end moment versus end rotation (M-θ) is shown in Fig. 4.9. The strains in the material do not enter the strain-hardening range

until the end rotation has reached a value of approximately 0.024 radians. For rotations greater than this, strain-hardening increases the strength of the member above that predicted by using the elastic-plastic assumption.

The use of an M-Ø-P relationship which includes the influence of strain-hardening enables a rational prediction of the onset of flange buckling to be made. According to the response predicted for an elastic-perfectly plastic material, at a rotation of 0.035 radians a strain equal to that at which strain-hardening occurs, ϵ_{st}, would have progressed to a point approximately 8 inches on either side of the mid-height of the column.[80] Since the flange b/t ratio of the column is 14.0 this should have caused flange local buckling. Detailed measurements of the flange movements during the test showed a negligible amount of movement and Fig. 4.10, which shows the column after test, shows no evidence of local buckling.

By considering the actual properties of the material, including the strain-hardening range, the answer to these discrepancies may be ascertained. This shows that at a rotation of 0.035 radians an area approximately 6 inches in length had been fully strain-hardened, less than half that required to produce a local buckle.

Thus at present no suitable method exists to determine the termination point for in-plane behavior. The analytical tools are available for such an investigation as illustrated above. However, with the use of compact sections and bracing rules as specified for beams, the optimum capacity will be supplied. Since information to the contrary is lacking, this optimum capacity is assumed to be adequate.

4.5 AXIALLY LOADED COLUMNS

The problem of compression members subjected to axial load has been a major topic of investigation.[81] Recent studies have concentrated on determining the influence of the residual stress distribution on the column strength.[32]

At the present time column strength is specified as that given by the Euler formula for elastic buckling:

$$\frac{P_{cr}}{P_y} = \frac{\pi^2}{\left(\frac{KL}{r}\right)^2} \frac{E}{\sigma_y} \qquad (4.10)$$

Equation 4.10 should apply up to $P_{cr}/P_y = 1.0$. However, residual stresses acting on the cross section, cause yielding to occur below this load, thus reducing the stiffness of the member.

The Column Research Council has proposed an equation which is based on a rational consideration of the residual stress effect for both strong and weak axis buckling.[52] From this point of view it is a compromise but it has been checked against the results of experiments on rolled shapes and has proven satisfactory. The equation is given in a modified form by:

$$\frac{P_{cr}}{P_y} = 1 - \frac{\sigma_y}{E} \frac{1}{4\pi^2} \left(\frac{KL}{r}\right)^2 \qquad (4.11)$$

In Eqs. 4.10 and 4.11, K is the effective length factor which is dependent on the boundary conditions at the ends of the member.

The column strength is defined over the complete range of slenderness ratios as the lower of the values given by Eqs. 4.10 and 4.11.

4.6 CONNECTIONS

A complete specification must provide safe guides for the design of connections as the elements which link together one or more members. In a rigidly jointed frame the connections must ensure that the rotations of all members meeting at the joint are compatible throughout the complete range of deformation required. The connection must have sufficient strength and rigidity to resist the applied forces without contributing excessively to the deformation of the structure.

The following discussion is restricted to square corner and beam-to-column connections. In this type of connection the basic requirements for proportioning the connection are based on principles of equilibrium.(82) However, the requirements dealing with web crippling and tensile distortion of the flanges are basically empirical.(83)

Since the tests used as the basis for these provisions were performed on low carbon steel connections there is little basis for extending the results to the low alloy steels.

An extensive program of investigation into the behavior of low carbon and low alloy steel connections has been proposed at Lehigh University. The completion of specifications for plastic design in high strength steels will have to wait for the results of this investigation.

4.7 OTHER CONSIDERATIONS

Another outstanding problem is the influence of shear on the behavior of members.[1] An investigation has also been proposed in this area. It is hoped that this will account for the influence of strain-hardening on the behavior as the two influences act together.

4.8 SUMMARY

The bases for the specifications relating to the design of beams under uniform moment and moment gradient have been described. These are in a form suitable for design use.

The in-plane behavior of beam-columns has been presented. Tools are available for the design of these members and together with the design rules formulated for beams will assure in-plane behavior of these members. More work remains to be done in connection with the termination of in-plane behavior due to local or lateral torsional buckling. The load-deformation behavior of the beam-column under biaxial bending situations has not been satisfactorily described.

The specifications relating to axially loaded columns are in a form suitable for design use. The main barrier to formulating complete specifications for low alloy steels is the lack of experimental knowledge on the behavior of connections.

5. BEHAVIOR OF STRUCTURAL SUBASSEMBLAGES

In the preceeding chapters the characteristics of the low alloy steels have been discussed. It has been shown that the plastic design of low alloy steel members presents no unusual difficulties provided that proper allowance is made for the increased strength and decreased strain-hardening modulus of the material. Before the low alloy steels can be used with confidence, however, it must be shown that structures fabricated of these steels behave in a satisfactory manner. It is the purpose of this chapter to present such evidence and to discuss the factors involved in the behavior of these structures. It will be shown that the behavior of structures fabricated from the low alloy steels may be predicted by the methods which have been used successfully for low carbon steel structures.

5.1 STRUCTURAL ACTION

Structural frames can be divided into two groups. The braced frames are those in which the relative lateral translation of any two vertically adjacent beam-to-column joints is negligible. The unbraced frame is characterized by the additional complexities introduced by consideration of the relative joint translation. Instead of dealing with the structure as a whole, it is convenient to subdivide the structure into units, or subassemblages, which are analytically simple, yet retain at least some of the characteristics inherent in the complete structure.[86]

Methods for the design of braced frames using the subassemblage concept have been presented and tests have been performed on subassemblages of low carbon steel.[87,88] A test has recently been performed on a subassemblage consisting of a low-alloy beam-column restrained by low carbon steel beams. This test will be discussed in the following section.

Design methods based on the subassemblage concept have been proposed for unbraced frames but only one frame which might be considered a subassemblage has been tested.[40,89] This test was performed on a single-story, single-bay, hybrid frame. The beam was of low carbon steel while the columns were of low alloy steel. The behavior of this frame will also be discussed.

5.2 BEHAVIOR OF A BRACED HYBRID SUBASSEMBLAGE

For testing simplicity the subassemblage is modified. The restraining beams are not loaded and the restraints provided by the columns above and below the column of interest are eliminated.[90]

5.2.1 Test Subassemblage

The hybrid subassemblage is shown in Fig. 5.1. In this figure R represents the reactions at the pinned ends of the restraining beams. The column height, measured between the centers of the restraining beams is denoted by, h, and the span of the beams L. The force, F, is applied through a stub beam of length, e.

The beams were butt welded to the column flanges, forming rigid joints. A diagonal stiffener was used to reinforce the connection as shown in Fig. 5.1. The connection was designed to transfer the moment, shear and axial thrust and to take into account the difference in strength between the beam and the column.[82] The moment was applied through a stub beam which was also framed rigidly into the column. This stub was not a part of the test specimen and remained elastic throughout the test.

The restraining beams were 12B16.5 sections of A36 steel and had been cold straightened by rotarizing. The physical properties of the beam sections as determined by measurement are shown in Table 5.1. In Table 5.1, d, b, t, w are dimensions of the cross section as shown in the inset and L/d is the span to depth ratio. The value of the full plastic moment, M_p, was computed from the results of tension tests on specimens taken from the unused portions of the member.

The material properties obtained from these tension tests are summarized in Table 5.2. This table shows the location of the specimen in the cross section and gives values for the static yield stress, σ_y, the yield strain, $\epsilon_y = \sigma_y/E$ and the ultimate stress, σ_{ult}. The value of E has been taken as 29,500 ksi.[36] Table 5.2 also gives the strain at the onset of strain-hardening, ϵ_{st}, the strain-hardening modulus, E_{st}, and the percent elongation at fracture. The measured residual strain distribution is shown in the inset to Table 5.2.

The cold straightening process has a decided effect on the material properties as discussed in Chapter 2. This is evidenced

first of all by the residual stress distribution which is typical of that obtained by adding the residual strains due to the rolling process to those caused by cold bending the section about its weak axis. More important, however, is the effect on material properties. The tests performed on specimens cut from the flanges exhibited an almost bilinear behavior with a very low strain-hardening modulus. The results on the web specimens are typical of those on virgin structural steel.

The beam-column was a 6WF25 section of A441 steel. The physical properties of the member are given in Table 5.1. In this table, L/r_x is the strong axis slenderness ratio of the column and M_{pc} is the plastic moment value reduced to account for the axial load on the member. The material properties and residual strain distribution are given in Table 5.2. This section was straightened by gagging and the material properties are more typical of those expected for this type of material.[29]

5.2.2 Test Procedure

The procedure for testing restrained columns has been presented previously.[90] Only enough of the method will be given for completeness.

A photograph of the subassemblage in the testing machine is shown in Fig. 5.2. The axial load is applied to the beam-column through the upper head of the testing machine. In this test the axial load in the column was held constant at 0.6 P_y, where P_y is the yield

load of the column. ($P_y = A\sigma_y$) The column is supported at the third points by two sets of articulated braces which allow in-plane movement but prevent lateral movement.

The horizontal restraining beams are rigidly connected to the ends of the column and the reactions at the unconnected ends of the beams are resisted by pins fitting into holes in the braced tower which can be seen in Fig. 5.2. The beams are braced laterally at the third points by knife edge arrangements.

From Fig. 5.1 it can be seen that the axial force in the column is made up of the direct force applied by the testing machine, P, the jack force, F, and the beam reaction, R. To simulate the situation existing in the lower stories of a multi-story frame the test was performed with the axial load held constant. Thus at each increment of load or deformation the direct force, P, was adjusted so that the total axial force in the column remained at $0.6\ P_y$.

Once the axial load has been applied, the beam-to-column joints are rotated by applying the jack force to the stub beams. The column is forced into a symmetrical, single curvature mode of deformation. In the early stages of loading this joint rotation is accompanied by an increase in applied moment; after unloading of the subassemblage begins an increase in joint rotation is accompanied by a decrease in the applied moment. In the test, the subassemblage was deformed well into the unloading range.

At each increment of rotation the direct axial load was recorded from the console of the hydraulic testing machine. The jack

load was computed from the oil pressure readings in the line and checked by strain measurements on the dynamometer. The dynamometer can be seen in Fig. 5.2 and is connected in series with the jack. The applied end moment is then the product of the jack load and the stub beam length (shown as 30 inches in Fig. 5.1). Strain readings were recorded during the test at the beam third points. These strains were in the elastic range throughout the test and could be used to compute the reactions at the pinned end of the beams and the portion of the applied moment which was resisted by the restraining beams.

At each increment of load or joint rotation the joint rotations were measured by level bars. In addition the overall contraction of the column was measured as well as the mid-span deflection of the restraining beams. The column was instrumented with SR-4 Type A strain gages at points adjacent to the beam-to-column connections. These locations remained elastic during the test and the strain readings in addition to the knowledge of axial load and joint rotation could be used to compute the portion of the applied moment which was resisted by the column. The mid-height column deflection in the plane of the applied moments was measured as well as the out-of-plane deflections at this point. To check for the occurrence of local buckling in the column, the flange deformations were observed at three locations in the mid-height vicinity.

Since the subassemblage is a rigid frame it may suffer initial moments due to the erection procedure.[90] In particular, the pinned ends of the restraining beam may not be the required distance apart. Forcing the frame into the testing apparatus may induce moments in the

subassemblage which are significant. The erection stresses were computed from strain measurements and found to be negligible (less than 1 percent of the capacity of the members).

The moments developed during the initial application of the axial load were also computed and found to be negligible (for example less than 2 percent of the column capacity).

5.2.3 Test Results

The test can best be described with reference to the moment rotation curve of Fig. 5.3. In Fig. 5.3 and other curves which present the results of this test the numbers adjacent to the curve represent stages at which data was taken during the test. Load numbers 1 through 7 refer to the stages used to apply the initial axial load. The dashed curve represents the predicted response.[75] The moments plotted as the open points represent the total applied moment as determined from the jack load. Compatibility at the joints ensures that the end rotation of the restraining beam is equal to that of the column. The applied moment is resisted partly by the column and partly by the beam. Equilibrium requires that the applied moment be equal to the sum of the end resisting moments developed in the beam and column. Thus at any value of the joint rotation θ, the applied moment is equal to the sum of the column resisting moment plus the beam resisting moment at that same value of rotation θ. The moments plotted as the closed points in Fig. 5.3 represent the total resisting moment of the subassemblage as computed from the measured strains in the beams and

column. The applied and resisting moments balance within 4 percent. The rotations plotted are the average of those measured at the top and bottom joints; the resisting moments are also averaged values. The agreement between the two is remarkably good. The solid line representing the experimental response is drawn as an average of the two.

In Fig. 5.4 the experimental M-θ curve for the beam is given by the solid lines joining the test points while the prediction as obtained from an elastic-plastic analysis is given by the dashed lines. For load numbers 23 to 26 the influence of strain-hardening increases the beam strength above that predicted on the basis of an elastic-perfectly plastic stress-strain relationship. Local buckling of the compression flange of the beams was observed visually and occurred between load numbers 22 and 23. The beams exhibited more than adequate post local buckling strength as the resisting moment increased beyond this point.

The moment plotted in Fig. 5.4 is the end moment at the intersection of the beam and column centerlines. The connection at this point has sufficient strength to force the beam to hinge at a point away from the connection, in this case 9 inches from the face of the column. Previous studies have shown that the connection constrains the adjacent regions of the framing members so that they behave elastically at stresses above the nominal yield point.[16,40,88] In previous tests on subassemblages of A36 steel the beam hinges formed at locations d removed from the face of the column (d is the depth of the beam). Thus the positions of the beam hinges were partially anticipated.

In the elastic-plastic prediction shown by the dashed line in Fig. 5.4 this shift of hinge (12 inches from center of joint) has been

accounted for. After the hinge forms the member is assumed to rotate with no increase in moment. Actually the strain-hardening characteristics of the beam force the moment at the center of the joint to increase as the yielded length spreads along the beam. The average material properties for the flange as given in Table 2 are $\epsilon_{st} = 13\ \epsilon_y$, $E_{st} = E/83$. If the section is assumed to have a shape factor of unity the end moment and the end rotation can be computed from the resulting bending moment and curvature distributions including the influence of strain-hardening.[25] The resulting curve is plotted in Fig. 5.4 as the broken line.

The unloading of a beam under moment gradient is precipitated by local buckling. For a compact section local buckling will occur when a sufficient length has yielded to allow the plate to buckle locally at the minimum stress. This optimum length is 9.6 in. and thus local buckling should occur at a rotation of 0.024 radians, as shown by the dashed arrow in Fig. 5.4. This assumes that the section meets the definition of a compact section as used by Lay.[25]

Since the beam section has been straightened by rotarizing, the material properties have been altered. A method of accounting for this is to use an effective modulus for the flange to account for the reduction in stiffness. It has been shown that the modulus may be reduced by approximately one-third for a typical straightening process. The current limitations for plastically designed structures limit the b/t value to 17 on the basis of $E_{st} = 900$ ksi. Assuming a reduced value of $E_{st} = 600$ ksi, the compact section limit would be 13.9. The section used had a b/t = 14.4 which is very close to the limit. Local

buckling was observed at a rotation of approximately 0.020 radians as shown by the full arrow in Fig. 5.4.

Local buckling is assumed to limit the rotation capacity of the member. However, it can be seen from the plot in Fig. 5.4 that the strength of the member continues to rise even after local buckling. The beam was braced at the third points so that the slenderness ratio, L/r_y, between braces was approximately 19. According to Lay, this bracing spacing is sufficiently close to delay the onset of lateral buckling until further deformation has occurred.[25] Thus even though the section is weakened by local buckling, it can still accept an increased load. At the end of the test the yielded length was almost double that at the onset of local buckling, yet the beam showed no signs of unloading.

It appears that beams which are continuously braced along the length of the compression flange will have a larger rotation capacity than those which are not. Research is needed to determine the behavior of closely braced beams under moment gradient before this factor can be taken into account for design purposes.

The M-θ curve for the column is shown in Fig. 5.5. In this figure the dashed line showing the predicted response has been obtained by direct numerical integration rather than by the extrapolation procedure outlined in Chapter 4.[8] In this manner the measured cross section dimensions, residual stress distribution, and yield strength presented in Table 5.2, were accounted for. The numerical procedure uses as input the elastic-plastic moment-curvature-thrust

relationship. This neglects the influences of strain-hardening and unloading and accounts for the somewhat conservative prediction of the strength in the unloading range. In general, the theory adequately predicts the response. The beam-column of the subassemblage is the one used as an example in Chapter 4, thus the remarks concerning local buckling and strain-hardening also apply to the behavior of the member as part of a subassemblage.

The subassemblage connection after testing is shown in Fig. 5.6. The local buckle in the compression flange of the beam can be seen in this figure, and also the rather large extent of the yielded section of the restraining beam. Note that there is no evidence of yielding in the connection itself.

During the test the out-of-plane deformations of the column were negligible. Near the central portion of the column the tension flange was entirely elastic while the compression flange and the major portion of the web exhibited considerable yielding. At the end of the test there were no visual signs of local buckling in this area. These observations are born out by the measurements of the local flange movements which show little change throughout the test. This behavior is to be expected from a consideration of the influence of strain-hardening on the response as shown in Chapter 4.

5.2.4 Summary of Test

Figure 5.3 compares the experimental results obtained from the test with those predicted by the theory. The experimental curves are shown by the full lines, the theoretical curves by the dashed lines.

The response for the beam has been idealized as elastic-strain-hardening, using the measured material properties. The influence of the shift in location of the hinge has been accounted for.

The response of the beam-column has been computed from the elastic-plastic M-Ø-P relationship using a direct integration procedure. The influence of the measured residual strains was included, however, the effects of strain-hardening and unloading were not included.

It is concluded from this test that the behavior of a properly designed subassemblage which contains low alloy steel members may be predicted by methods which have been previously tested on subassemblages of low carbon steels. The beam-column in the subassemblages considered exhibited the expected strength and deformation capacities.

5.2.5 Previous Subassemblage Tests

Table 5.3 summarizes previous tests performed on subassemblages of A36 material. In these tests the purpose was to investigate restrained columns having relatively high slenderness ratios and low axial load ratios. This was due to the then current interest in the plastic design of low rigid frames.[1] In Table 5.3, G is the relative beam-to-column stiffness ($G = I_b h/I_c L$ while θ represents the end rotation at which the various events occur. Of the tests performed, only RC-6 with a slenderness ratio of 29.9 and an axial load ratio of 0.84 could be called representative of the situation which exists in a multi-story frame. The axial load ratios range from 0.40 to 0.60 with

the above noted exception of RC-6.

There exists a need for tests at slenderness ratios of 20, 25, 30, 35, and 40 with axial load ratios of from 0.75 to 0.95. It is in this range that considerable elastic unloading of previously yielded regions would occur on the application of the bending moment. This has only recently been taken into account theoretically and experimental verification is necessary.(75) In addition, slenderness ratios of 20 to 40 lie within the range in which the strain-hardening characteristics of the beam-column material would play a more significant role. As these properties are not normally considered, it would be valuable to examine this range experimentally.

In the design methods presently proposed it is required that the beam reach its full plastic moment and rotate at or above this value while the column continues to accept additional moment.(87) Tests SC-8 and RC-10 are the only ones in which this condition is fulfilled. Future tests should take into consideration practical G values for subassemblages to attempt to cover the case in which the beam hinges before the column attains its peak moment.

In summary, although the present theory adequately predicts the behavior of subassemblages of A36 steel and hybrid subassemblages, the tests performed cover only those axial load values, restraint conditions and slenderness ratios that are typical of low building frames. Although the present theory results in a conservative prediction, more tests are needed to cover those cases of more practical interest for braced multi-story frames.

5.3 BEHAVIOR OF AN UNBRACED HYBRID SUBASSEMBLAGE

Recently a design method for unbraced frames has been developed which is also based on the subassemblage concept.[89] The design subassemblage is shown in Fig. 5.7 and is obtained by passing two horizontal cuts through the building at the mid-height of two adjacent columns. The subassemblage then consists of the girder plus the half-lengths of the columns framing into it, as shown in Fig. 5.7. Since the cuts are assumed to pass through points of inflection, the axial loads and shears shown are the only forces acting on the subassemblage. In the design process the design subassemblage is broken into windward, interior and leeward sway subassemblages as shown in Fig. 5.8(a), (b), (c), and (d), each sway subassemblage consisting of a half-length of the column, restrained by one or more girders and subjected to the moments, shears and axial forces shown. The response of each subassemblage may be determined and the total response of the story determined by summing the individual responses.[86,89]

Possibly because of its recent emergence as a design possibility, no tests have been performed on such structural steel sway subassemblages. In fact, no full size tests have been performed on frames under any appreciable axial load until very recently.[40,91]

The hybrid portal frame test reported in Ref. 40 could be classified as a subassemblage. The test will be discussed in detail in a separate report. Only a brief description of the procedure will be given herein, along with additional background information.

The frame is shown in Fig. 5.9. The columns were 5WF18.5 sections of A441 steel, rigidly connected to a 10I25.4 beam of A36 material. The behavior of the hybrid frame will be compared with a theory which has been used to predict the behavior of low carbon steel structures. The pertinent dimensions of the frame are shown in Fig. 5.9. The bases of the columns were essentially fixed.

The frame was subjected to vertical loads, W, of 20 kips, applied approximately at the quarter points of the beam, and column top loads of 60 kips. The vertical loads were applied at the start of the test and were held constant during the test. The axial load in each column was initially 0.26 P_y. This simulates the loading in a story of a large frame subjected to vertical loads due to the dead and live load on the frame and then to the action of wind. The vertical loads were applied through gravity load simulators, which offered no restraint to the sway of the frame. The vertical loading system may be seen in Fig. 5.10. The test frame is marked A, the simulator B. The simulators deliver the load through tension jacks, C, attached to spreader beams, G. The reactions from the simulators are taken by the base beams, F, which are bolted to the structural floor.

The center spreader beam, G, is attached by short lugs to the test frame, A, and delivers the quarter point loads. The outside spreader beams, G, are attached to the vertical lugs, D, which run to arms rigidly connected to a horizontal loading beam, E. This loading beam reacts through pedestals over each column top and thus delivers the vertical column top loads.

The test was performed by deforming the frame in a sidesway mode by the application of a horizontal force, H, at the mid-depth of the beam as shown in Fig. 5.9. The response of the frame as characterized by the relationship between the horizontal force, H, and the sway deformation, Δ, is of interest. During this response the vertical loads are held constant.

The response of the frame has been predicted by a second order elastic-plastic analysis.[90] The analysis is simply an elastic analysis, which considers the secondary moments due to the axial loads, and is performed between points of hinge formation. The load-deformation response is shown in Fig. 5.11. This analysis predicts a peak horizontal load of 16.9 kips at a deflection of 2.8 inches. At this point, plastic hinges have formed at the top and bottom of the leeward column, at the base of the windward column and under the windward beam load. The prediction makes allowances for the imperfect fixity of the base plates as well as the strengthening influence of the connections.[40]

After the four hinges have formed, the elastic-plastic analysis would predict that the frame behaves as a mechanism as shown by the rigid plastic line shown in Fig. 5.11.

It has been observed in previous tests of simple frames that strain-hardening will effectively increase the strength of the frame above that expected on an elastic-plastic basis.[4,92,93] Other authors have attempted to account for this influence but their efforts have been directed towards finding the increase in the load required to form a mechanism usually by an analysis which considers compatibility in the frame.[4,94] Thus the method is tedious.

In the subassemblage concept of design for unbraced frames the post-mechanism response is important as this region for one subassemblage may coincide with a loading region of an adjacent subassemblage and thus contribute to the maximum story strength.[89] For this reason, the inclusion of the influence of strain-hardening on the response of the subassemblage should be investigated.

The influence of strain-hardening will be illustrated with reference to the simple cantilever beam of Fig. 5.12(a). Under a load, P, the bending moment distribution is shown in Fig. 5.12(b) and the corresponding curvature distribution in Fig. 5.12(c). The load P is greater than that producing M_p at the support. At this load, the cantilever does not deform indefinitely, as predicted by the elastic-plastic theory, but continues to deform at an ever-increasing load, due to the spread of the fully-yielded zone along the member. This process continues until the yielded length is sufficient to cause local flange buckling.

The hinge angle corresponding to any yielded length, τL, is approximately equal to the area under the curvature diagram over the yielded length, τL, minus the elastic rotation over this length. This is shown as the shaded area in Fig. 5.12(c). As discussed in Chapter 3, the hinge angle can be approximated with a fair degree of accuracy (for the structural steels) by the shaded rectangle shown in Fig. 5.12(d). Thus for any assumed yielded length, τL, the inelastic joint rotation, θ_H, is given by:

$$\theta_H = \phi_{st} \tau L \qquad (5.1)$$

the moment at the support is, $M_p L/(L-\tau L)$ and the load, P, is given by:

$$P = \frac{M_p}{L - \tau L} \tag{5.2}$$

Thus the load deformation response of the cantilever may be constructed.

In a statically indeterminate structure the response is not as easily obtained. However, in Chapter 2, the propped cantilever shown in Fig. 2.9 has been analyzed and will be used for the purposes of discussion. The relationship between the load and the bending moments at the support and under the load point are shown in Fig. 5.13. At $P = 0.89\ P_p$, the moment at the fixed support is equal to M_p. At $P = 1.01\ P_p$ the moment at the load point reaches M_p. Thus the increase in the load causing a mechanism to form is approximately 1 percent due to strain-hardening. In most portal frames this small increase would seem to be expected, although in special types of structures a larger increase is possible.[49]

The reason for the very small increase in the mechanism load can be seen in Fig. 5.13. For $0.89\ P_p \leqslant P \leqslant 1.01\ P_p$ the moment at the support is increased above that predicted by the elastic-plastic theory due to the presence of strain-hardening. On the other hand, due to the redistribution of stiffness in the structure, the moment at the load point drops below that predicted by the elastic-plastic theory. In Fig. 5.13 the dashed lines represent the response predicted by the elastic-plastic theory.

Since the applied load is determined from the equation of equilibrium involving the two moments, the overall response of the structure does not differ appreciably from that predicted by the elastic-plastic analysis, up to the point of mechanism formation. The load-deflection relationship is shown in Fig. 5.14. Up to the point of mechanism formation the difference between the elastic-plastic curve and that predicted by a more exact analysis is negligible. Thus it appears to be reasonable to neglect the increase in load caused by strain-hardening before the mechanism and use the state of the frame at the formation of the mechanism for the starting point of the strain-hardening analysis.

For the hybrid frame considered, the loading scheme and failure mechanism are shown in Fig. 5.15. According to the rigid plastic assumption, the rotations at each of the hinges are shown in Fig. 5.15 for an assumed post-mechanism sway angle, ρ. Thus for a given increment in sway angle, $d\rho$, the inelastic hinge angles required to maintain the mechanism motion may be computed.

For a given increment in hinge angle the yielded length at the hinge may be computed using Eq. 5.1 and the increased moment at each hinge is then computed from the geometry of the bending moment diagram as shown in Fig. 5.12(b). In this case the length of the equivalent simple cantilever will be the distance from the hinge to the point of zero bending moment.[4] The applied force is then computed from the equations of equilibrium for the deformed shape of the frame.

The response predicted by this process is shown as the dashed line in Fig. 5.11. The difference between the response including

strain-hardening and the rigid plastic response is significant.

The experimental response of the frame is compared with that predicted by including the influence of strain-hardening in Fig. 5.16. The agreement is excellent. The validity of the assumptions made in the analysis is illustrated with reference to the plot of Fig. 5.17. This figure shows the variation in the moment at point C, in the column, as the applied horizontal load, H, varies. The agreement between measured and predicted responses is excellent. It should be noted that the agreement at other hinge locations was not always this good but that the maximum moment, and the shape of the response curve agreed remarkably well with those predicted.(40)

It is concluded from this test that the behavior of sway subassemblages of low alloy or low carbon steel can be predicted with confidence provided the pertinent factors involved are considered. It is noted that those factors would be important in subassemblages of low carbon or low alloy structural steels. In particular the plastic hinges form in the low alloy columns were forced to undergo large inelastic rotations. These hinges behaved as predicted by consideration of the in-plane theory.

5.4 FRAME BUCKLING

The problem of instability under vertical loading has not been discussed. At present, research is underway at Lehigh University to investigate the influence of this factor. When completed, the results

will be applicable to the structural steels considered herein.

5.5 SUMMARY

The results of two tests have been presented in this chapter. The subassemblages tested each contained a beam-column of low alloy steel restrained by low carbon steel beams. The results of tests on sway and non-sway subassemblages were predicted using an analysis which had been previously tested on subassemblages of low carbon steel. Since the subassemblages are considered to be representative portions of full scale frames, it is concluded that the behavior of such frames, either of low carbon or low alloy steel, can be adequately predicted.

6. SUMMARY AND CONCLUSIONS

The purpose of this dissertation is to summarize the present state of knowledge for plastic design of low alloy steels and to point out the additional research necessary before these steels can be used with confidence.

Provided the material has an adequate strain-hardening modulus, it was found that the behavior would be satisfactory and moment redistribution could take place in an indeterminate structure. The influence of the length of the inelastic plateau was found to be relatively minor. It was concluded that the structural steels considered had material characteristics that would facilitate the redistribution of moments in an indeterminate structure.

It was shown that the rotary straightening process can reduce the effective stiffness of the flange in the strain-hardening range. The recent test results on rotarized sections were explained by considering the effects of this process. It was concluded that more research needs to be performed both to obtain statistical information on the process itself and to document its influence on structural behavior before definite recommendations can be made. This applies to both low carbon and low alloy steels.

The effect of the web restraint was used to delineate the differences in local buckling action of the cross section under various loading conditions. The contribution of the web restraint to the strength of the flange plate is small. It was concluded that the

presently used solutions for the buckling of the web plate under uniform strain are conservative and could probably be liberalized by considering the post buckling strength of the web plate. A test series is proposed to investigate this problem.

The present solution for the web plate subjected to a strain gradient was found to have little rational basis. A second test series is proposed to investigate the influence of web slenderness on rotation capacity. The test arrangement used for these series will be unique in that the cross section will be subjected to an axial load and applied moment in such a manner that the progression of the yielded zone will proceed in the same manner as in an actual beam-column. Thus the web buckling capacity can be related directly to the rotation capacity of the member.

A method is presented which relates the local buckling strength of the flange to the rotation capacity required of the member. By considering this factor, present flange width to thickness limitations could be liberalized in certain situations. The method looks particularly attractive for low alloy columns used in multi-story frames.

The presently proposed design rules for beams under uniform moment and moment gradient were found to be satisfactory. The design of beam-columns is also on sound footing. The problems of local buckling and lateral torsional buckling of beam-columns require more research effort as does the problem of biaxial bending. The design of corner connections can be accomplished by modifying the presently used procedures to account for the differing steel strengths that might be

used. Connections subjected to axial load in addition to bending moment require further research effort. The problems of shear and web crippling require large scale investigations.

It is concluded that the behavior of the braced subassemblage containing either low carbon or high alloy steel members may be derived from a knowledge of the response of the component members. The principles of equilibrium and compatibility are used to link the responses of the various members of the subassemblage. The agreement with the predicted response is excellent.

The behavior of the unbraced hybrid subassemblage has been predicted by the use of a second order elastic plastic analysis. The analysis accounts for the presence of axial load in the frame, both with respect to the reduction in the flexural capacity of the columns and with respect to the secondary moments produced in the structure. The analysis also accounts for the increased strength in the area of the structural connections.

The influence of strain-hardening has been included in the response of the subassemblage by a simple yet rational method. The background for the method is presented, and a brief comparison of theory with the experimentally obtained response is included.

It is concluded that plastic design of structures fabricated from low alloy steels having yield stress levels up to 50 ksi is feasible and presents no unusual difficulties. The problems connected with the plastic design of such structures have not been completely solved. However, the problems which are still outstanding are those

which have not been solved completely for the low carbon steels, even after extensive use. This list would include web buckling, biaxial bending, design of connections, web crippling, shear and frame buckling. In all of these areas major research efforts are in progress or are proposed.

At present (1966) it appears feasible to use low alloy steel members in low rigid frame structures as covered by the present specifications.[58] Before these members can be used the restrictions relating to those problems mentioned above must be adjusted in a conservative manner. For multi-story building frames, the low alloy steel members exhibit behavior which can be predicted with the same confidence as that of corresponding low carbon steel members. Thus the use of the higher strength steel should involve no unusual difficulties.

7. TABLES

TABLE 2.1

PROPERTIES OF MASSONNET'S TEST BEAMS

Test No.	α	σ_y ksi	Z(in.^{3})
5	2.0	39.8	2.58
6	2.0	29.8	2.58
13	2.0	64.4	2.52
14	2.0	64.4	2.52

TABLE 2.2 MATERIAL CONDITION AT SIMPLE PLASTIC THEORY LOAD

$\frac{\epsilon_{st}}{\epsilon_y}$	$\frac{E}{E_{st}}$	$\frac{M_s}{M_p}$	$\frac{\epsilon_{max}}{\epsilon_y}$	$\frac{v}{d}\ \frac{1}{\epsilon_y}\ \frac{1}{(L/d)^2}$	$\frac{\theta_H}{\phi_p L}$	$\frac{\tau L}{L}$
Elastic-Plastic		1.000	--	0.1240	0.0416	0
1.0	45	1.062	3.80	0.1172	0.0221	0.0154
1.0	450	1.025	12.06	0.1220	0.0338	0.0061
12.0	45	1.013	12.60	0.1232	0.0372	0.0033
12.0	450	1.011	17.03	0.1240	0.0376	0.0028
20.0	45	1.008	20.36	0.1236	0.0375	0.0020
20.0	450	1.007	23.35	0.1236	0.0377	0.0019

TABLE 3.1

WEB BUCKLING PROGRAM

Material A441

Test No.	b/t	P/P_y	d/w
WB-1	14.0	0.40	60
WB-2	14.0	0.70	60
WB-3	14.0	0.80	60
WB-4	14.0	0.90	60

TABLE 4.1

BEAMS UNDER HIGH MOMENT GRADIENT

Test No.		$\frac{L}{r_y}$	$\frac{b}{t}$	Section	Material	$\frac{\theta_H}{L\emptyset P}$
LB6	0.706	38.5	16.9	10WF21	A7 (38)	4.6
LB7	0.912	28.8	16.9	10WF21	A7 (38)	8.9
LB8	0.980	28.8	16.9	10WF21	A7 (38)	10.4
HT-38	0.800	45.0	13.4	10WF25	A441 (52 ksi)	12.2

TABLE 4.2

BRACING SPACING REQUIREMENTS

Material	Effective Length Factor	$\frac{L}{r_y}$ (Eq. 4.5)	Rotation Capacity From Experiment
A36	0.54	44	6.5 (L/r_y = 45)
	0.80	30	4.5 (L/r_y = 30)
A441	0.54	32	5.7 (L/r_y = 35)
	0.80	22	No Test Available

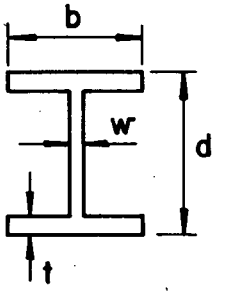

Section	b IN.	d IN	t IN.	w IN	b/t —	d/w —	h/r_x	L/d	M_p IN-K	M_{pc} IN-K
12 B 16.5	4.02	12.04	0.280	0.240	14.4	50.2	-	7.5	786	-
6 WF 25	6.12	6.25	0.438	0.300	14.0	20.8	45.4	-	-	420

Table 5.1 Member Properties

Section	Specimen No.	σ_y KSI	ϵ_y	ϵ_{st}	E_{st} KSI	σ_{ult} KSI	Elong. %	Residual Stresses KSI
12 B 16.5	1	35.9	.0012	.021	425	59.6	30	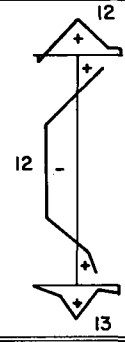
	2	35.8	.0012	.017	228	*	26	
	3	38.7	.0013	.031	365	60.3	31	
	4	39.5	.0013	.030	358	59.9	29	
	5	36.0	.0012	.012	424	60.1	30	
	6	35.9	.0012	.012	385	59.1	30	
	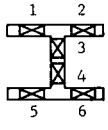							
6 WF 25	1	50.5	.0017	.016	655	76.5	22	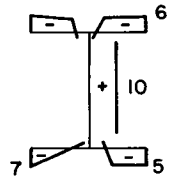
	2	50.3	.0017	.017	576	76.4	24	
	3	48.8	.0017	.016	644	75.9	24	
	4	48.8	.0017	.016	629	75.4	22	
	5	50.1	.0017	.017	635	76.6	23	
	6	50.0	.0017	.017	638	75.2	24	

*Not recorded

Table 5.2 Material Properties

TABLE 5.3

SUBASSEMBLAGE TESTS

Test No.	$\frac{h}{r_x}$	$\frac{s}{d}$	G	$\frac{P}{P_y}$	θ At Column Peak	θ At Beam Hinge	θ At Column Local Buckle
RC-1	59.4	37.0	4.13	.50	.014	.040	.054
RC-2	59.4	27.8	3.10	.40	.023	.038	.052
RC-3	59.5	18.5	2.11	.42	.020	.021	.040
RC-4	40.0	36.9	5.87	.57	.014	.038	.032
RC-5	39.9	27.5	4.47	.56	.012	.030	.040
RC-6	29.9	27.5	5.97	.84	.006	.030	.032
RC-7	59.7	27.6	2.80	.40	.010	.022	.042
RC-10*	60.5	18.5	2.11	.43	.022	.020	.036
SC-8	45.4	7.5	0.34	.60	.014	.010	

*Column not braced.

8. APPENDIX A

8. APPENDIX A - EFFECT OF LARGE STRAINS

It has been suggested that the criterion for applying plastic design procedures to a material should be the materials susceptibility to fracture.[21] For the structural steels, however, fracture of a flexural member has never been observed under normal conditions. The mode of failure for a braced member has always been that of local buckling. It appears that a proper criterion for the application of plastic design procedures is the resistance of the material to local buckling.[22]

To support this point of view, consider the member segment of length, L, shown in Fig. A.1(a). It is subjected to a bending moment distribution which varies from M_o at the left end to ρM_o at the right. In this figure ρ is the moment ratio and is positive as shown. is chosen so that $1.0 \geq \rho \geq -1.0$. The maximum moment M_o is assumed to be greater than M_p over a yielded length, τL. The corresponding curvature distribution is shown in Fig. A.1(b).for the curve typical of the structural steels. In the usual structural situation the yielded length is bounded on one side by a load or reaction point and on the other by a stiff elastic portion, thus the local flange buckle must take the shape shown in Fig. A.1(c).

If the moment, M_o, is increased to the point where fracture occurs the value of the maximum stress, σ_o, is given by:

$$\sigma_o = \sigma_y + E_{st} (\epsilon_{ult} - \epsilon_{st}) \qquad (8.1)$$

In this analysis the value of E_{st} has been assumed constant up to the fracture strain and a shape factor of unity assumed for the cross section.

The curvature distribution which would result from a more exact analysis would not appreciably change the results obtained. Instead of a distribution bounded by linear segments, smooth transition curves would join the distribution over the yielded portions to that over the elastic parts of the member.

At fracture the yielded length can be computed as:

$$\tau L = \frac{L}{(1-\rho)} \frac{(\epsilon_{ult} - \epsilon_{st})}{\left(\frac{\sigma_y}{E_{st}} + \epsilon_{ult} - \epsilon_{st}\right)} \tag{8.2}$$

Lay has developed an expression for the local buckling strength of a flange which has a yielded length equal to the optimum.[27] This yielded length can be related to the material properties and cross sectional dimensions by:

$$\tau L = 2\pi \sqrt[4]{\frac{E_{st}}{G_{st}} \frac{21}{2304} \frac{A_w}{A_f} \left(\frac{bt}{w}\right)^4} \tag{8.3}$$

where

$$A_w = w(d - 2t) \tag{8.4}$$

$$A_f = bt \tag{8.5}$$

$$G_{st} = \frac{2G}{1 + \frac{E}{4\ (1 + u)\ E_{st}}} \tag{8.6}$$

G_{st} is the torsional rigidity in the inelastic range and has been developed from a consideration of the yielding process for structural metals.[27] G is the elastic torsional rigidity and u is Poisson's ratio. In the above expressions d is the cross section depth, b and t are the flange width and thickness and w is the web thickness.

The flange width to thickness ratio necessary to prevent local buckling until the optimum length has yielded is given by:

$$\left(\frac{b}{t}\right)^2 = \frac{1}{\sigma_y + E_{st}\,(\epsilon_{ult} - \epsilon_{st})} \left\{ 4G_{st} + \frac{1}{2}\sqrt{\frac{7}{3}\,E_{st}\,G_{st}\,\frac{A_f}{A_w}\left(\frac{w}{t}\right)^2} \right\} \quad (8.7)$$

Solvings Eqs. 8.2 and 8.3 for $(w/t)^2\sqrt{\frac{A_f}{A_w}\,G_{st}}$ and substituting this result and Eq. 8.6 into 8.7 the result becomes:

$$\left(\frac{b}{t}\right)^2 = \frac{1}{\sigma_y + E_{st}\,(\epsilon_{ult} - \epsilon_{st})} \left\{ 4G_{st} + \frac{7}{96}\,E_{st}\left(\frac{b}{L}\right)^2 \left[\frac{2\left(\frac{\sigma_y}{E_{st}} + \epsilon_{ult} - \epsilon_y\right)(1-\rho)}{(\epsilon_{ult} - \epsilon_y)} \right]^2 \right\} \quad (8.8)$$

Equation 8.8 gives the b/t ratio at which local buckling of the compression flange occurs simultaneously with the occurence of the fracture strain in the tension flange. For b/t ratios above this value, local buckling will occur before the tension flange fractures, while if b/t is less than that given by Eq. 8.8 fracture will occur before local buckling.

The most severe condition with respect to fracture is when $\rho = -1.0$. For this case and for practical ratios of b/L, the limiting value of b/t is about 9 for the structural steels of the low carbon and low alloy groups. Thus, even under these assumptions, for the majority of the wide flange shapes in present use member ductility is limited not by fracture but by local buckling and it is on this problem that effort should be concentrated.(58)

It should be remembered that in the analysis above E_{st} has been assumed constant up to fracture. For the structural steels E_{st} is not constant but increases from its initial value at the onset of strain-hardening to zero at the ultimate stress. It is not possible to draw any definite conclusions as to the effect of this variation on the failure mode. It should be noted that fracture under static loading conditions and normal temperature has never been observed for structural steel members.(16)

9. SYMBOLS

A	Area
A_f	Flange area
A_w	Web area
D_x, D_y	Plate stiffness coefficients - direct stiffness
D_{xy}, D_{yx}	Plate stiffness coefficients - cross stiffness
E	Modulus of elasticity
E_{st}	Strain-hardening modulus
G	Shear modulus
G_{st}	Strain-hardening shear modulus
I	Moment of inertia
I_w	Warping moment of inertia
K	Effective length
K_T	St. Venant's torsion constant
L	Length
M	Moment
M_o	Maximum moment in span
M_p	Plastic moment
M_{pc}	Plastic moment reduced for axial load
P	Axial load
P_y	Yield load ($A\sigma_y$)
R	Rotation capacity
W	Load
Z	Plastic modulus

b	Breadth of section
d	Depth of section
f	Ratio of strain at ultimate stress to yield strain
k	Web spring constant
n	Number of half-wave lengths
r_x, r_y	Radius of gyration about strong and weak axes, respectively
t	Flange thickness
u	Lateral movement
v	In-plane movement
w	Web thickness
α	Proportionality constant
δ	Axial deformation
ϵ	Strain
ϵ_{st}	Strain-hardening strain
ϵ_y	Yield strain
ρ	Moment ratio
σ	Stress
σ_y	Yield stress
σ_{rc}	Maximum compressive residual stress
τL	Yielded length
ϕ	Curvature
ϕ_{pc}	Curvature corresponding to attainment of M_{pc}, assuming ideally elastic material
θ	Rotation
θ_H	Inelastic hinge rotation

10. FIGURES

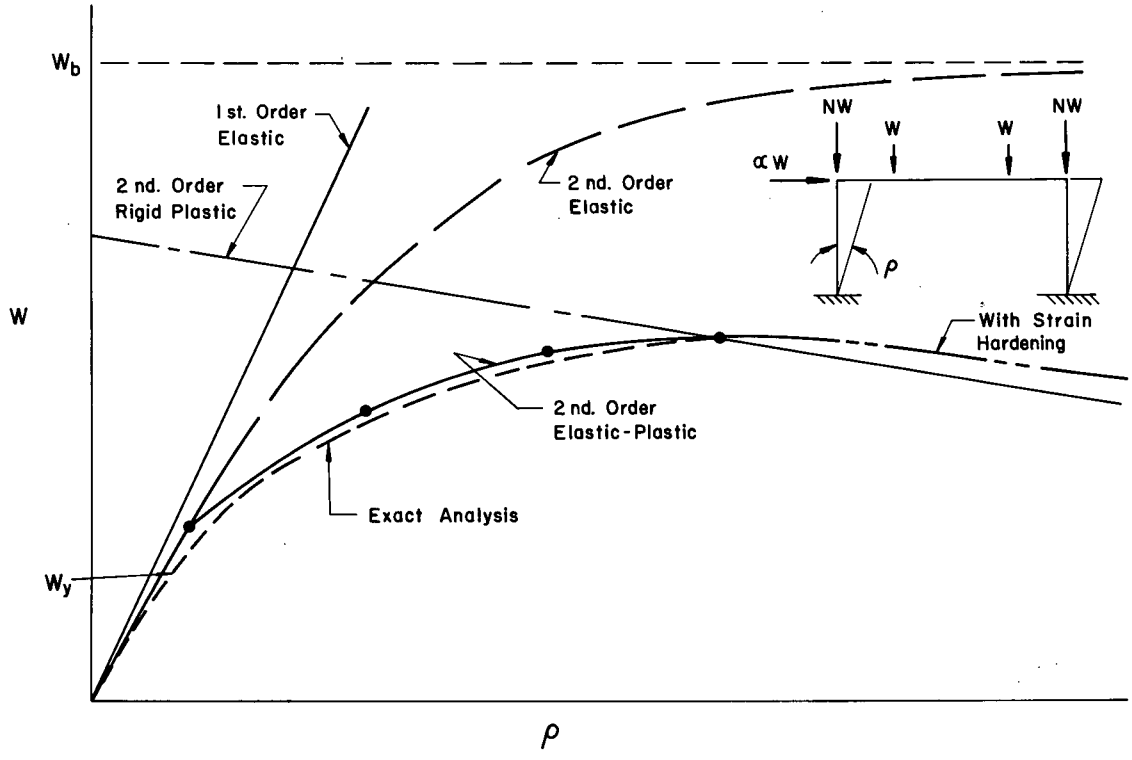

Fig. 1.1 Load-Deformation Relationships

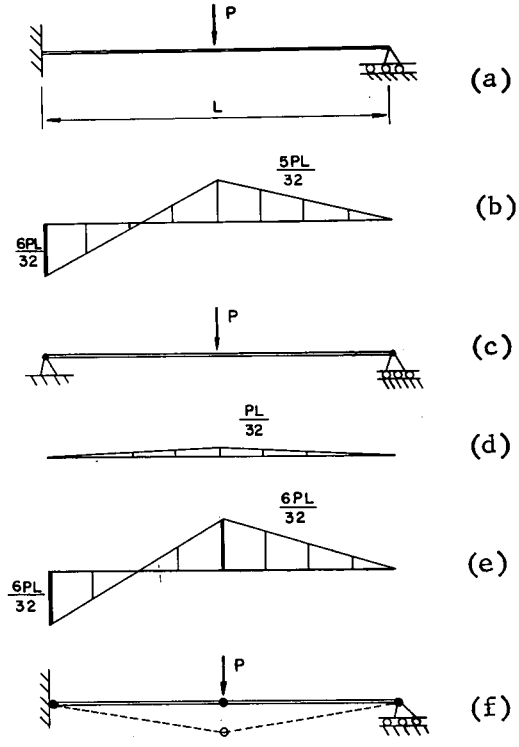

Fig. 2.1 Propped Cantilever

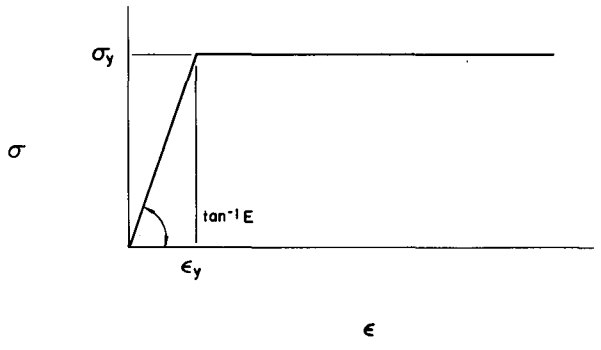

Fig. 2.2 Stress-Strain Relationship

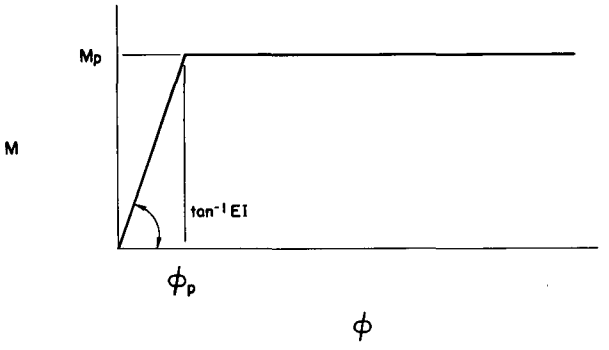

Fig. 2.3 Moment-Curvature Relationship

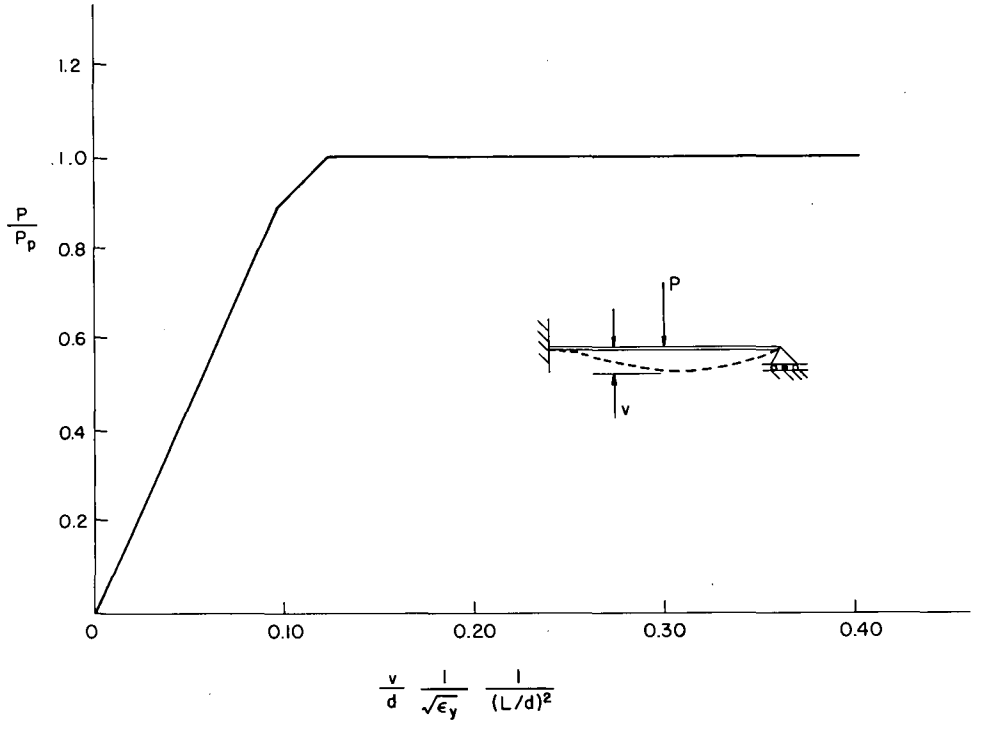

Fig. 2.4 Load-Deflection Curve for Cantilever

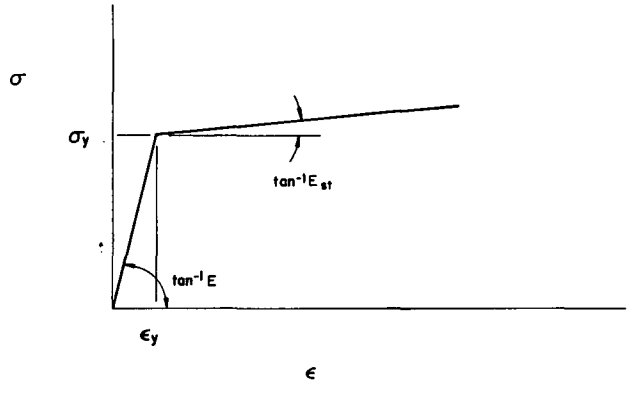

Fig. 2.5 Bilinear Stress-Strain Curve

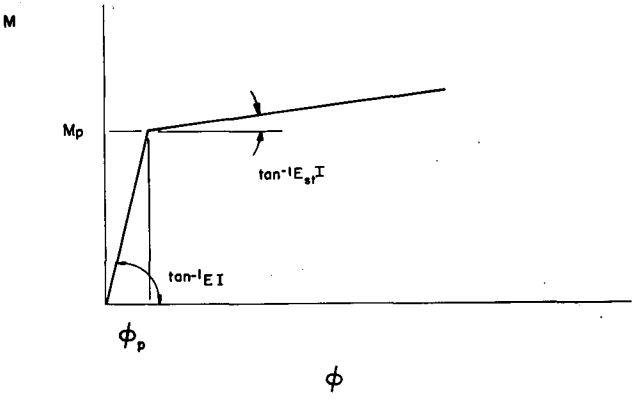

Fig. 2.6 Bilinear Moment-Curvature Relationship

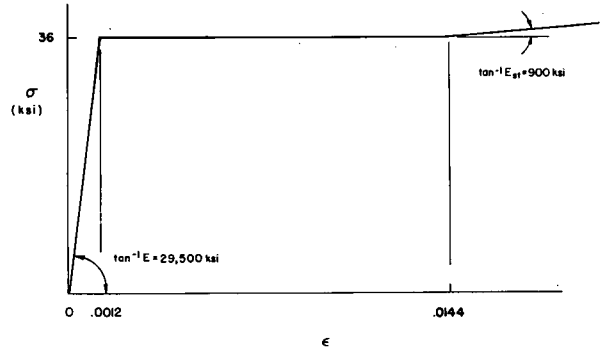

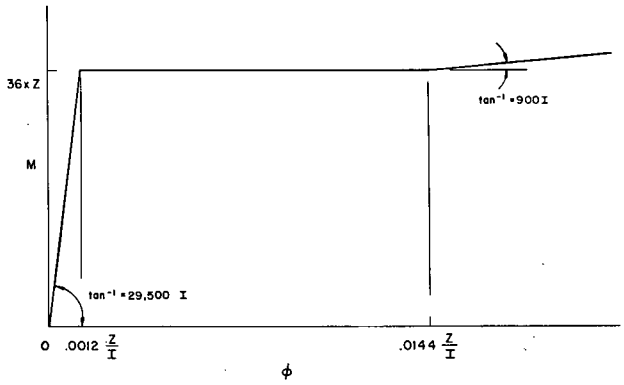

Fig. 2.7 Stress-Strain Curve for A36 Steel Fig. 2.8 Moment-Curvature Relationship

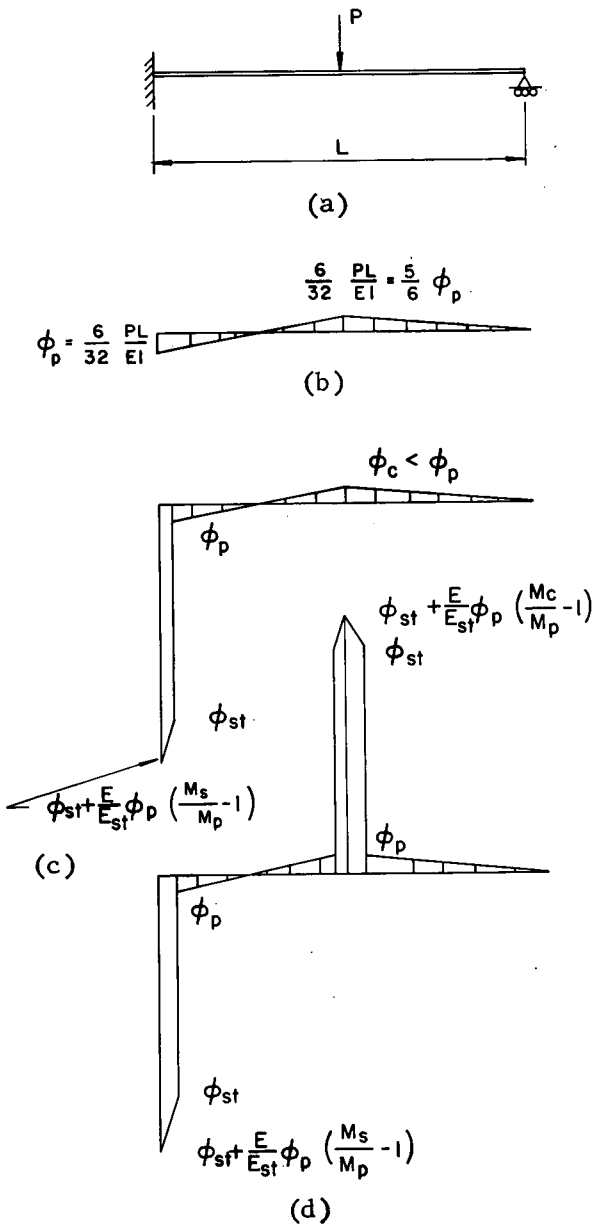

Fig. 2.9 Propped Cantilever

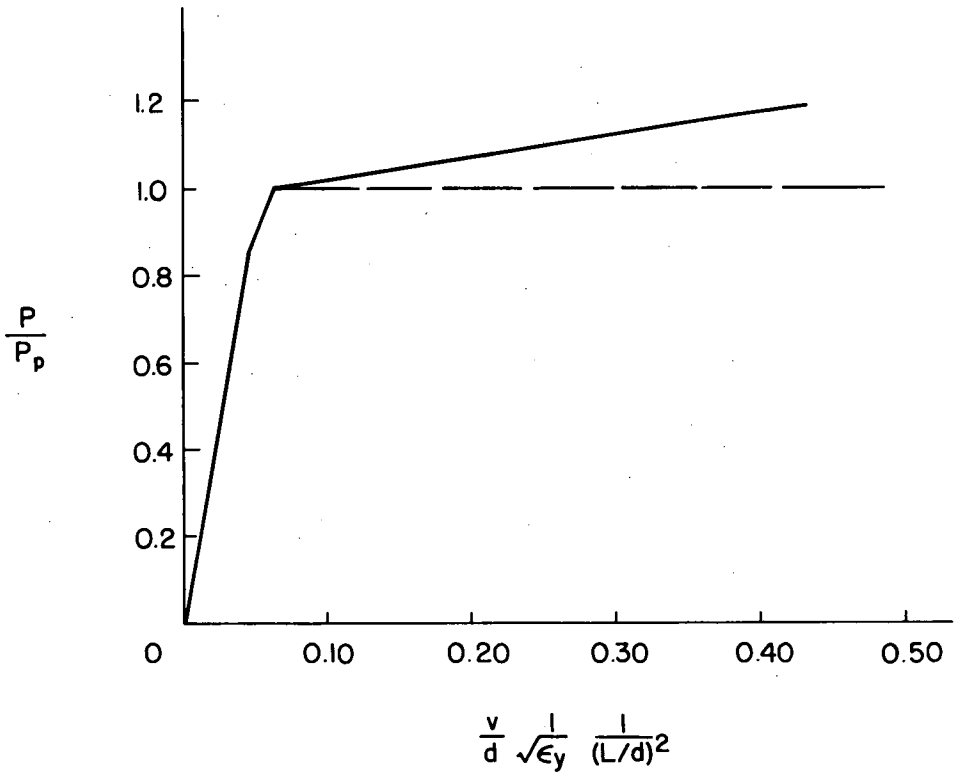

Fig. 2.10 Load-Deformation Curve

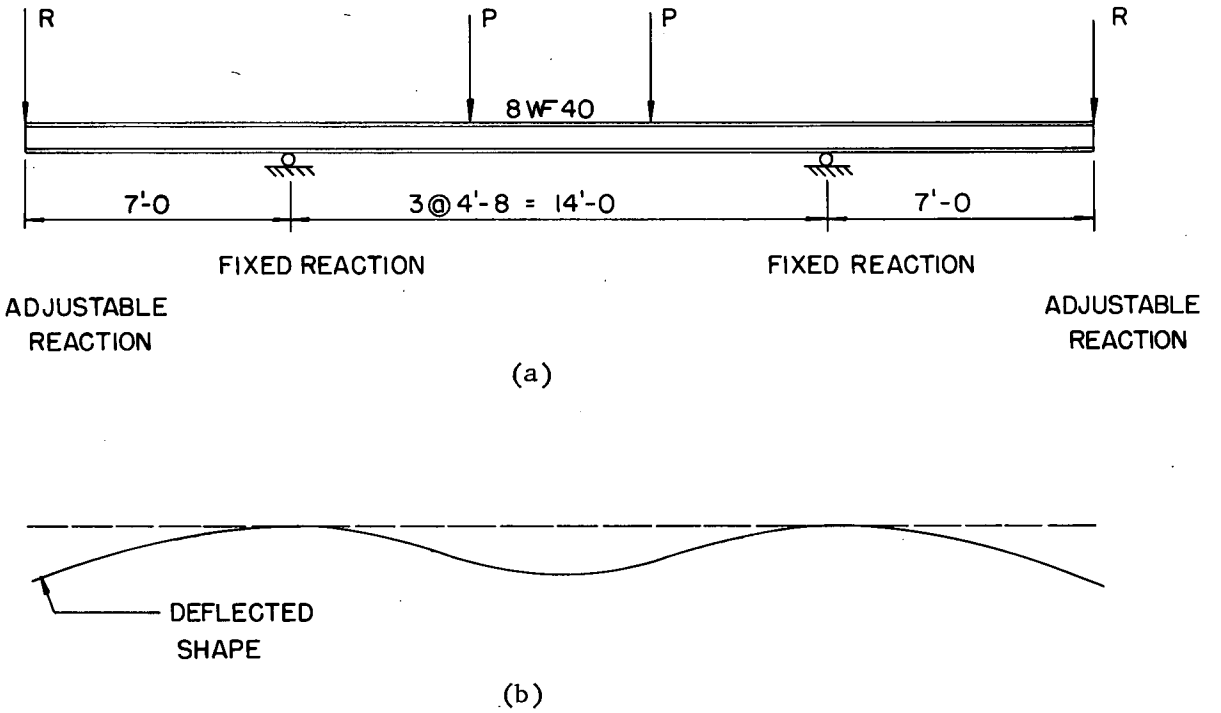

Fig. 2.11 Test Arrangement for Yang's Beam

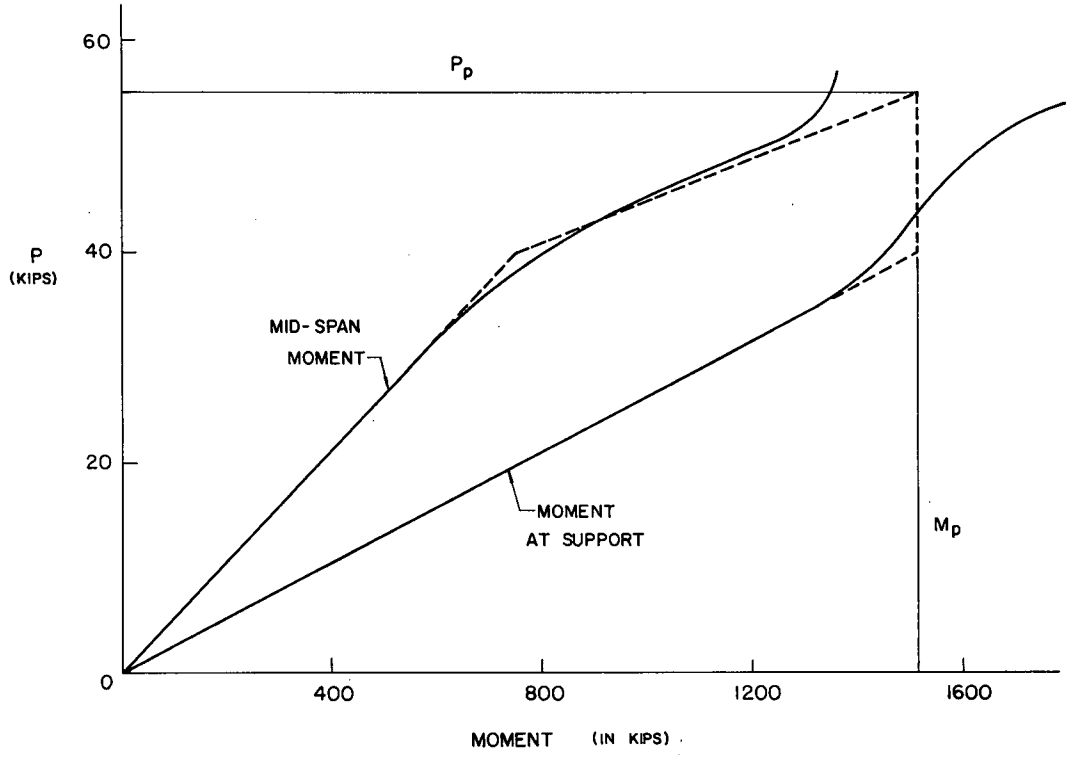

Fig. 2.12 Load-Moment Results for Yang's Beam

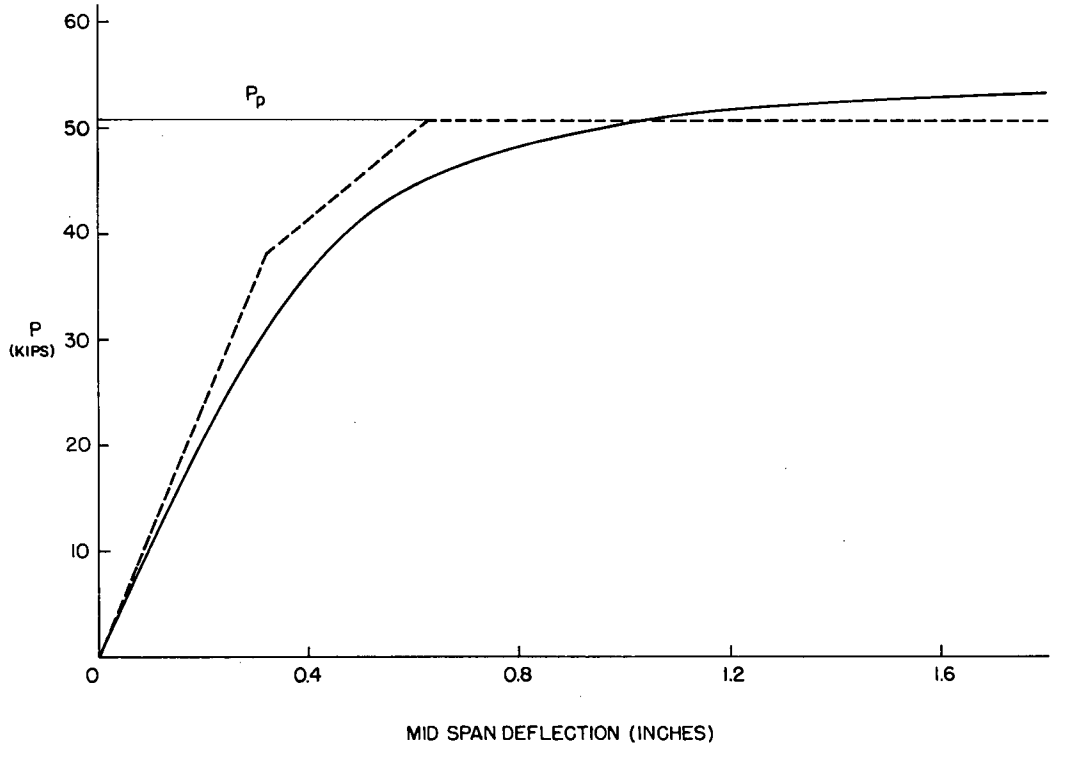

Fig. 2.13 Load-Deflection Results for Yang's Beam

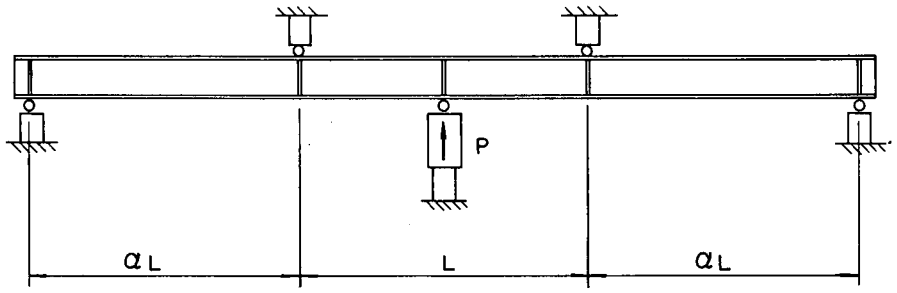

Fig. 2.14 Test Arrangement for Massonnet's Beams

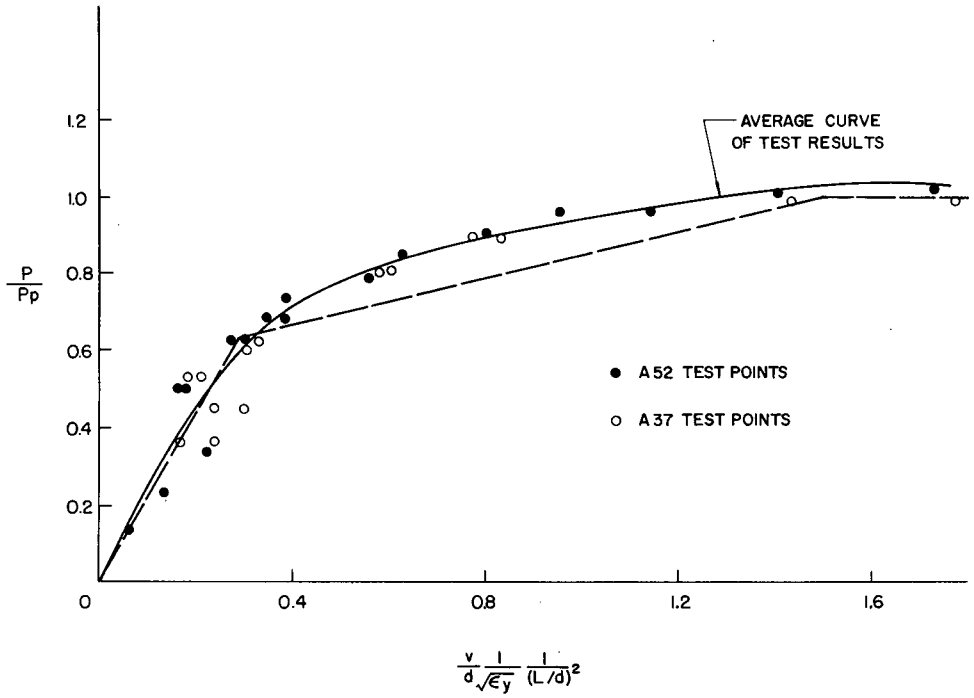

Fig. 2.15 Load-Deflection Results for Massonnet's Beams

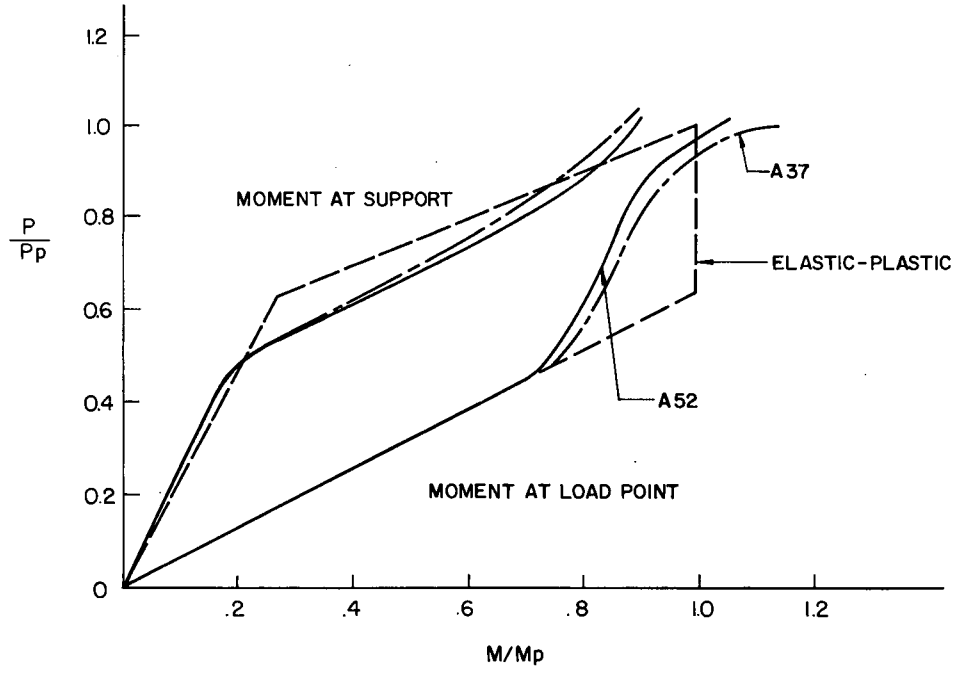

Fig. 2.16 Load-Moment Results for Massonnet's Beams

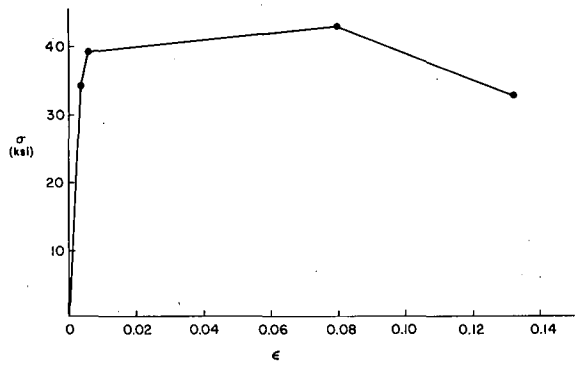

Fig. 2.17 Stress-Strain Curve for Aluminum Alloy

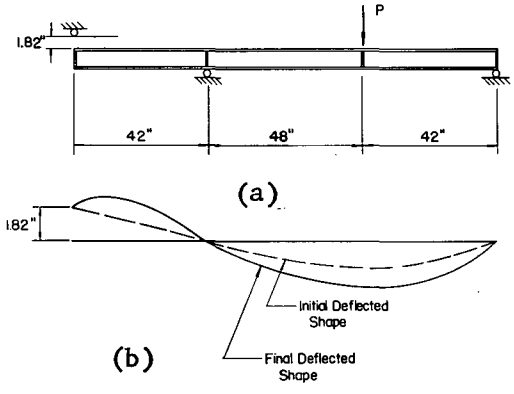

Fig. 2.18 Test Arrangement for Two Span Beam

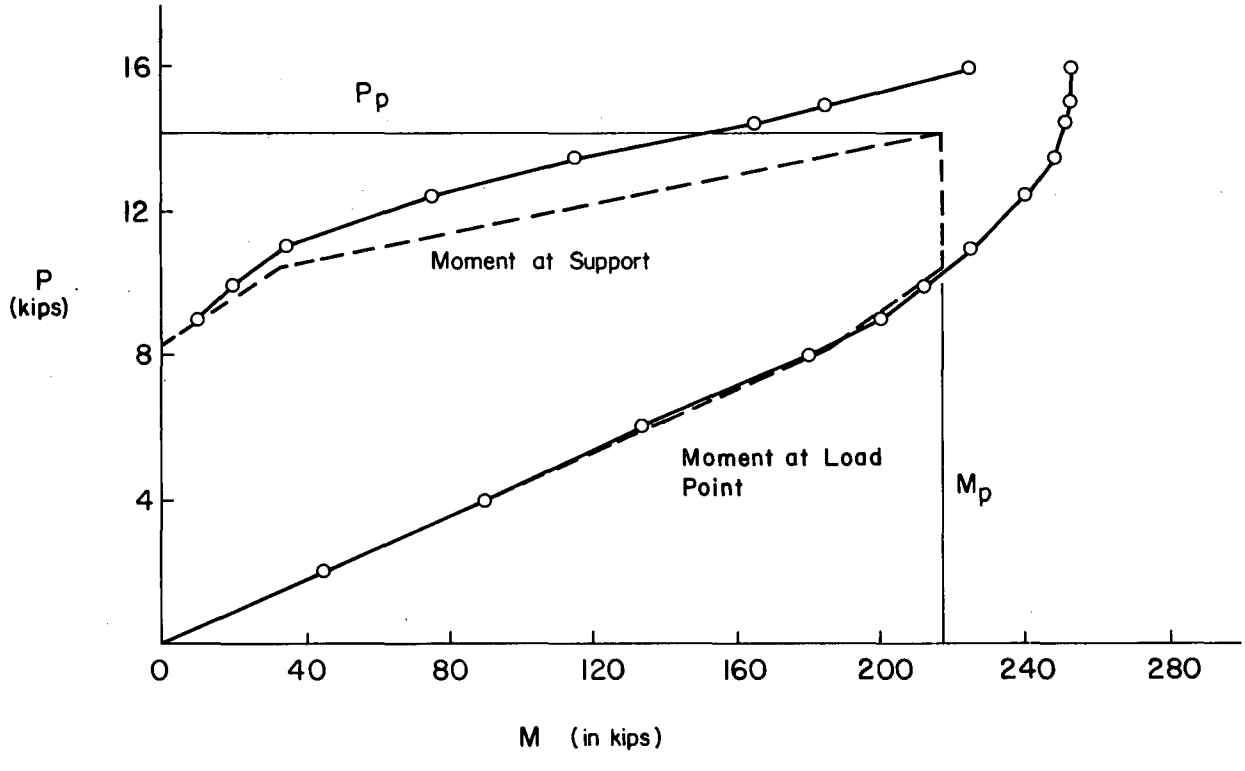

Fig. 2.19 Load-Moment Results for Two Span Beam

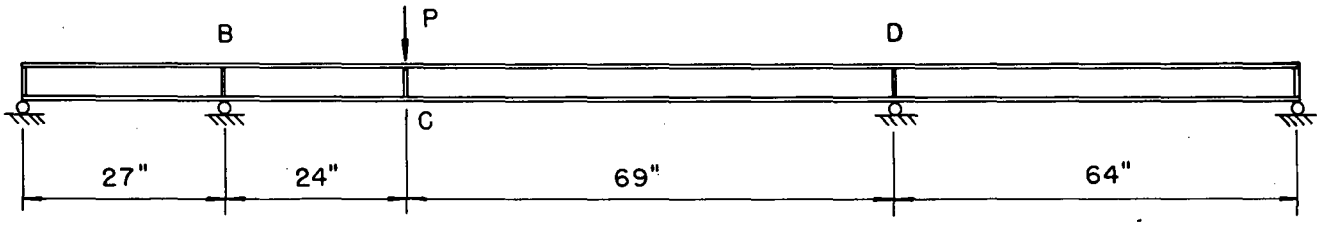

Fig. 2.20 Test Arrangement for Three Span Beam

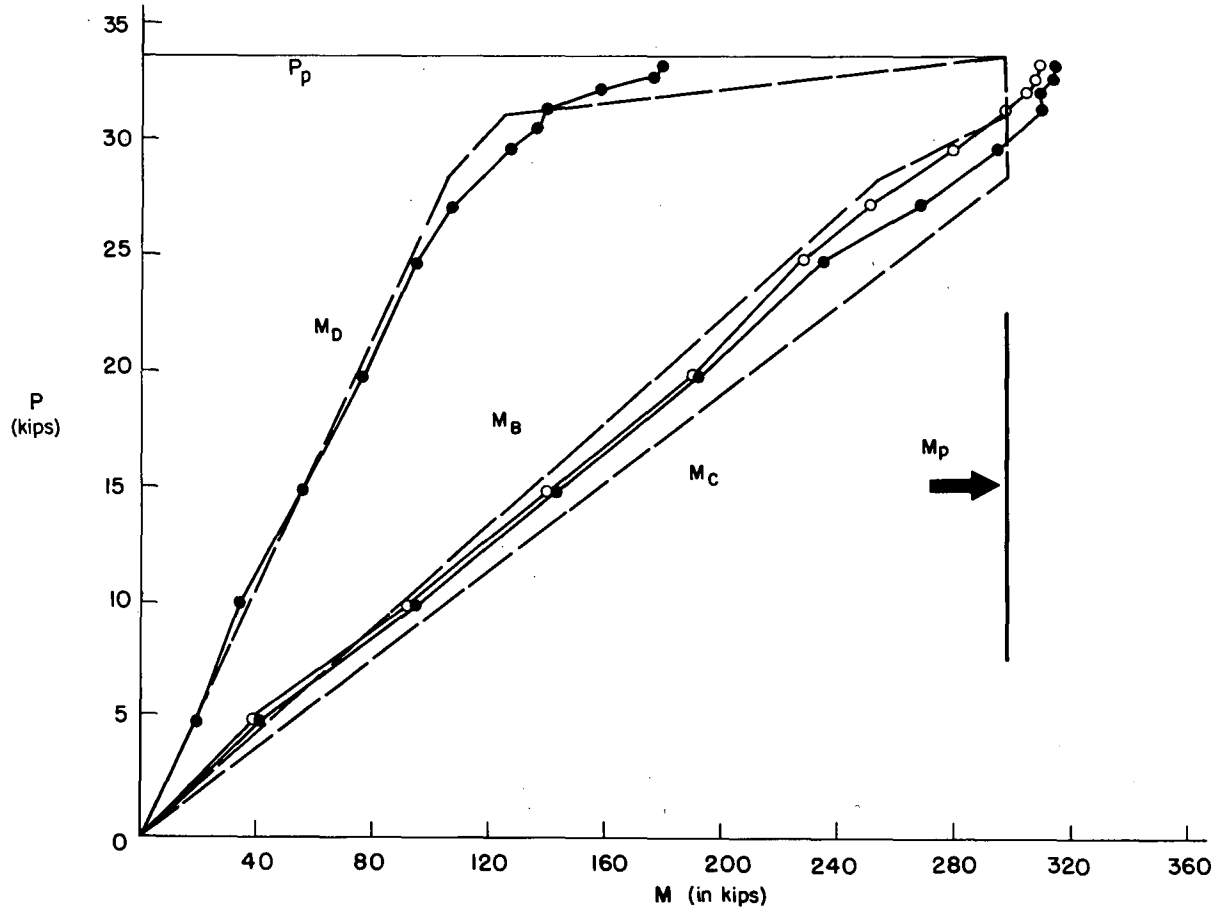

Fig. 2.21 Load-Moment Results for Three Span Beam

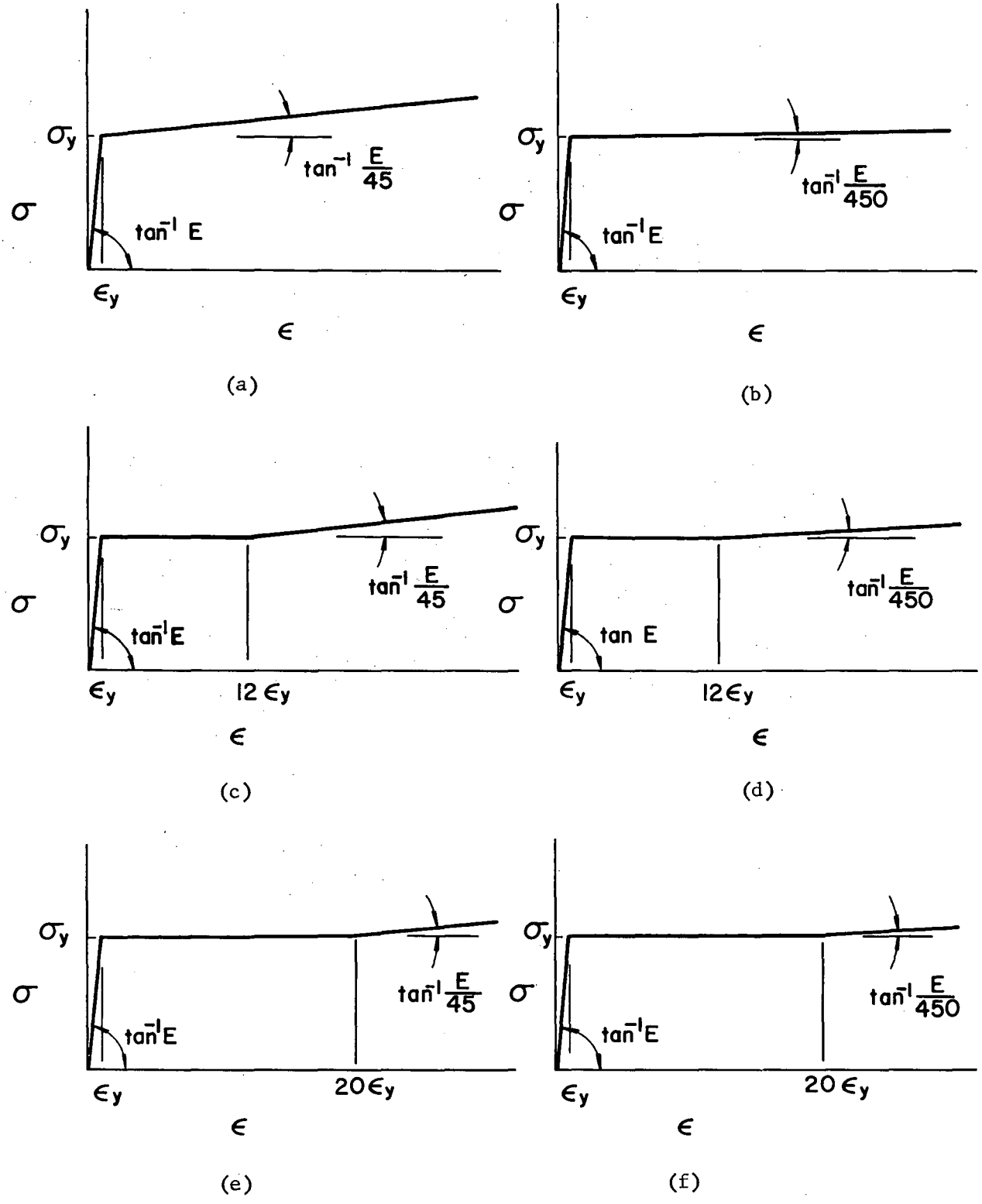

Fig. 2.22 Stress-Strain Relationships

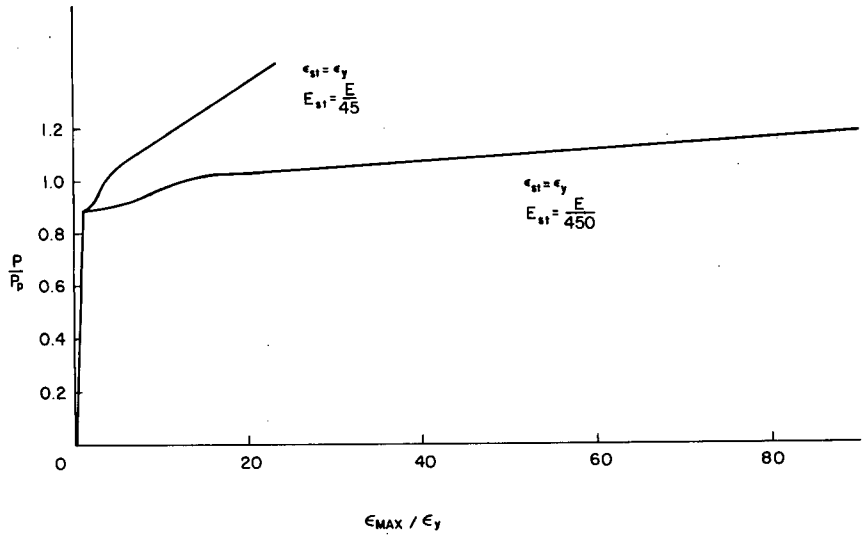

Fig. 2.23 Load-Strain Curves $\epsilon_{st} = \epsilon_y$

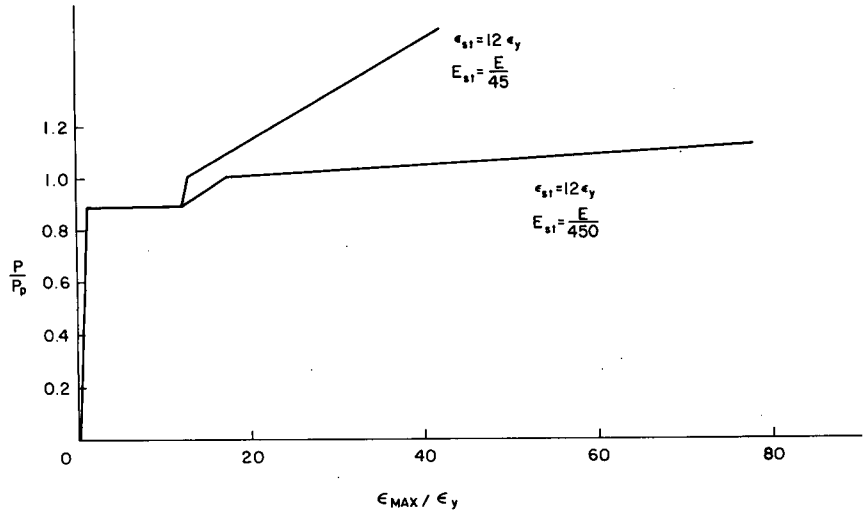

Fig. 2.24 Load-Strain Curves $\epsilon_{st} = 12\epsilon_y$

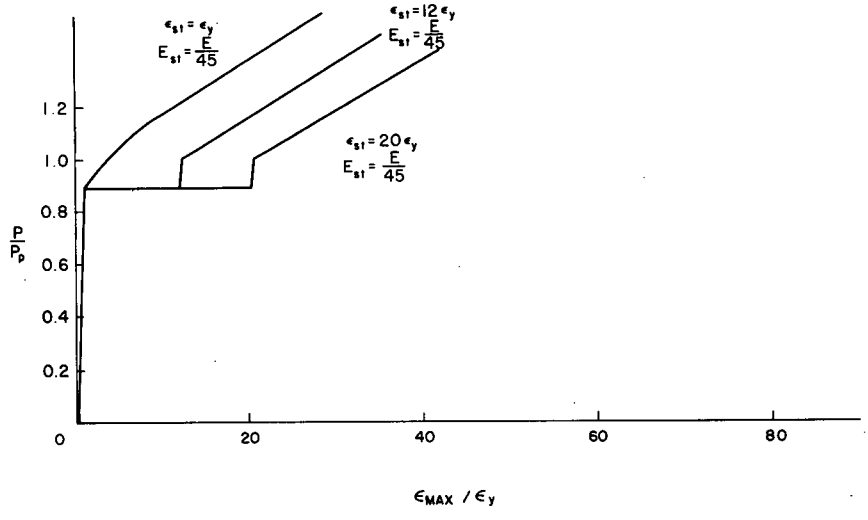

Fig. 2.25 Load-Strain Curves $E_{st} = E/45$

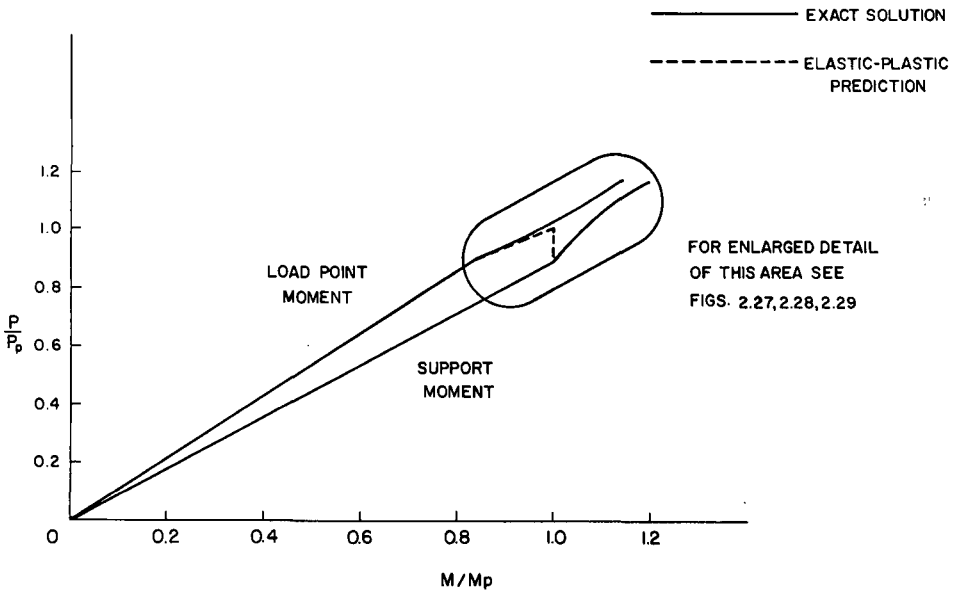

Fig. 2.26 Load-Moment Curves

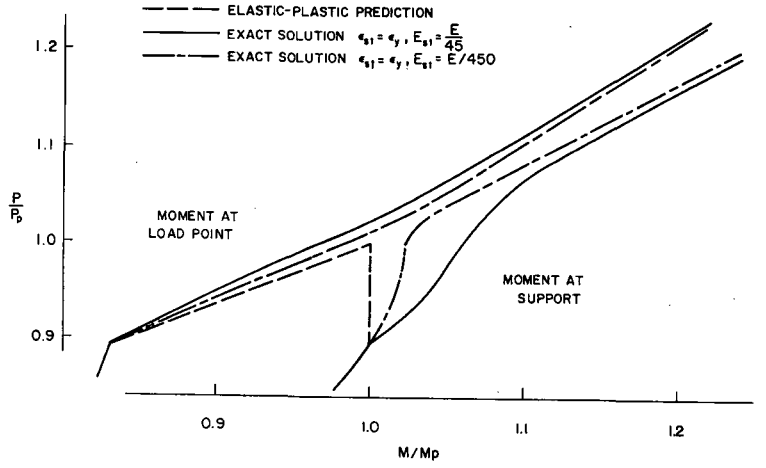

Fig. 2.27 Load-Moment Curves $\epsilon_{st} = \epsilon_y$

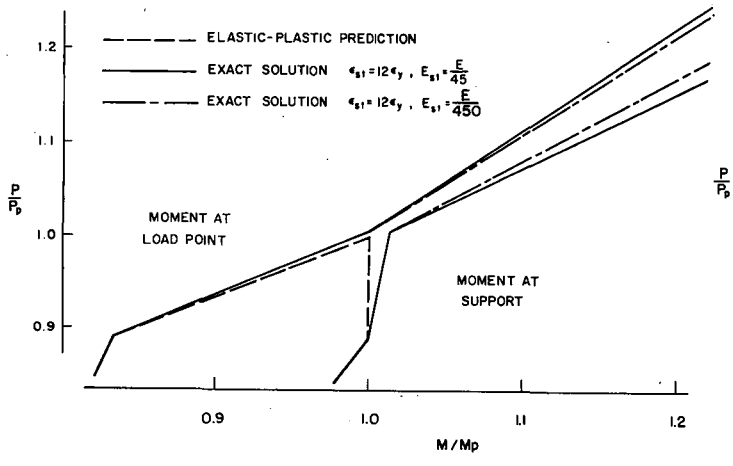

Fig. 2.28 Load-Moment Curves $\epsilon_{st} = 12\epsilon_y$

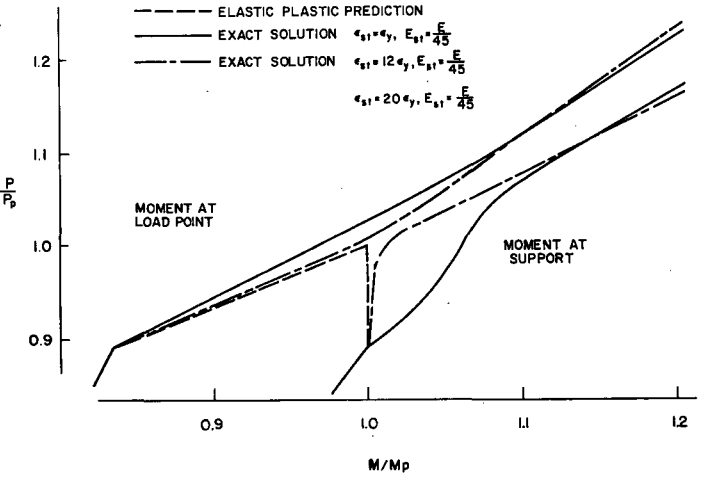

Fig. 2.29 Load-Moment Curves $E_{st} = E/45$

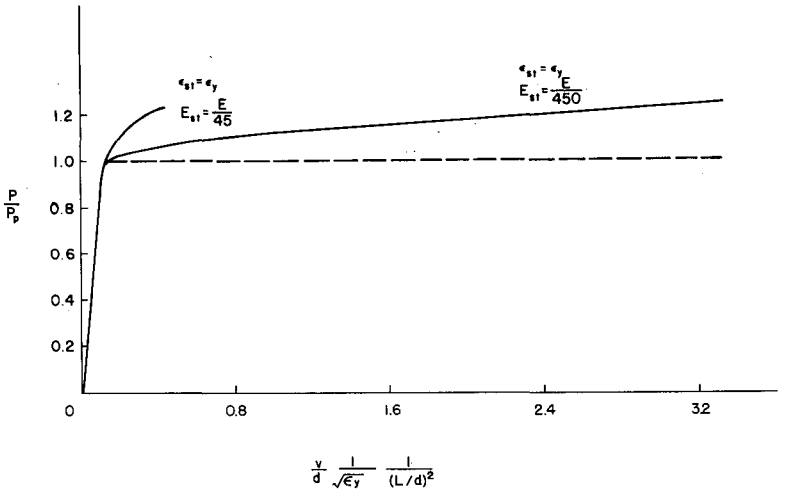

Fig. 2.30 Load-Deflection Curves $\epsilon_{st} = \epsilon_y$

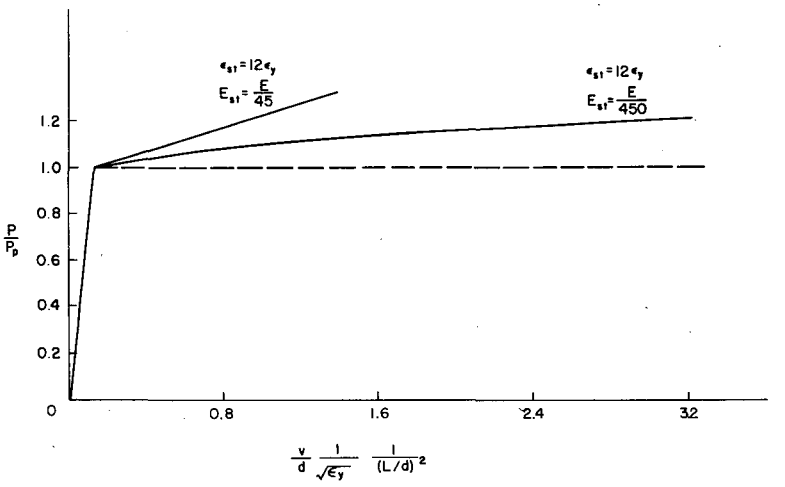

Fig. 2.31 Load-Deflection Curves $\epsilon_{st} = 12\epsilon_y$

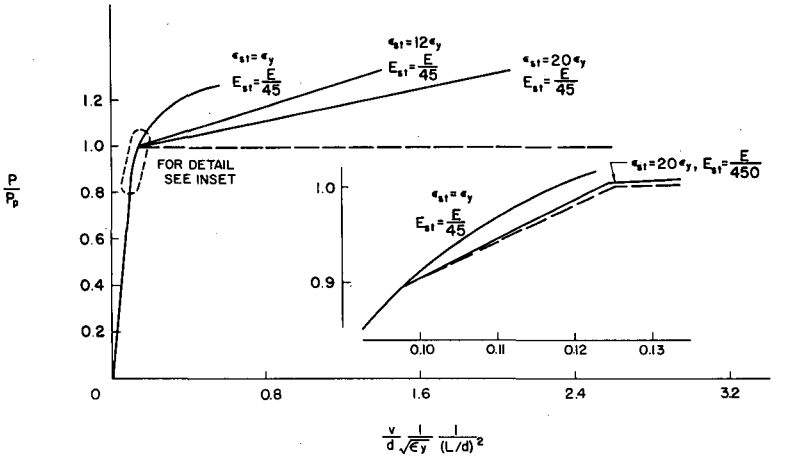

Fig. 2.32 Load-Deflection Curves $E_{st} = E/45$

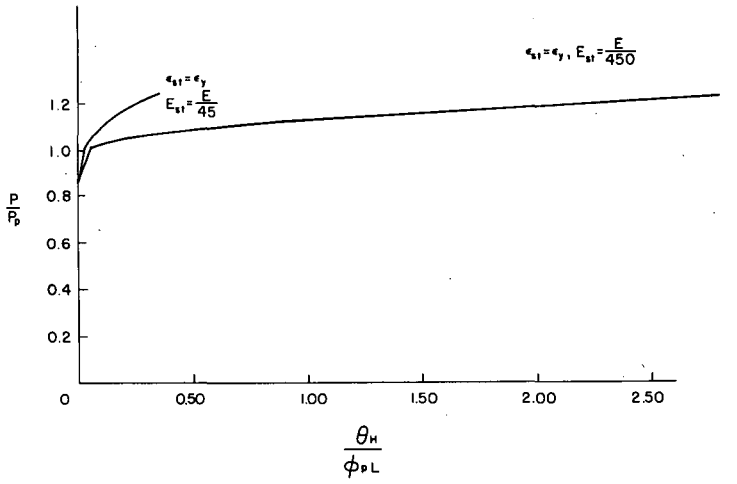

Fig. 2.33 Load-Hinge Angle Curves $\epsilon_{st} = \epsilon_y$

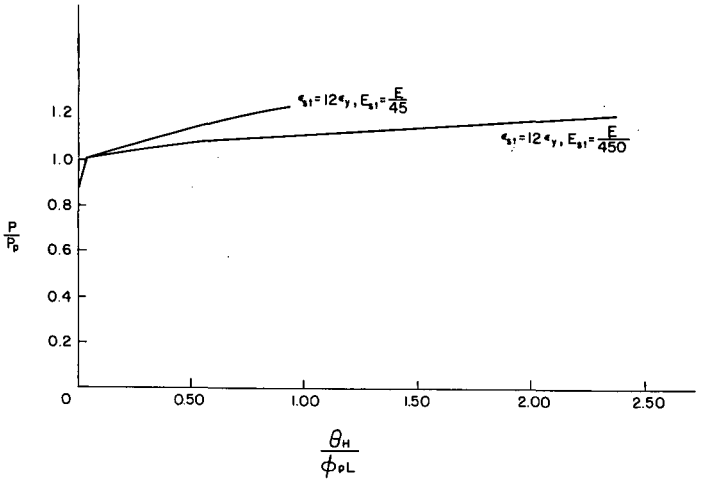

Fig. 2.34 Load-Hinge Angle Curves $\epsilon_{st} = 12\epsilon_y$

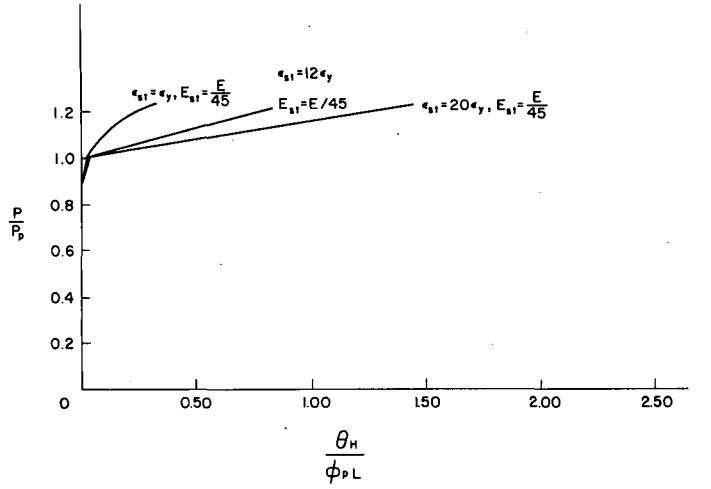

Fig. 2.35 Load-Hinge Angle Curves $E_{st} = E/45$

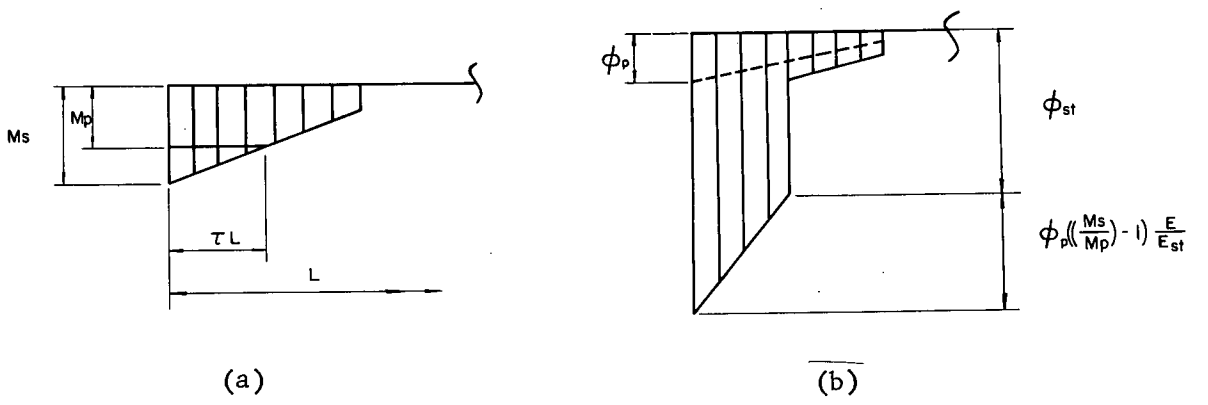

Fig. 2.36 Bending Moment and Curvature Distributions

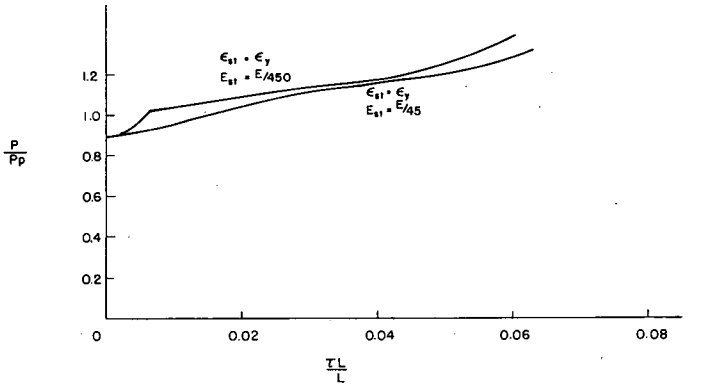

Fig. 2.37 Load-Yielded Length Curves $\epsilon_{st} = \epsilon_y$

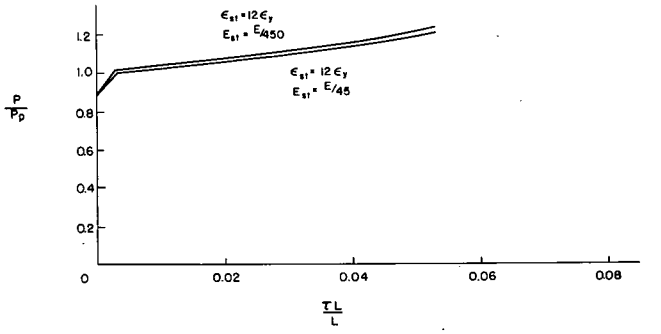

Fig. 2.38 Load-Yielded Length Curves $\epsilon_{st} = 12\epsilon_y$

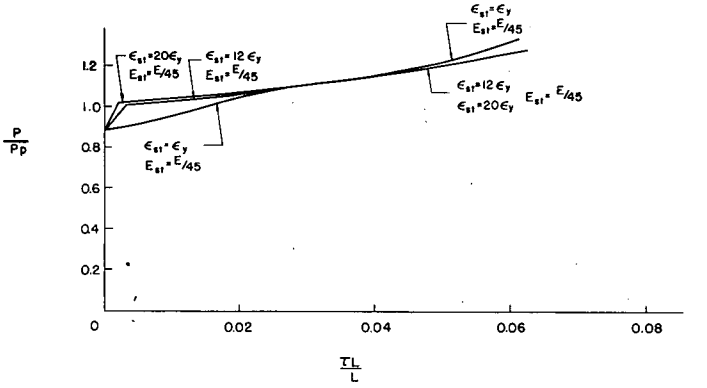

Fig. 2.39 Load-Yielded Length Curves $E_{st} = E/45$

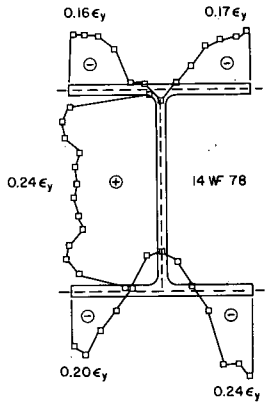

Fig. 2.40 Residual Strains Due to Rolling Process

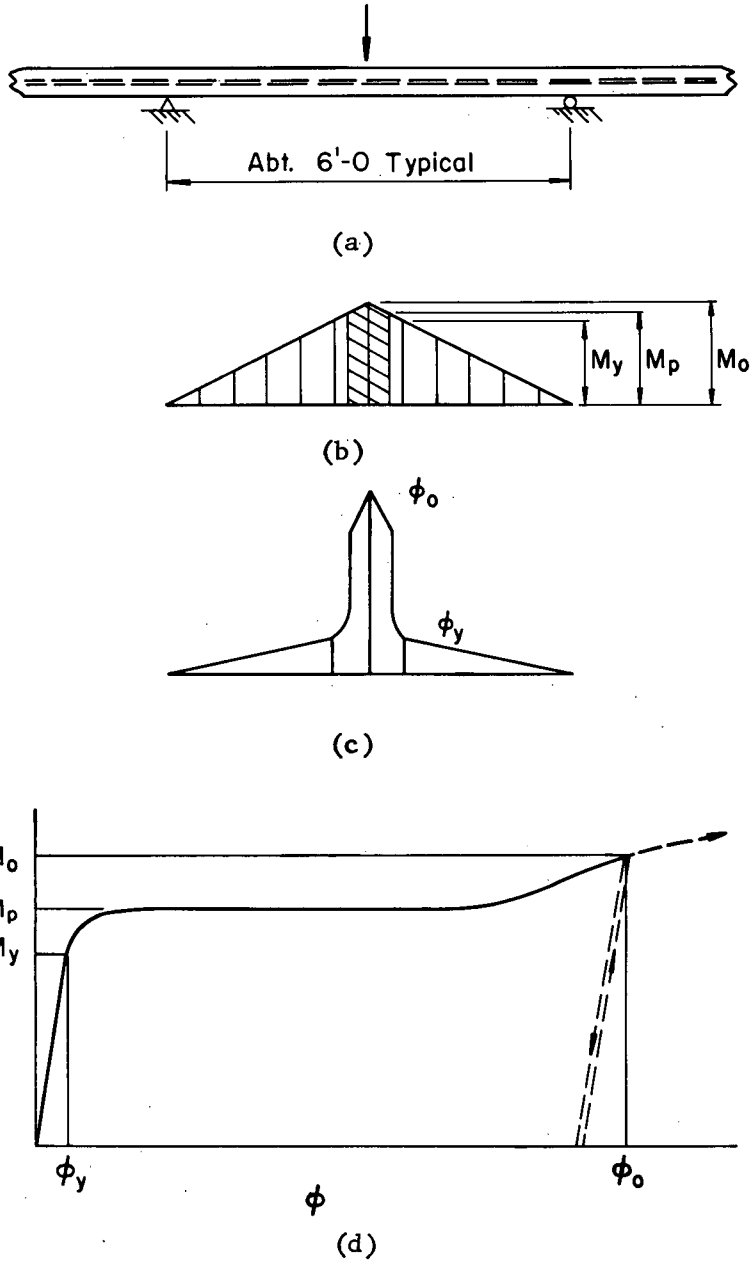

Fig. 2.41 Gag Straightening Process

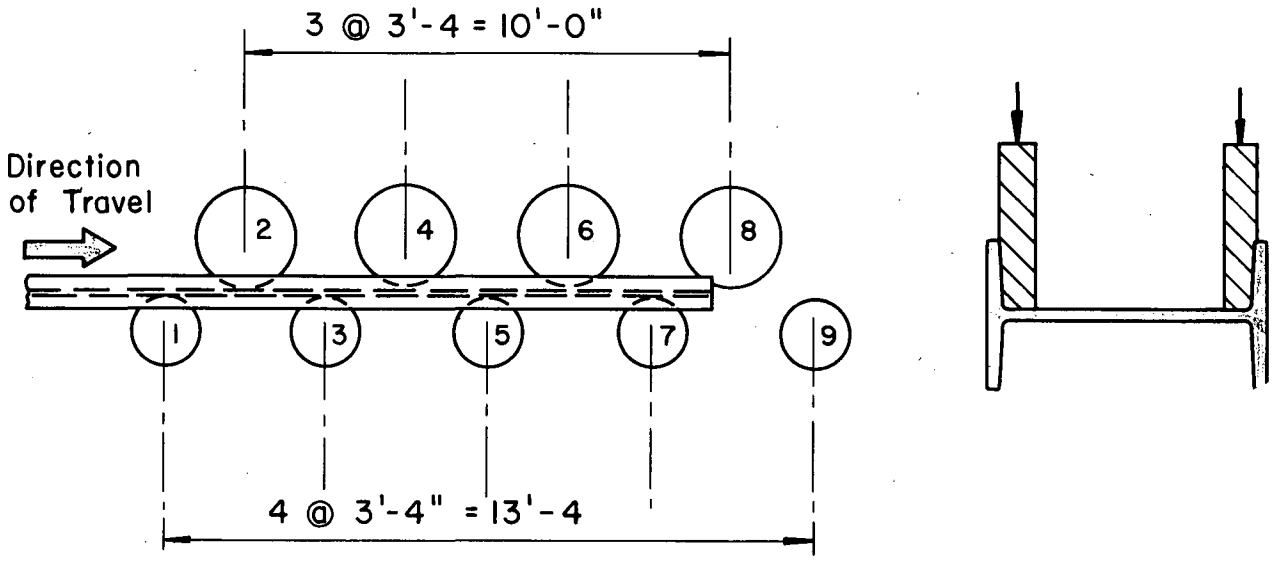

Fig. 2.42 Rotary Straightening Process

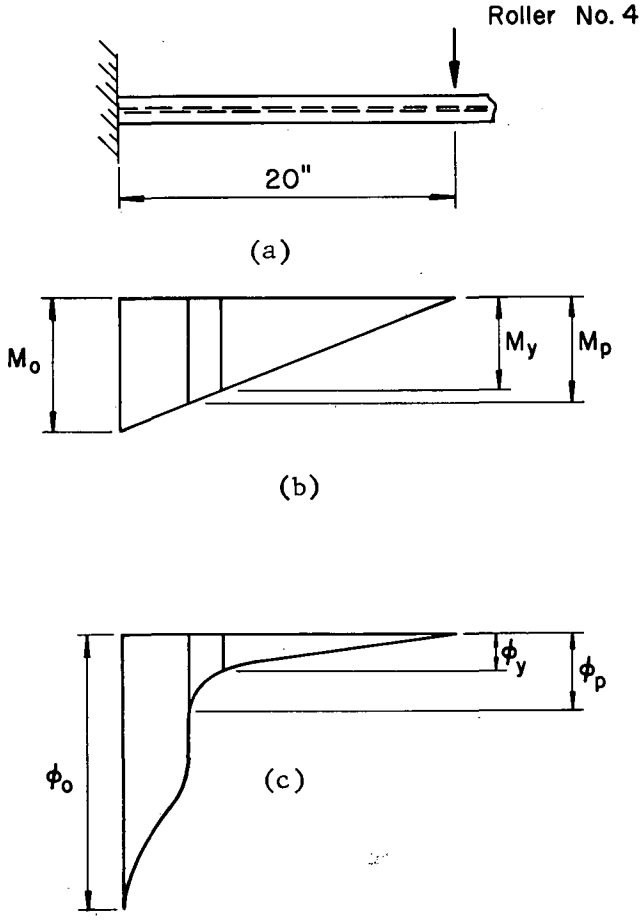

Fig. 2.43 Action of Roller

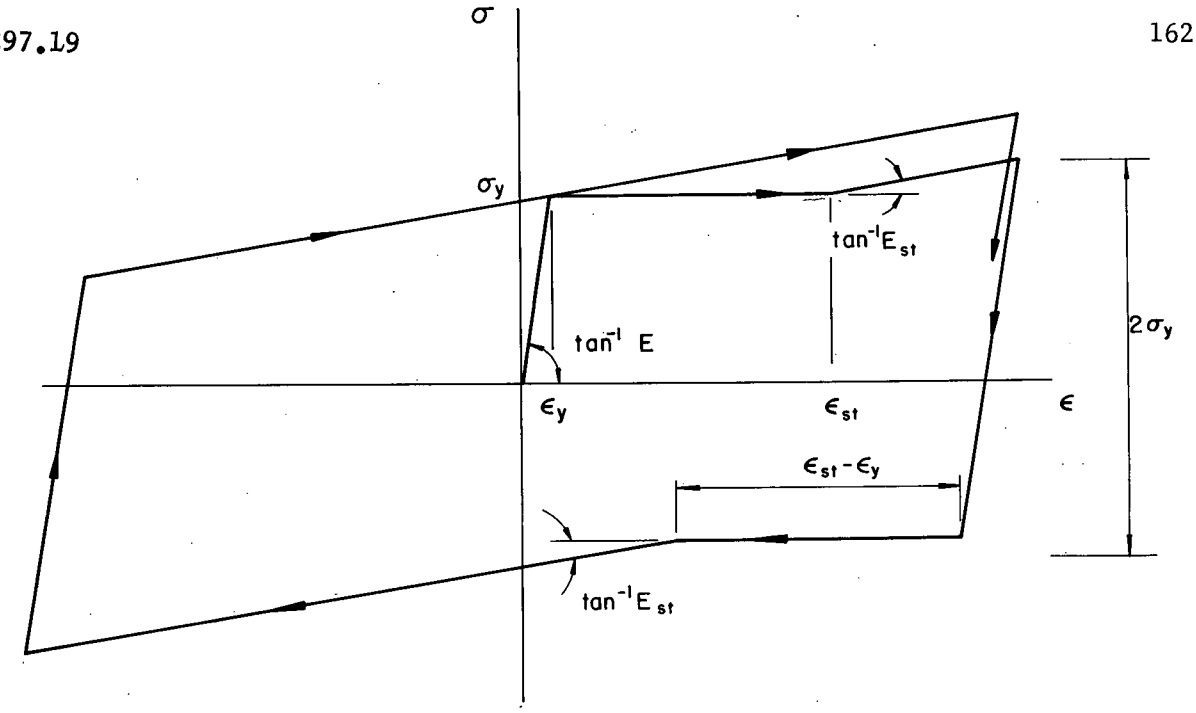

Fig. 2.44 Stress-Strain Diagram for Reversal of Strain

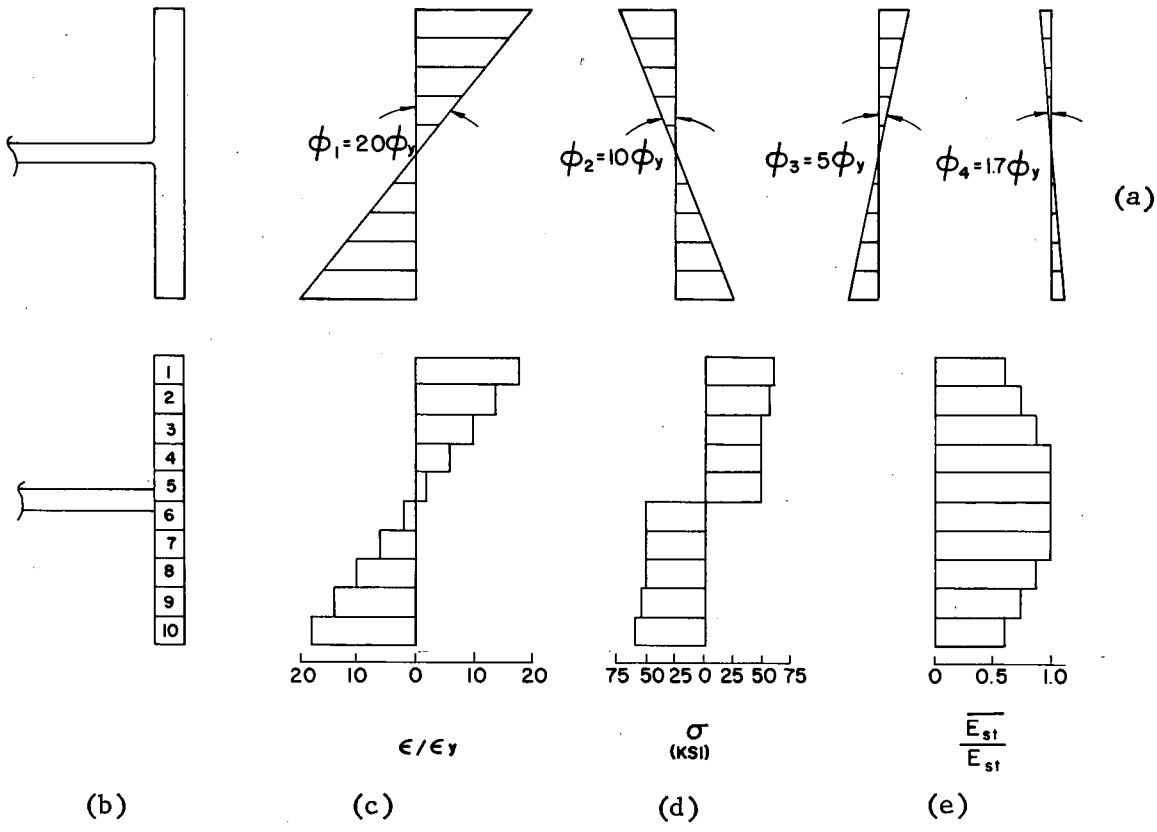

Fig. 2.45 Typical Rotary Straightening Process

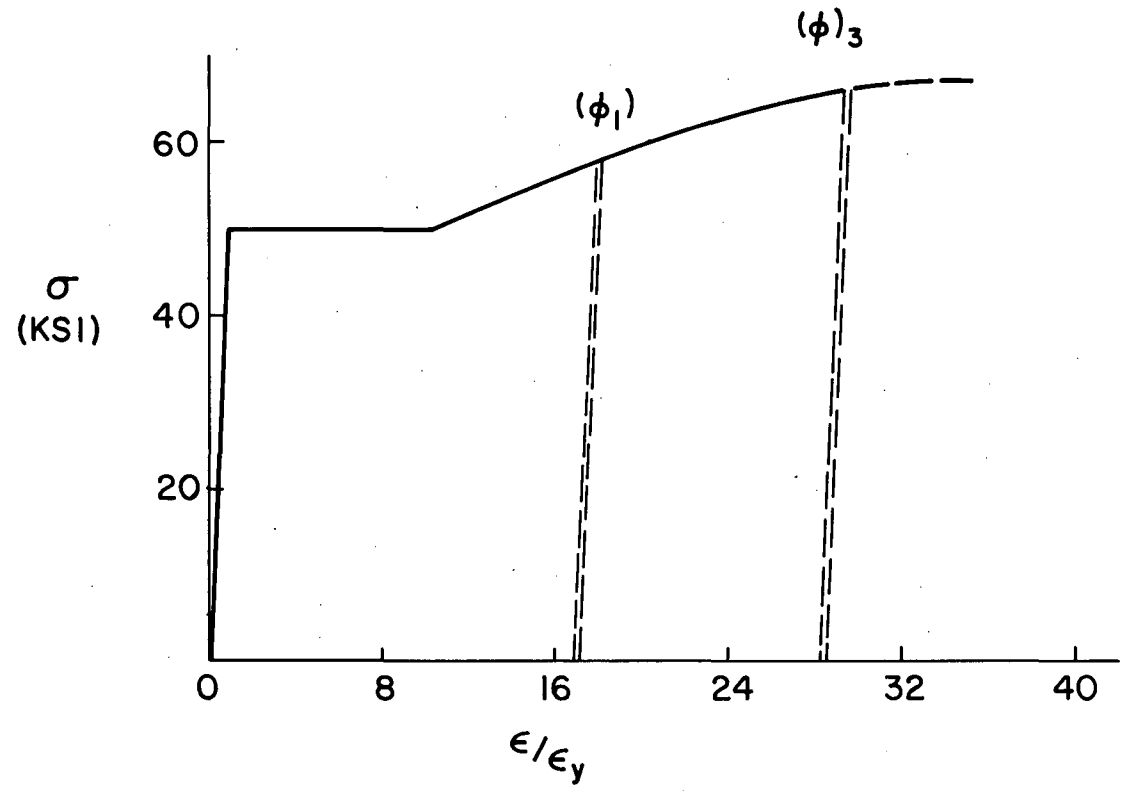

(a)

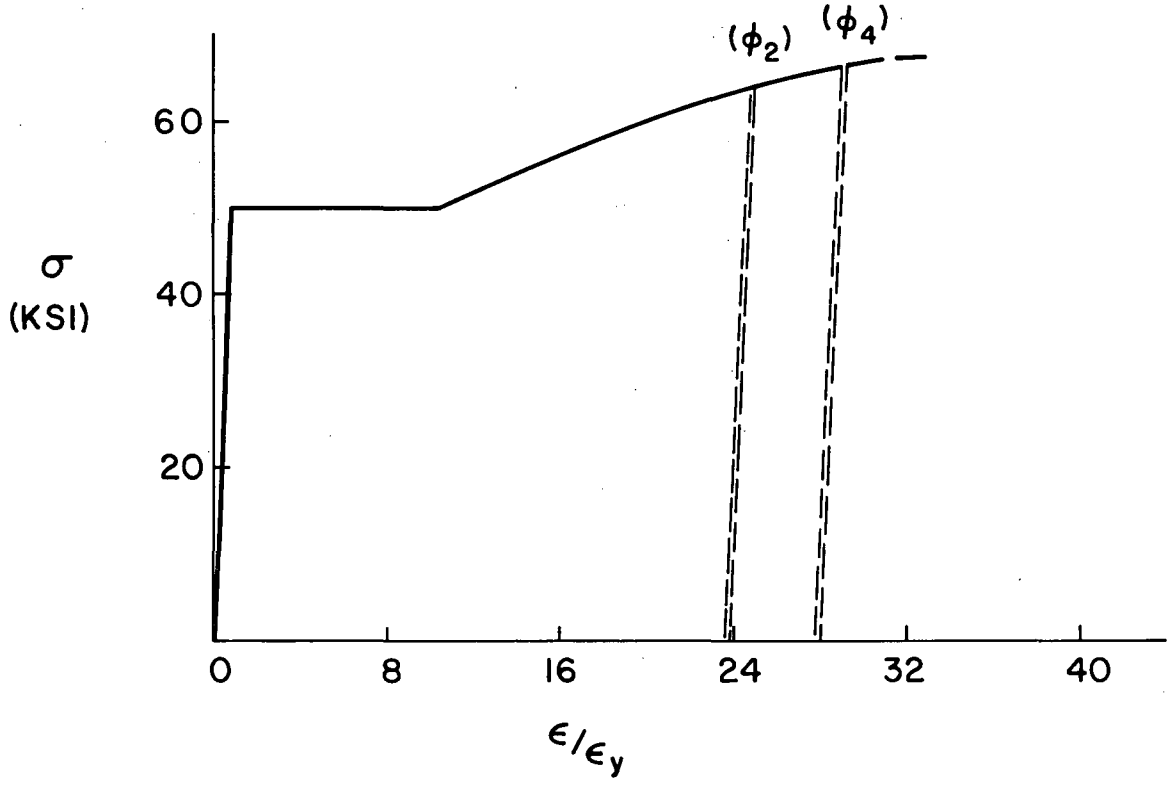

(b)

Fig. 2.46 Strain History of Extreme Element

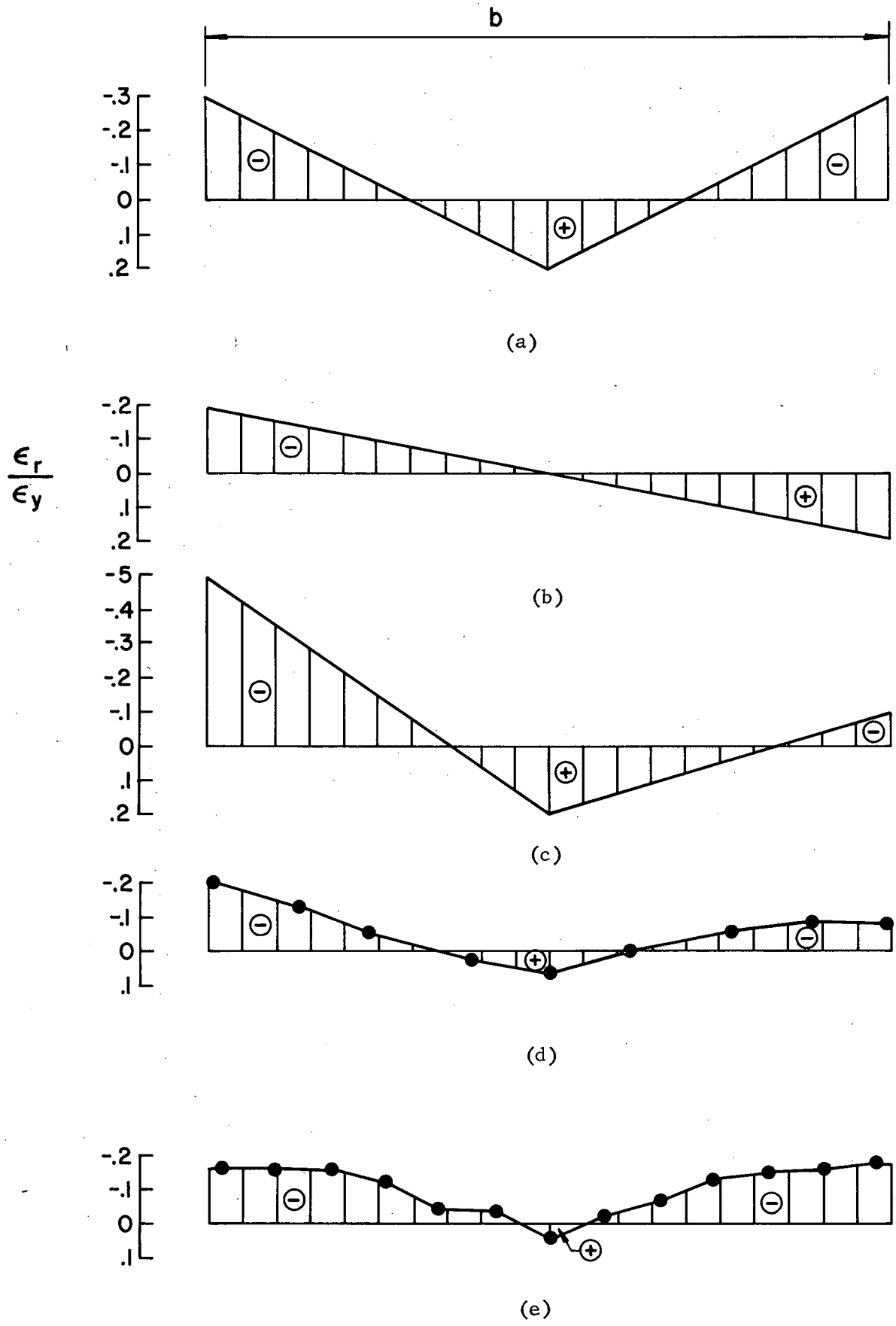

Fig. 2.47 Residual Strains

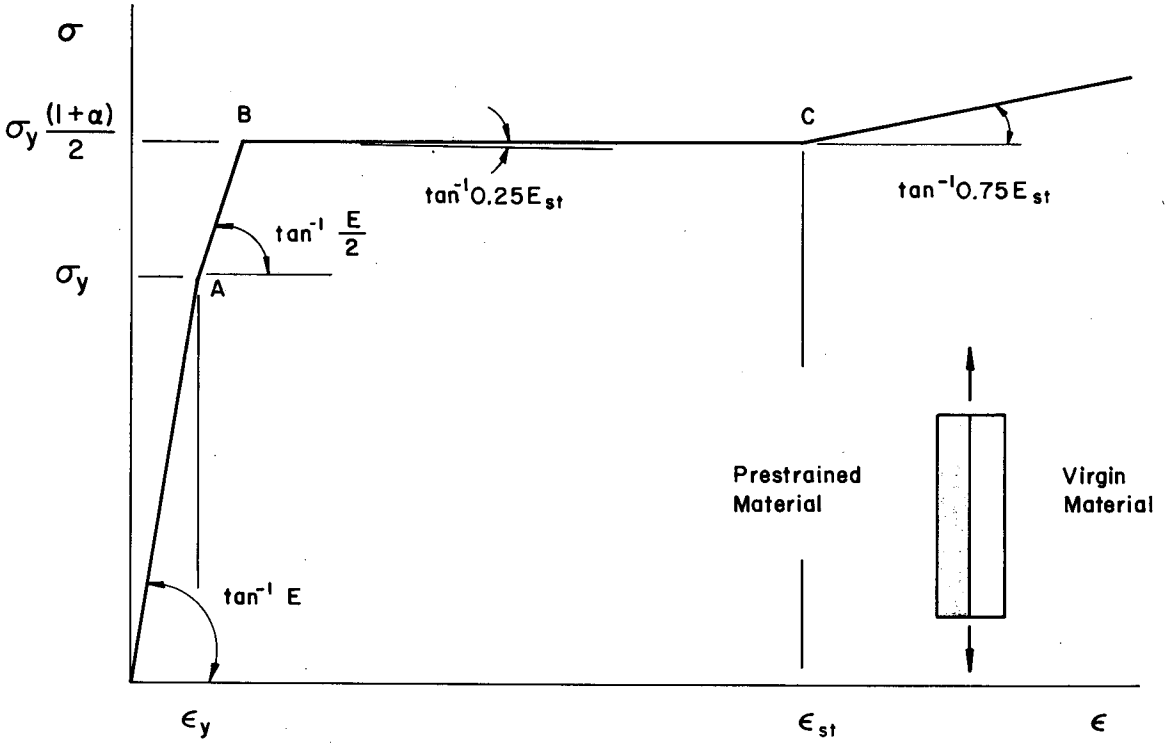

Fig. 2.48 Model for Tensile Specimen

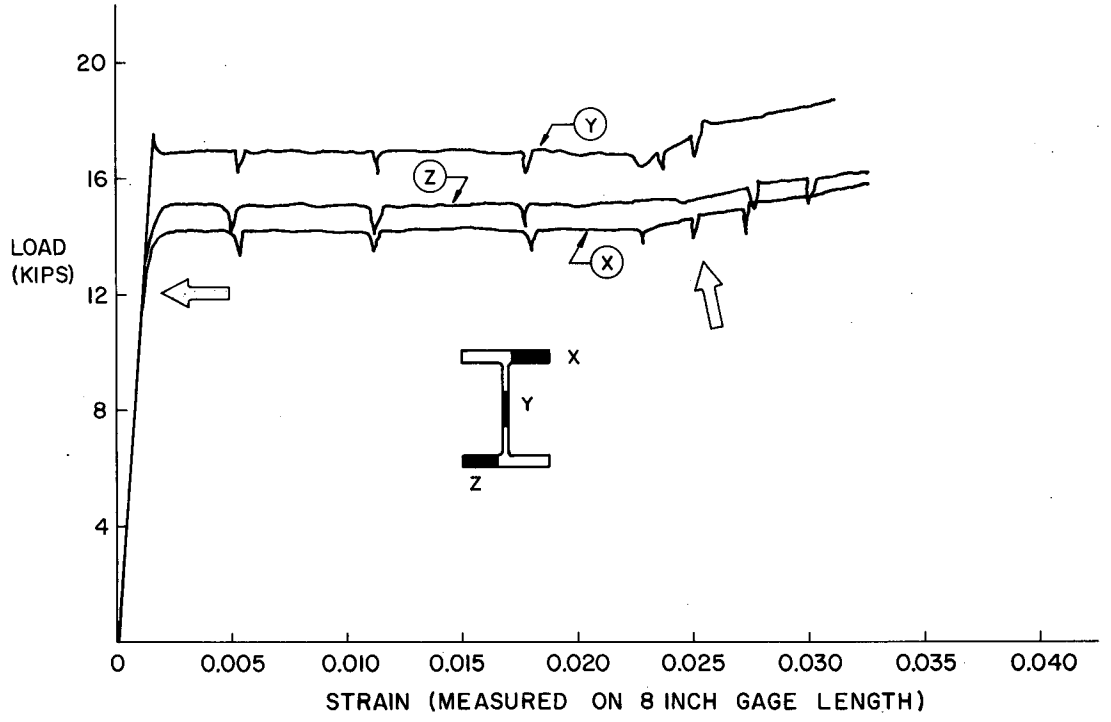

Fig. 2.49 Load-Strain Curves

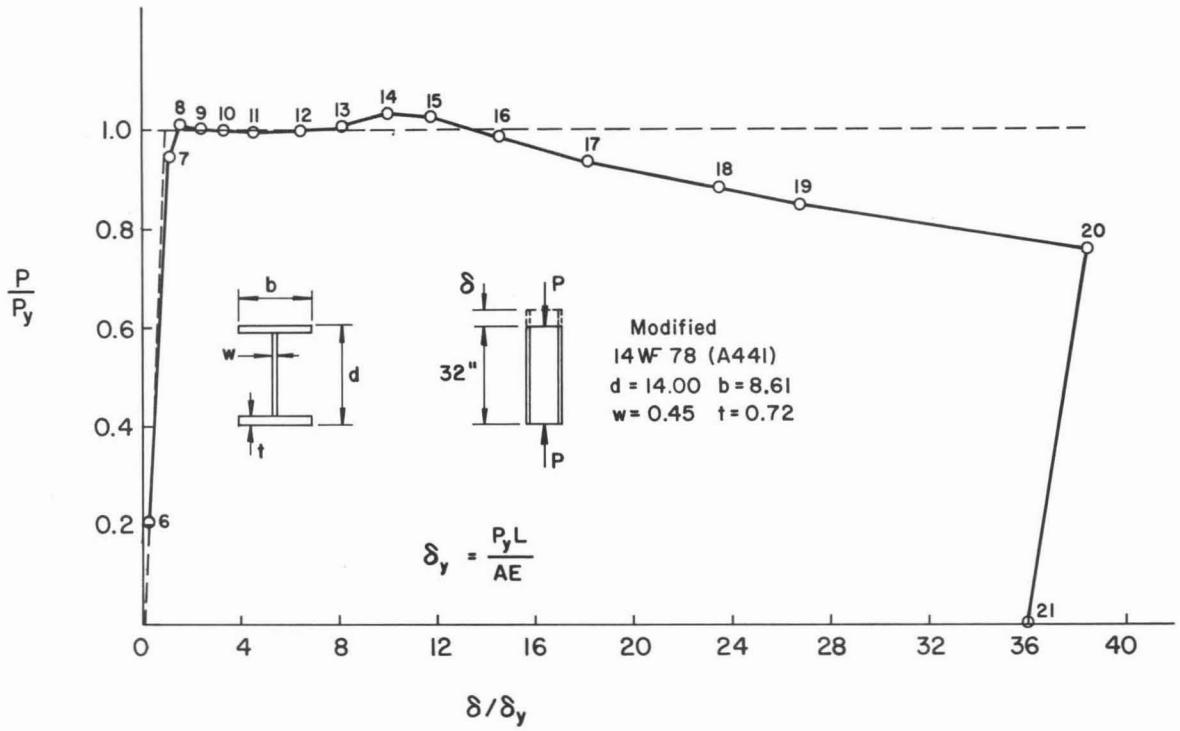

Fig. 3.1 Load-Deformation Curve for Stub Column

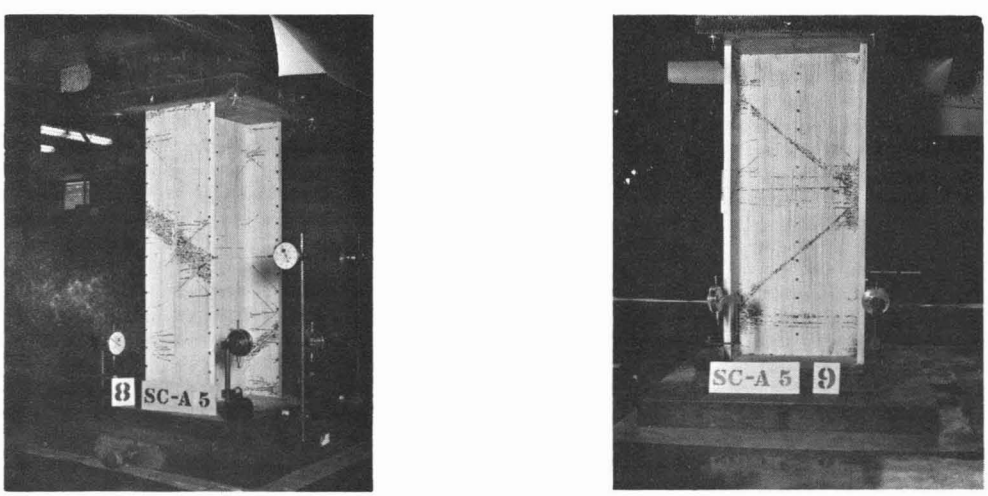

(a) (b)

Fig. 3.2 Progression of Yielding

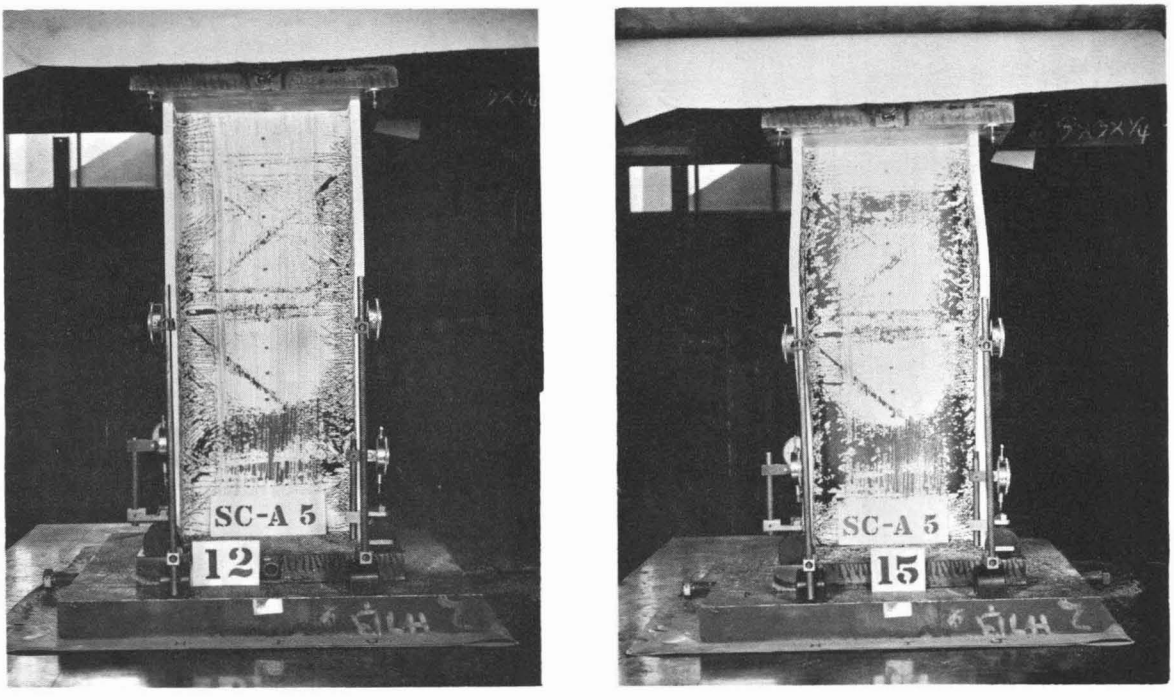

(a) (b)

Fig. 3.3 Condition at Onset of Local Buckling

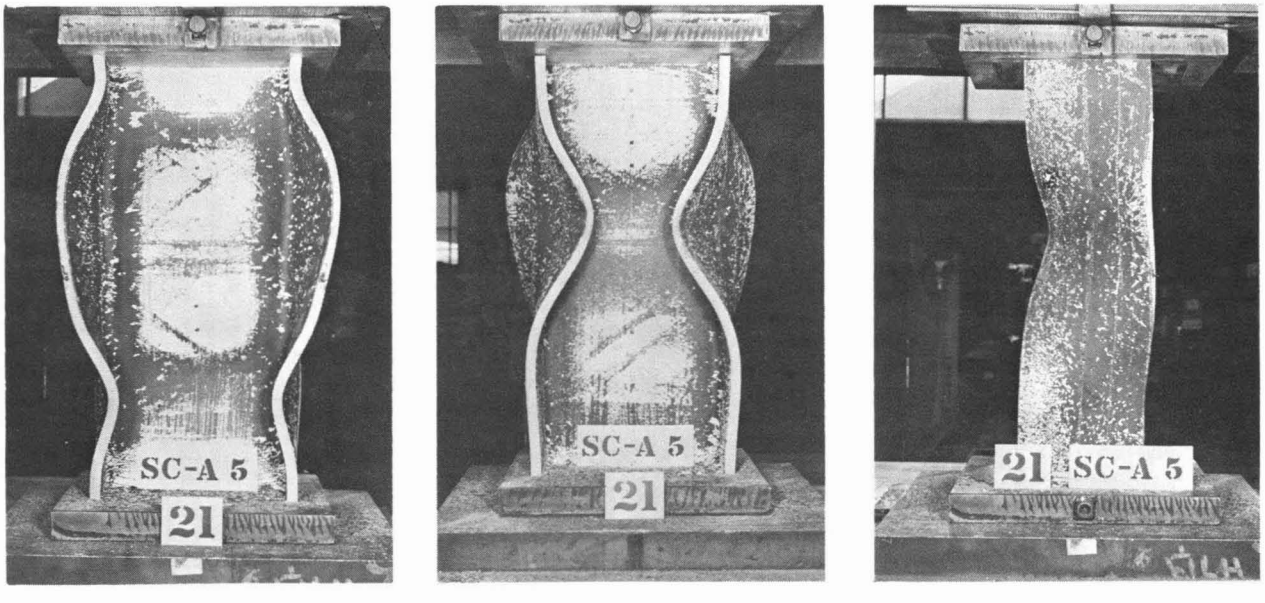

(a) (b) (c)

Fig. 3.4 Condition at Termination of Test

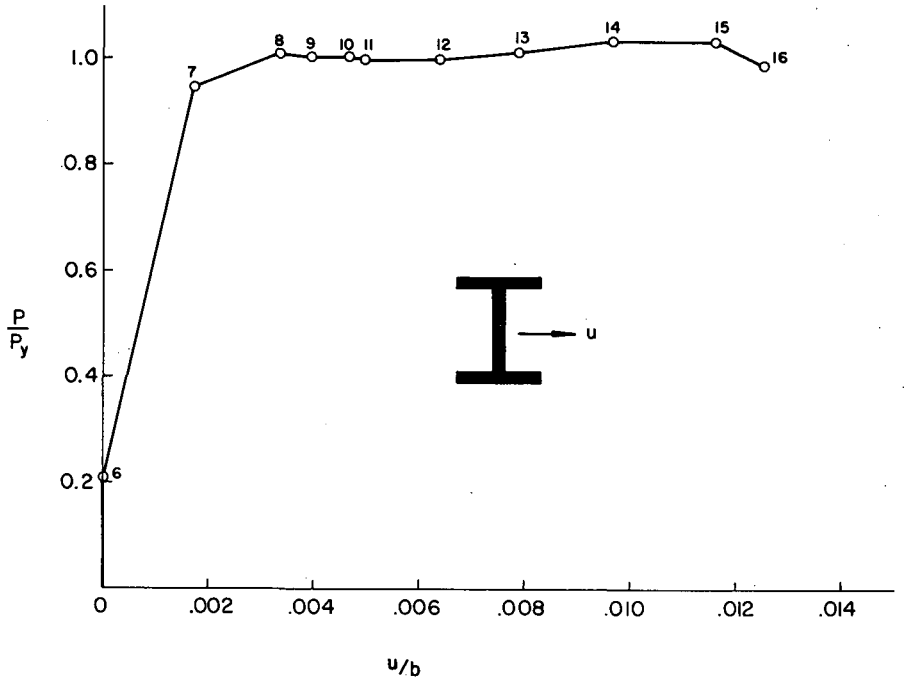

Fig. 3.5 Lateral Deflections

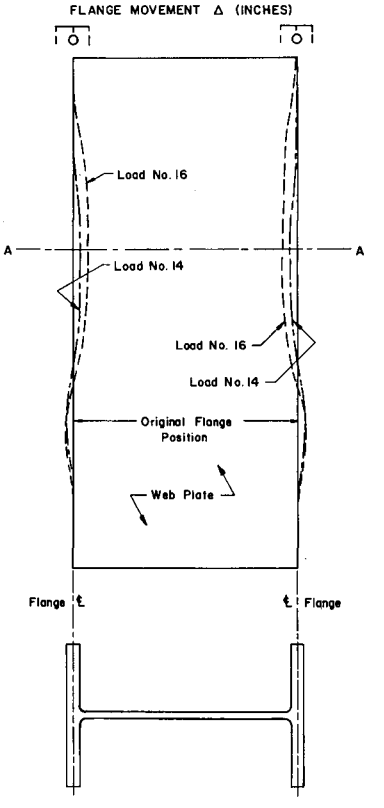

Fig. 3.6 Flange Movements

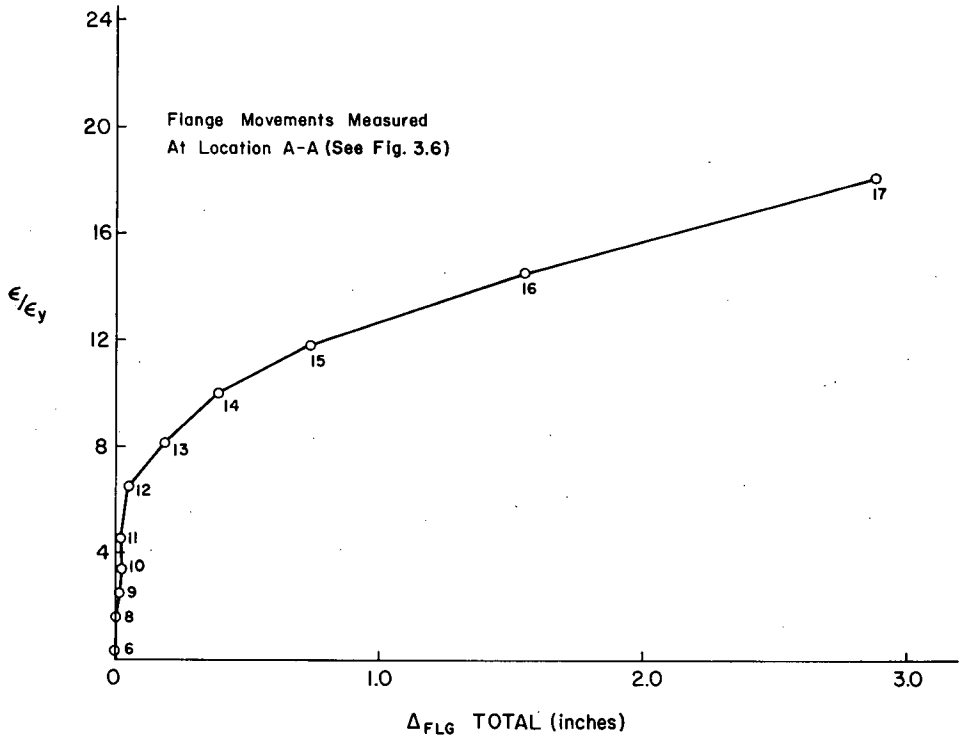

Fig. 3.7 Strain-Flange Deformation Curve

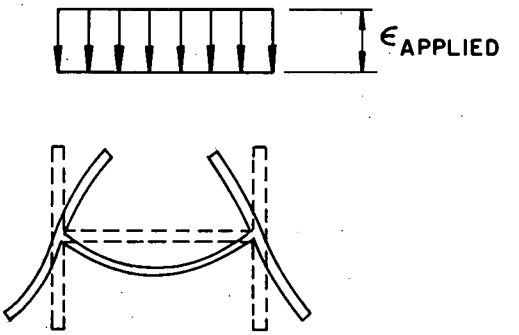

Fig. 3.8 Deformed Shape of Cross-Section

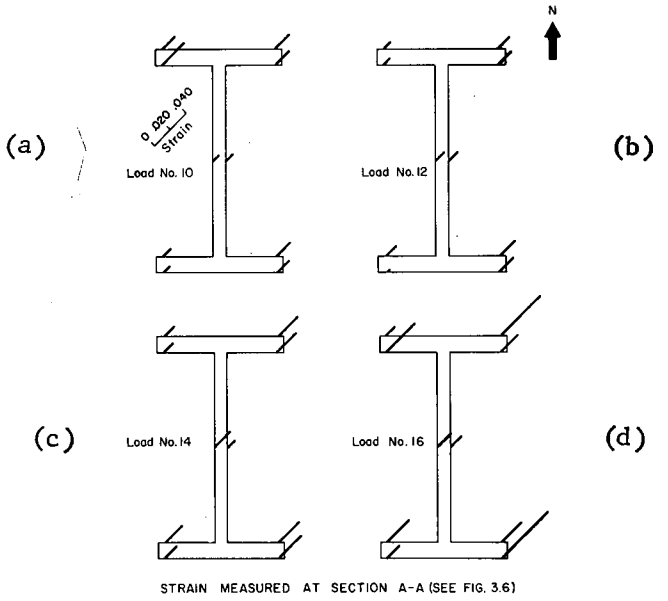

Fig. 3.9 Strain Distributions

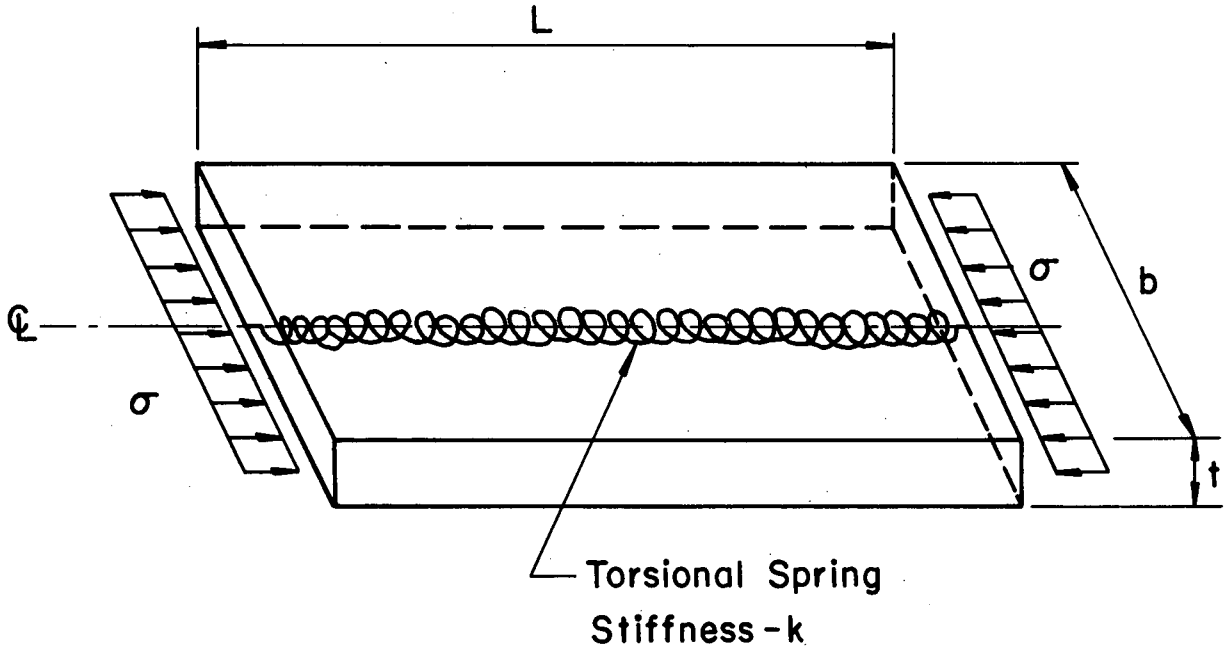

Fig. 3.10 Torsional Buckling Model

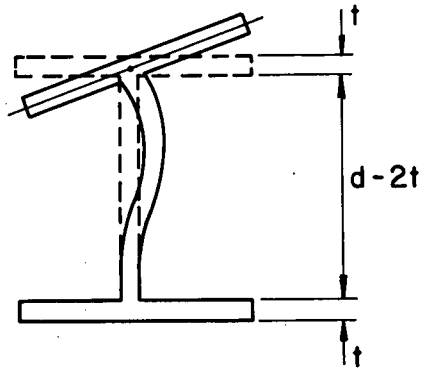

Fig. 3.11 Action of Web

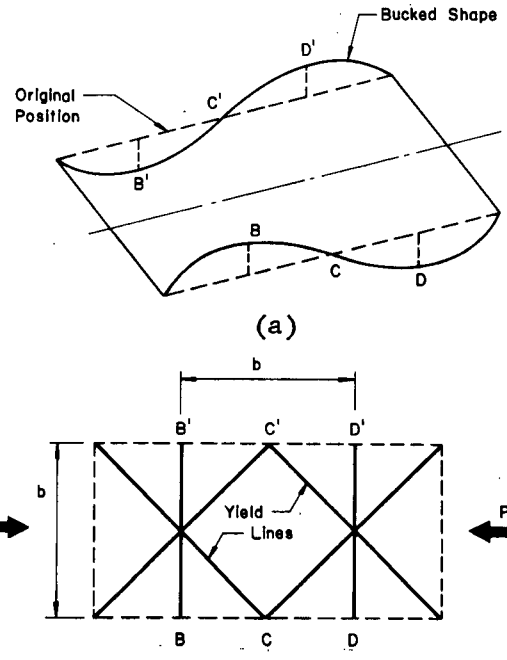

Fig. 3.12 Flange Buckling Model

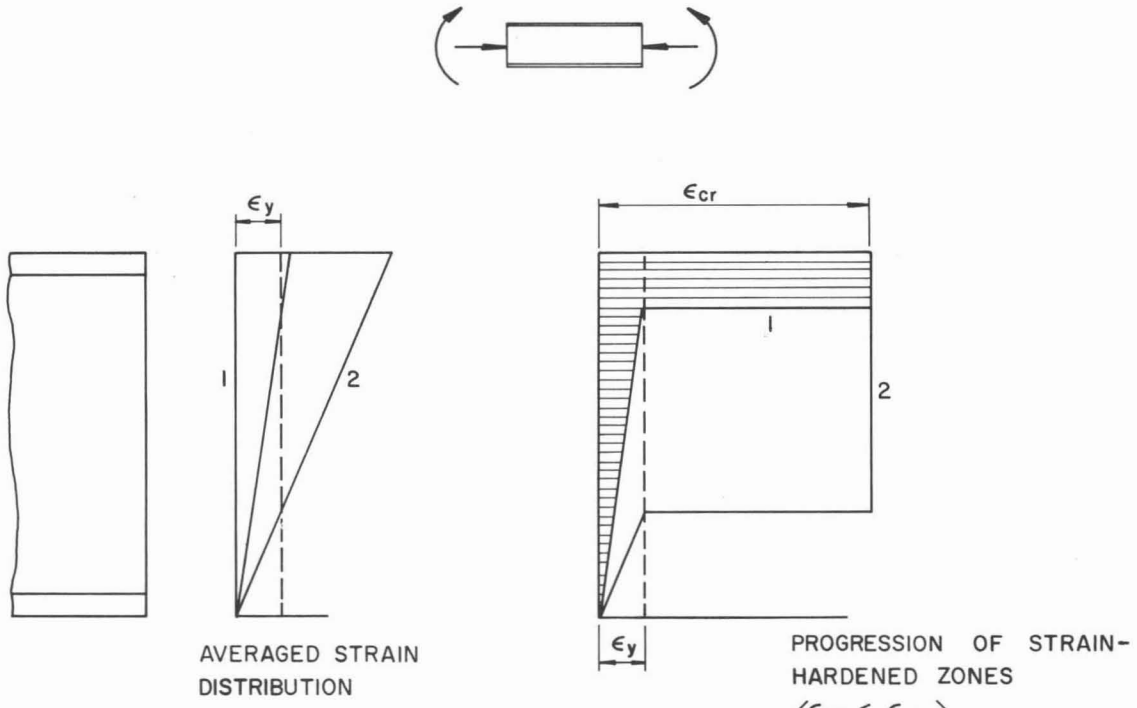

Fig. 3.13 Condition of Web Plate

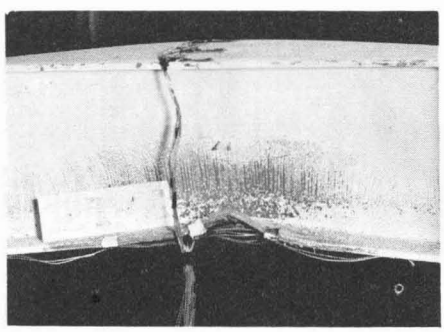

Fig. 3.14 Local Flange Buckling

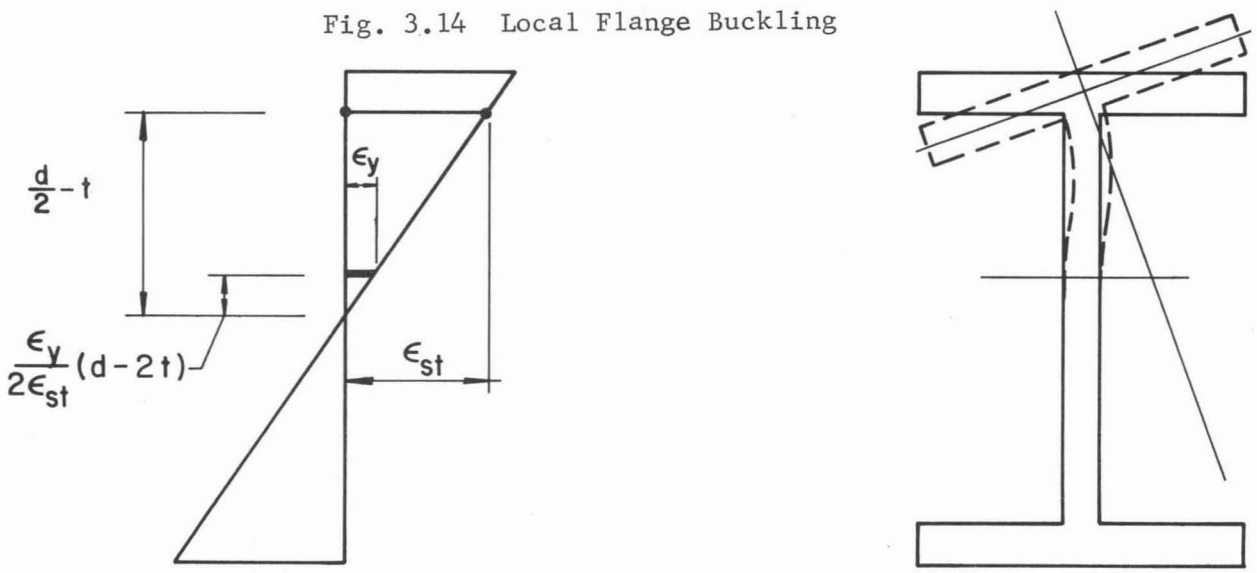

Fig. 3.15 Restraint Due to Web

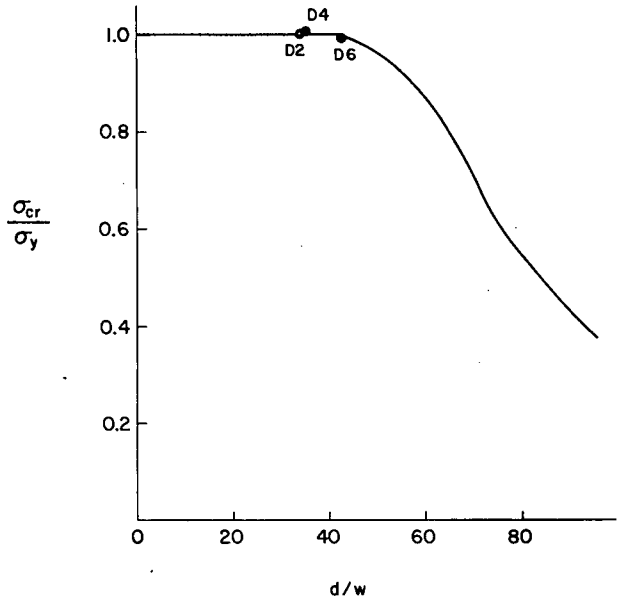

Fig. 3.16 Critical Stress for Web Buckling

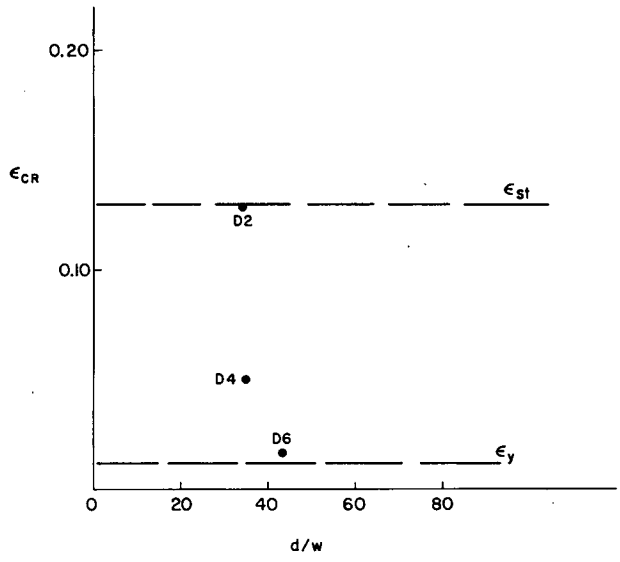

Fig. 3.17 Critical Strain for Web Buckling

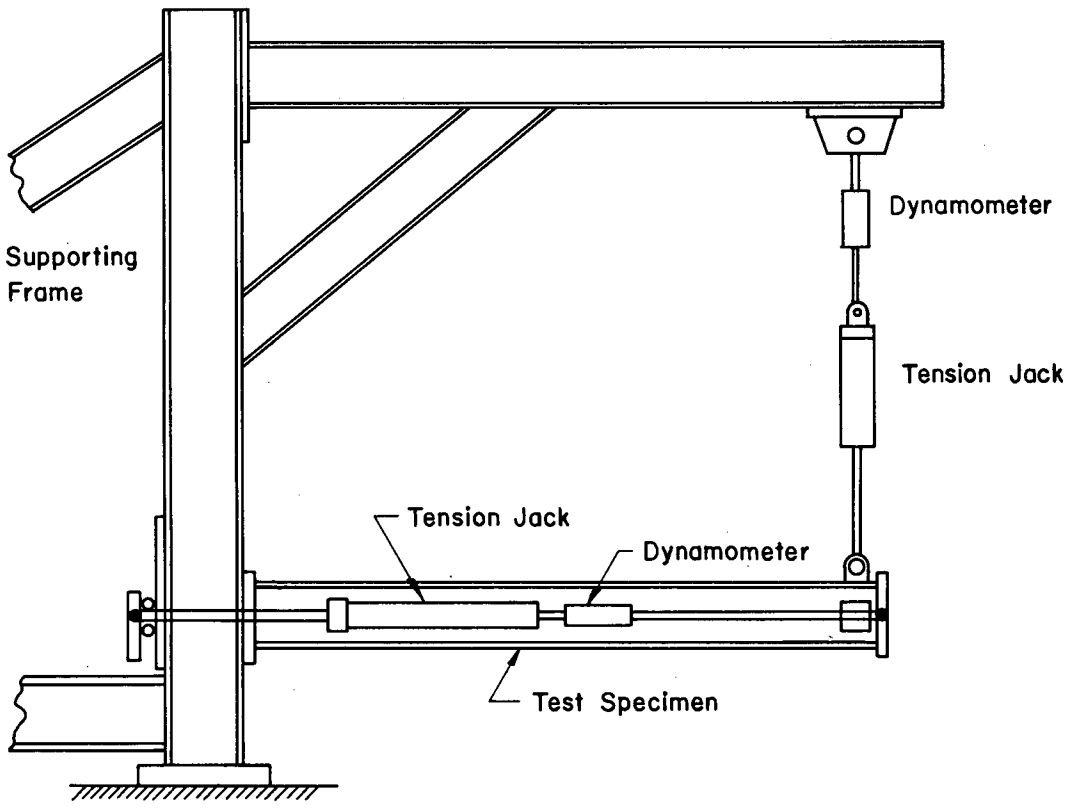

Fig. 3.18 Test Arrangement

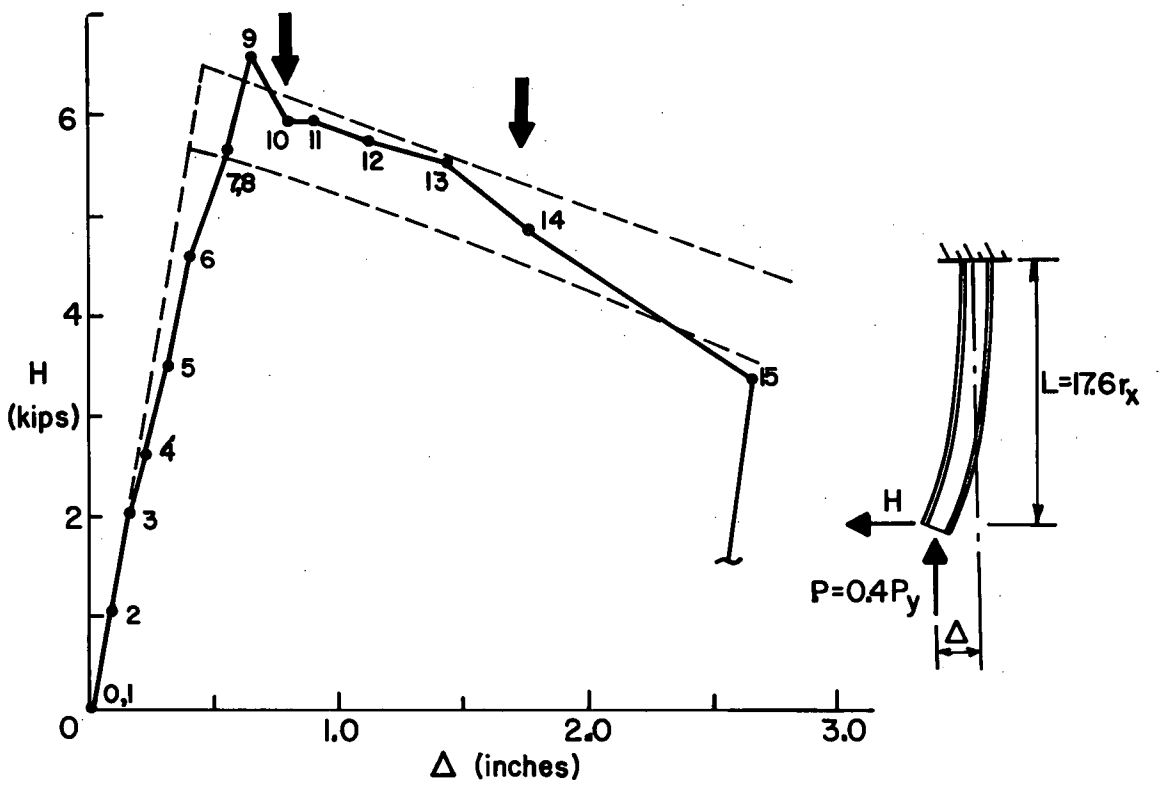

Fig. 3.19 Load-Deflection Relationship

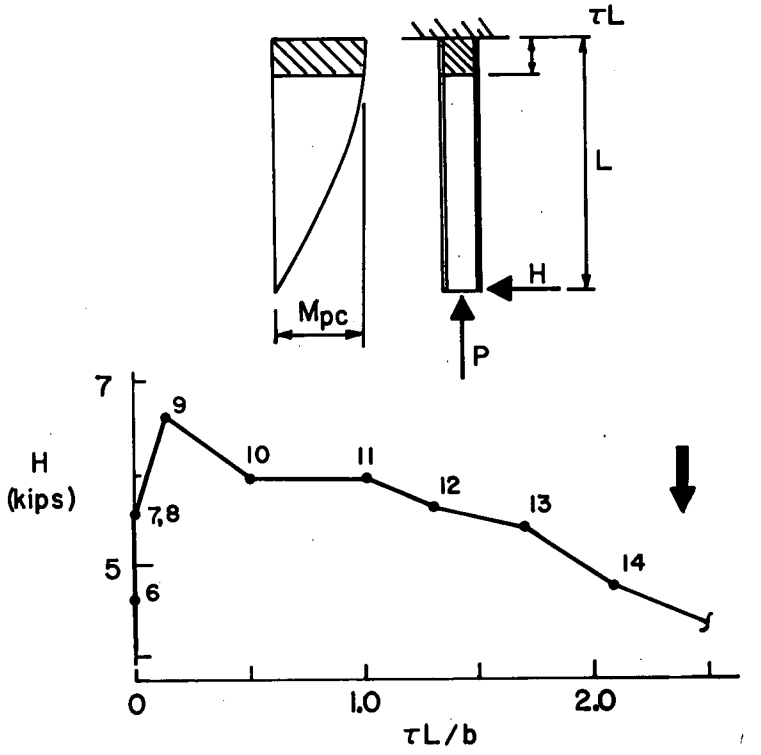

Fig. 3.20 Progression of Yielded Length

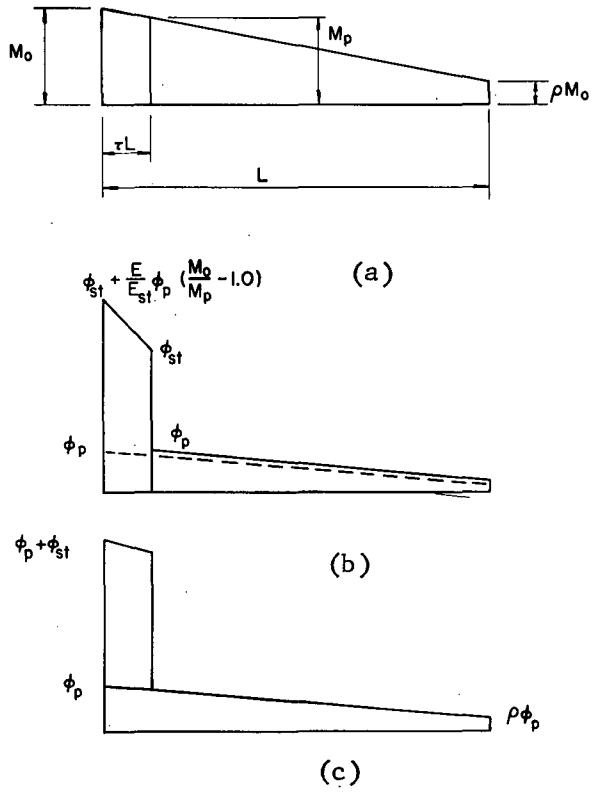

Fig. 3.21 Yielded Member Segment

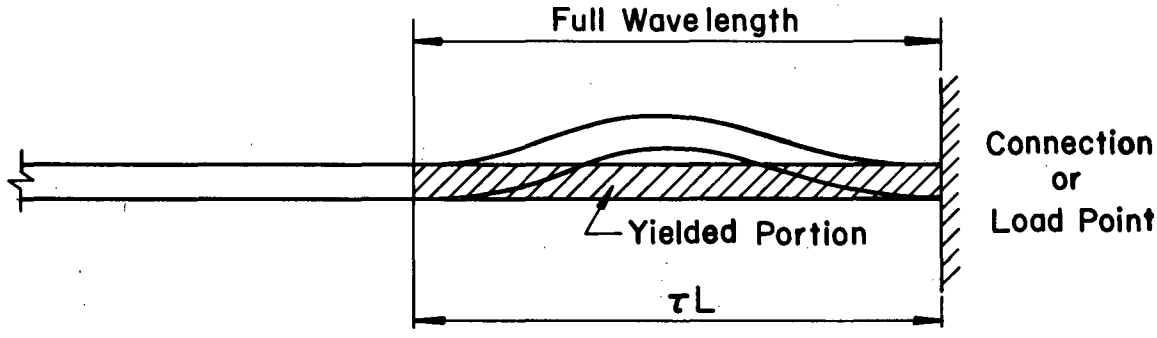

LOCAL BUCKLE UNDER
MOMENT GRADIENT

Fig. 3.22 Buckled Shape of Flange Plate

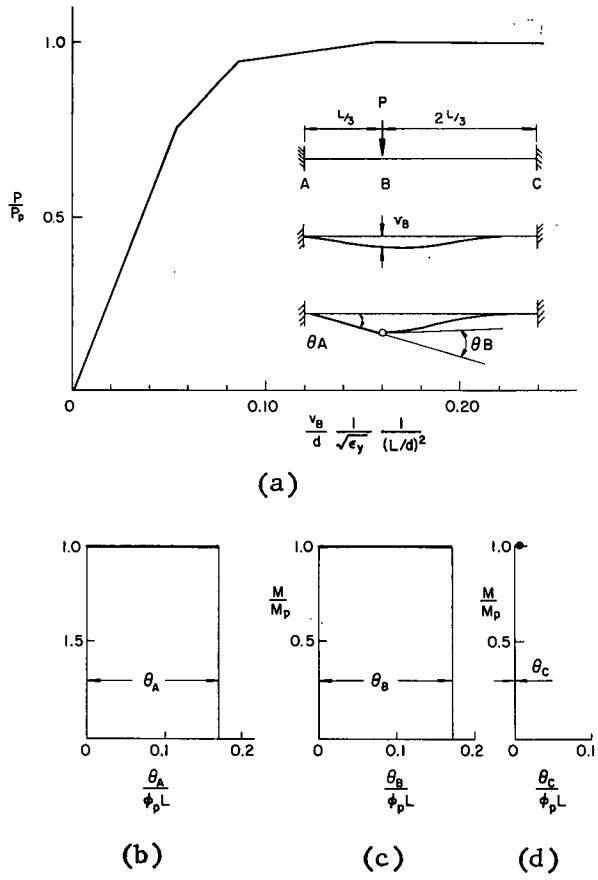

Fig. 3.23 Fixed-End Beam

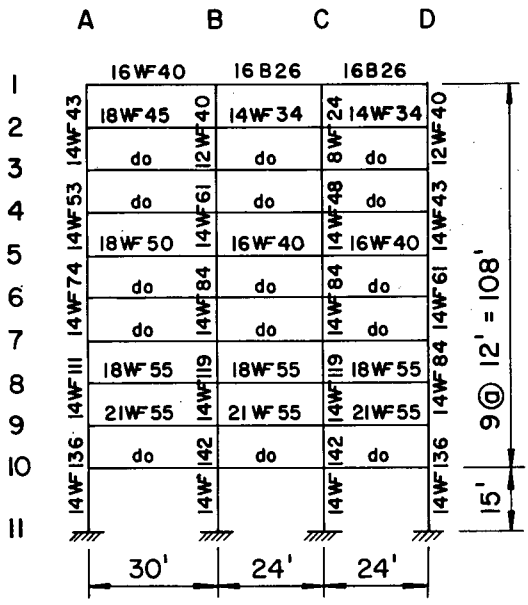

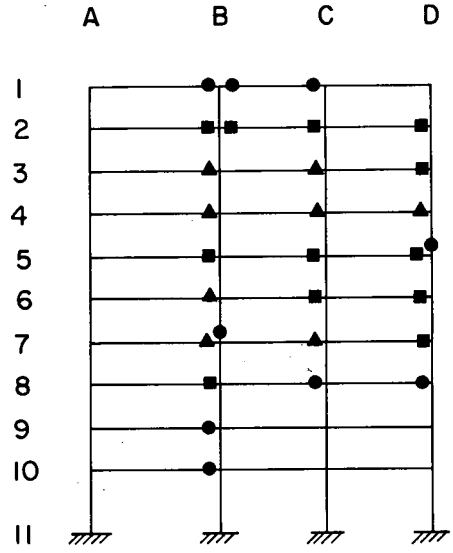

▲ Hinge forms between 0.8 and 0.9 x design ultimate load.

■ Hinge forms between 0.9 and 1.0 x design ultimate load.

● Hinge forms between 1.0 and 1.1 design ultimate load.

Fig. 3.24 Ten Story Frame

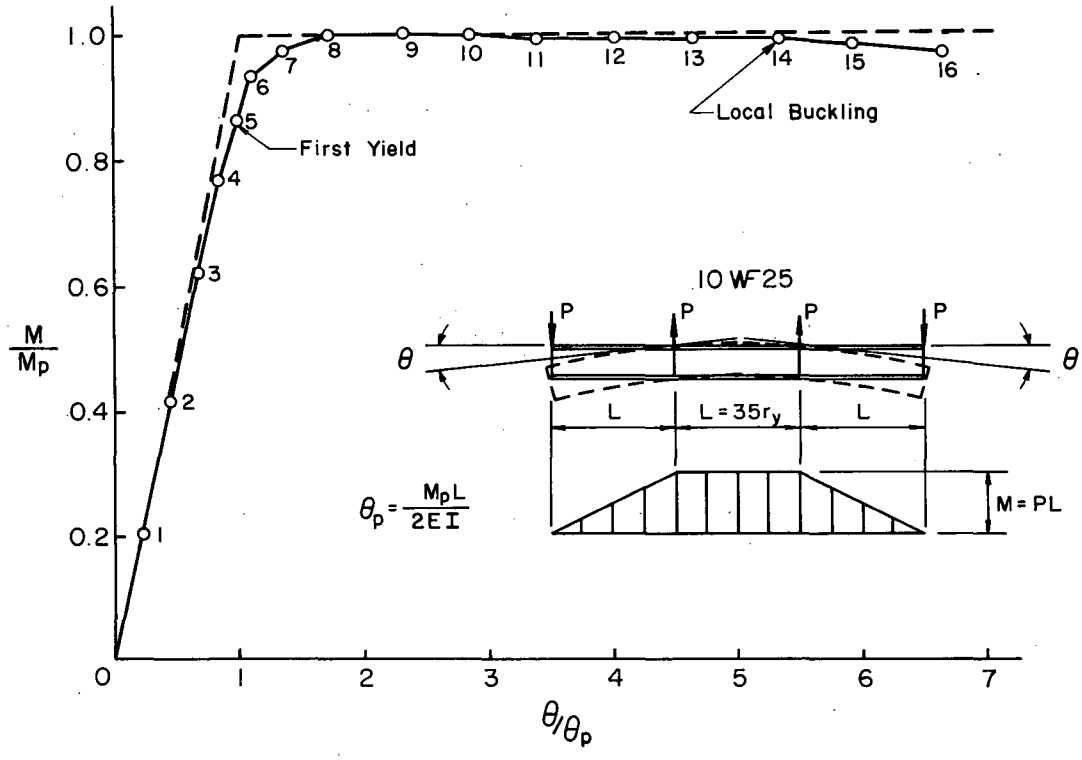

Fig. 4.1 Moment-Rotation Relationship

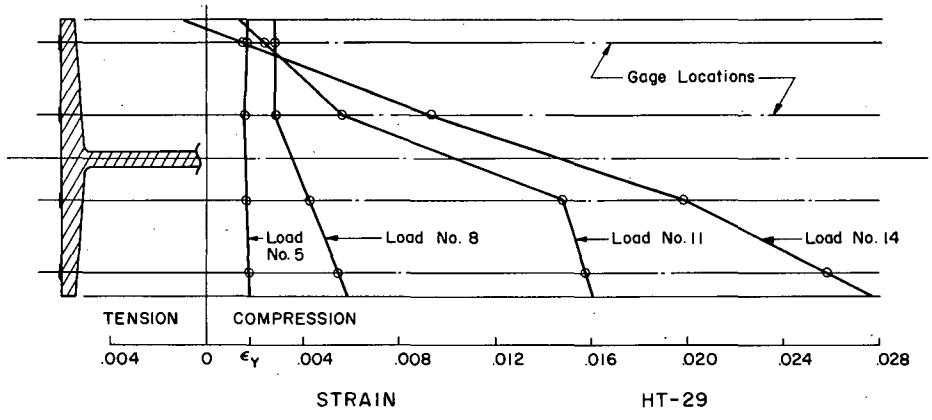

Fig. 4.2 Lateral Bending Strains

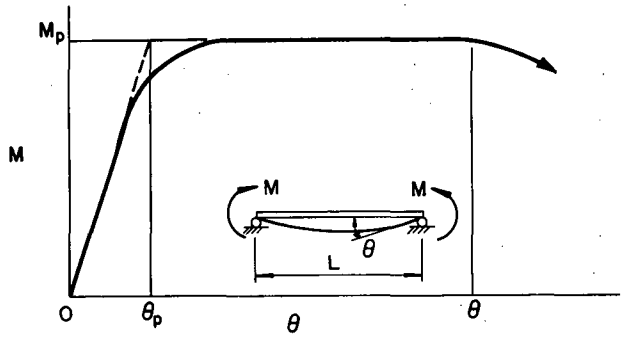

Fig. 4.3 Rotation Capacity Definition

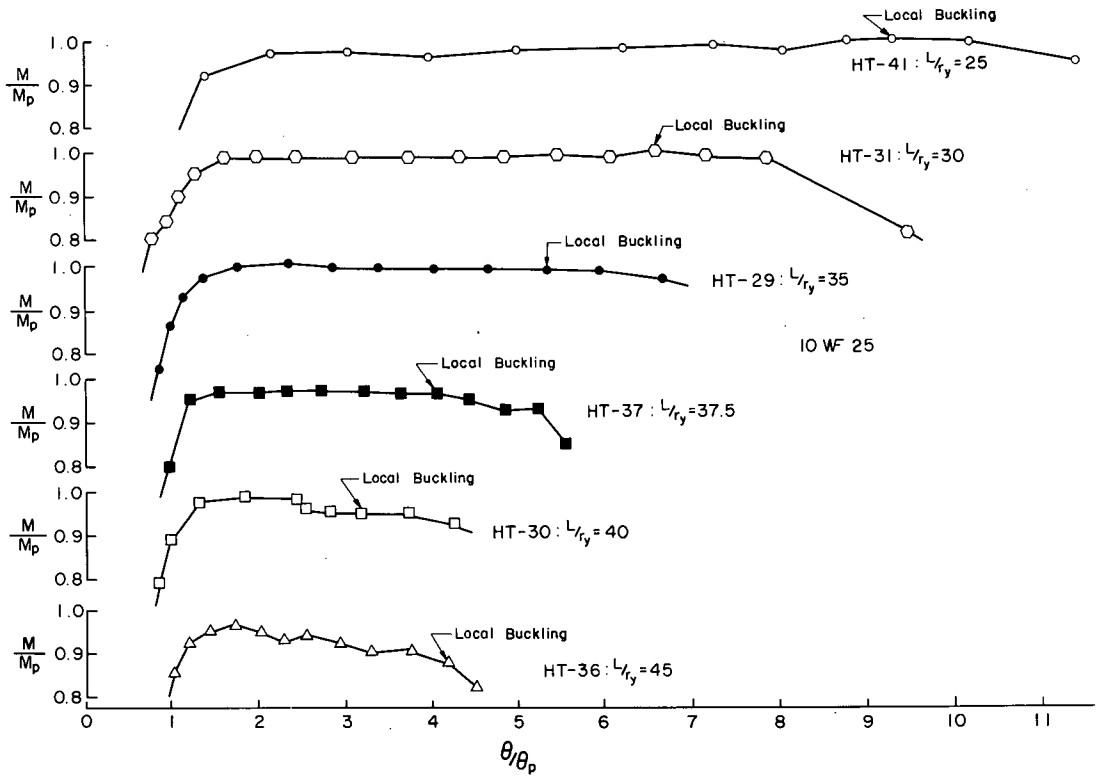

Fig. 4.4 Beams Under Uniform Moment

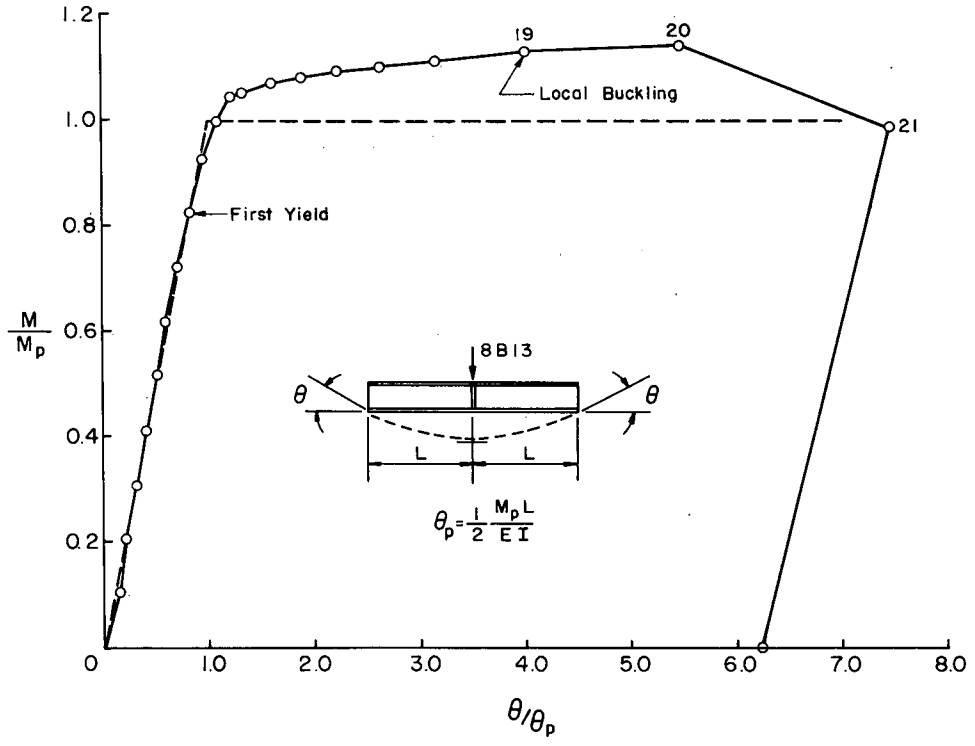

Fig. 4.5 Moment-Rotation Curve

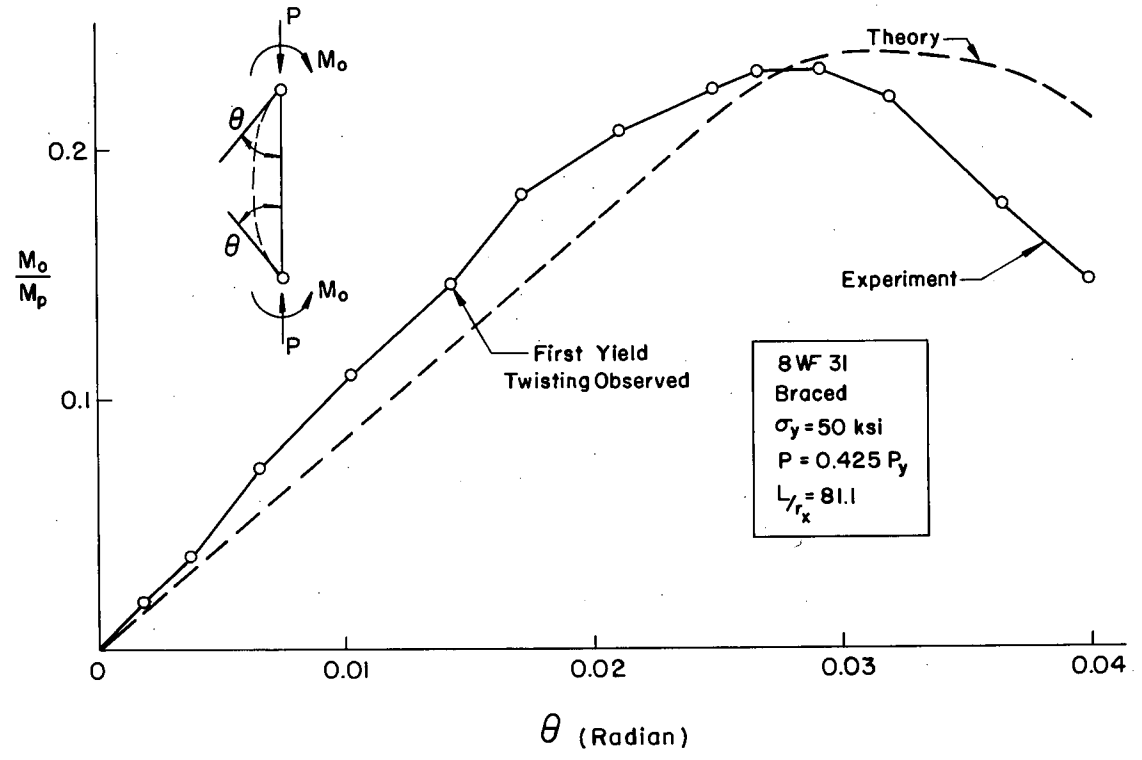

Fig. 4.6 Moment-Rotation Curve for Braced Beam-Column

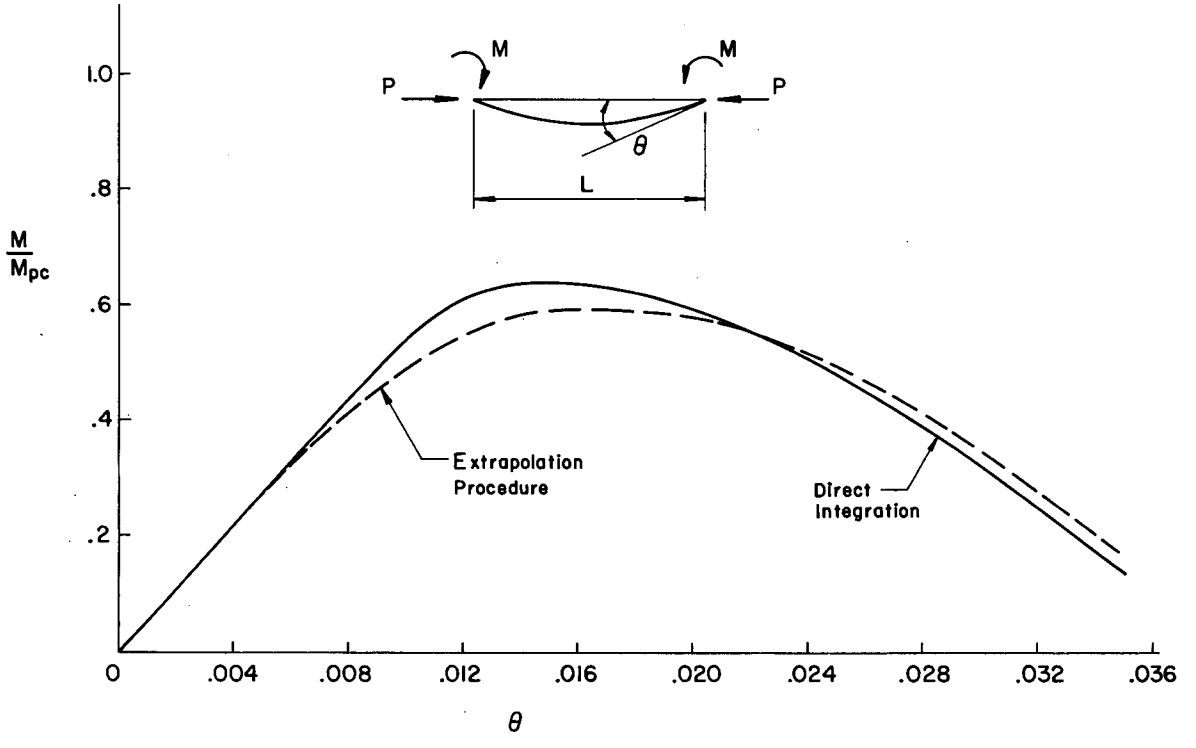

Fig. 4.7 Comparison of Extrapolation Procedure

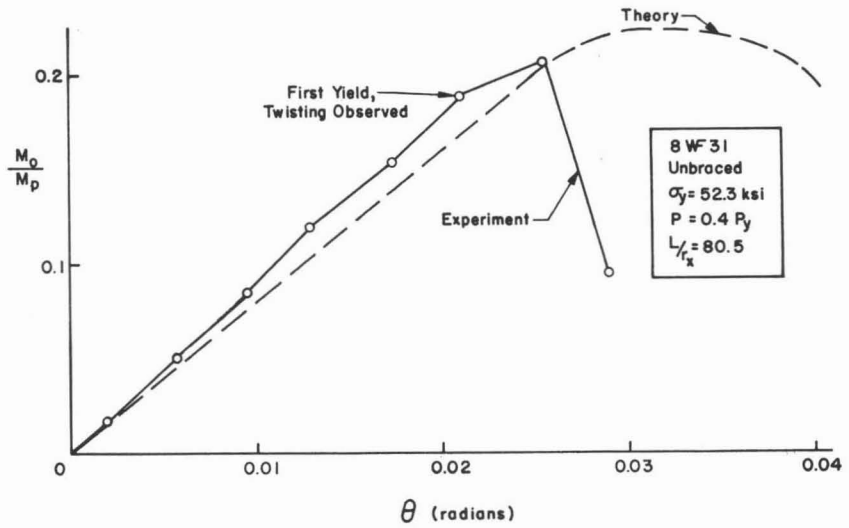

Fig. 4.8 Moment-Rotation Curve for Unbraced Beam-Column

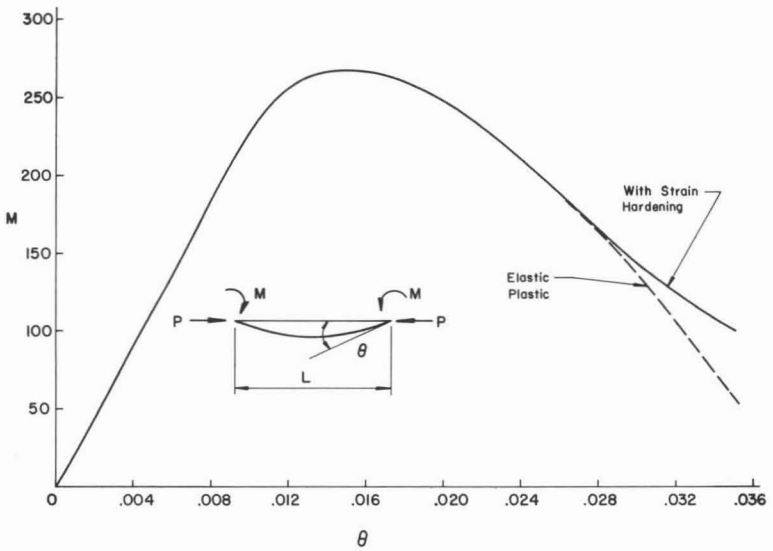

Fig. 4.9 Moment-Rotation Curve Including Strain-Hardening Influence

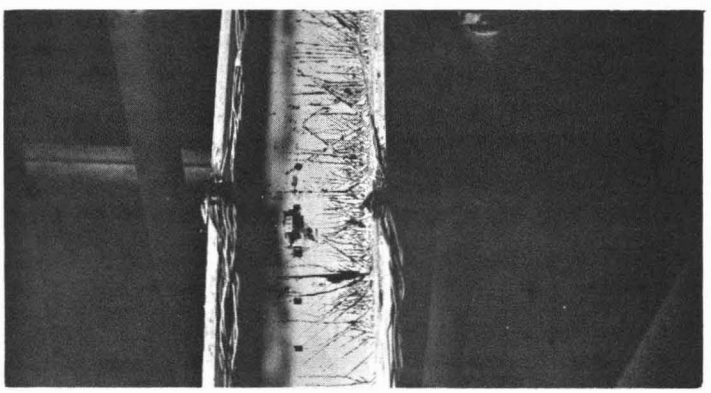

Fig. 4.10 Mid-Height Area of Beam-Column After Test

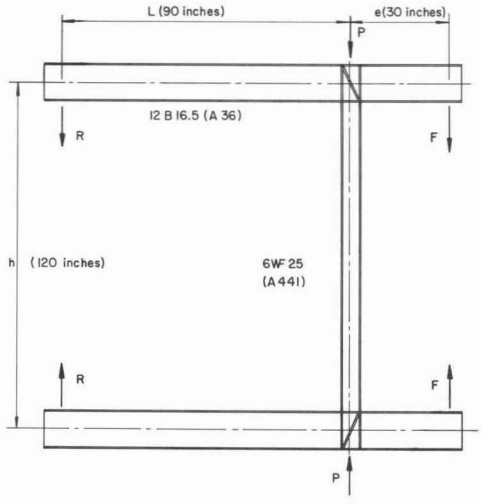

Fig. 5.1 Braced Hybrid Subassemblage

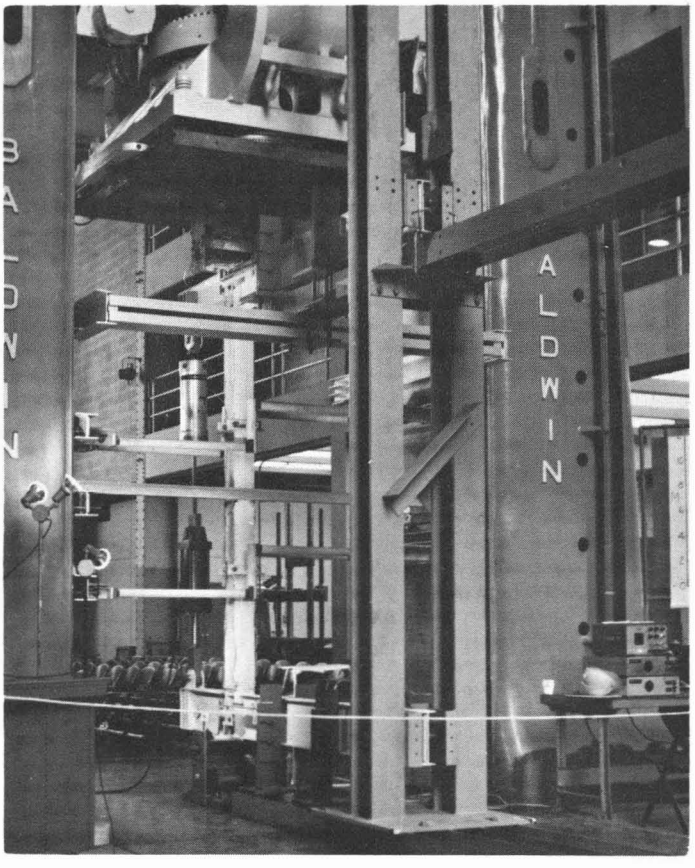

Fig. 5.2 Braced Subassemblage Under Test

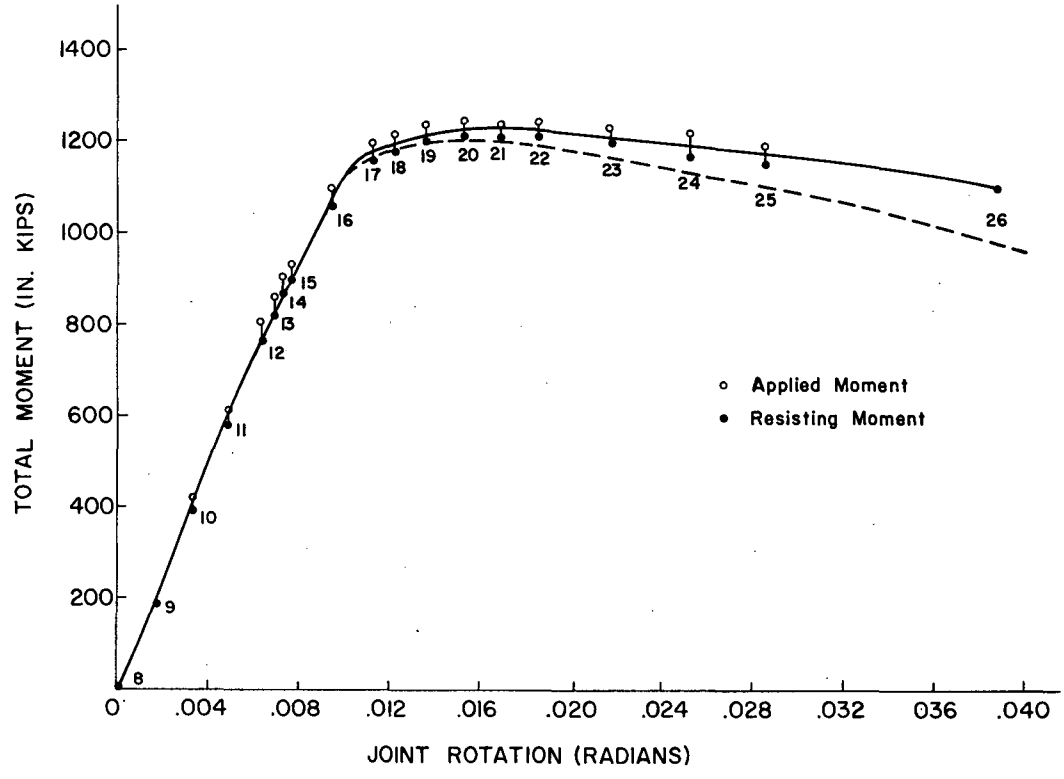

Fig. 5.3 Moment-Rotation Curve for Subassemblage

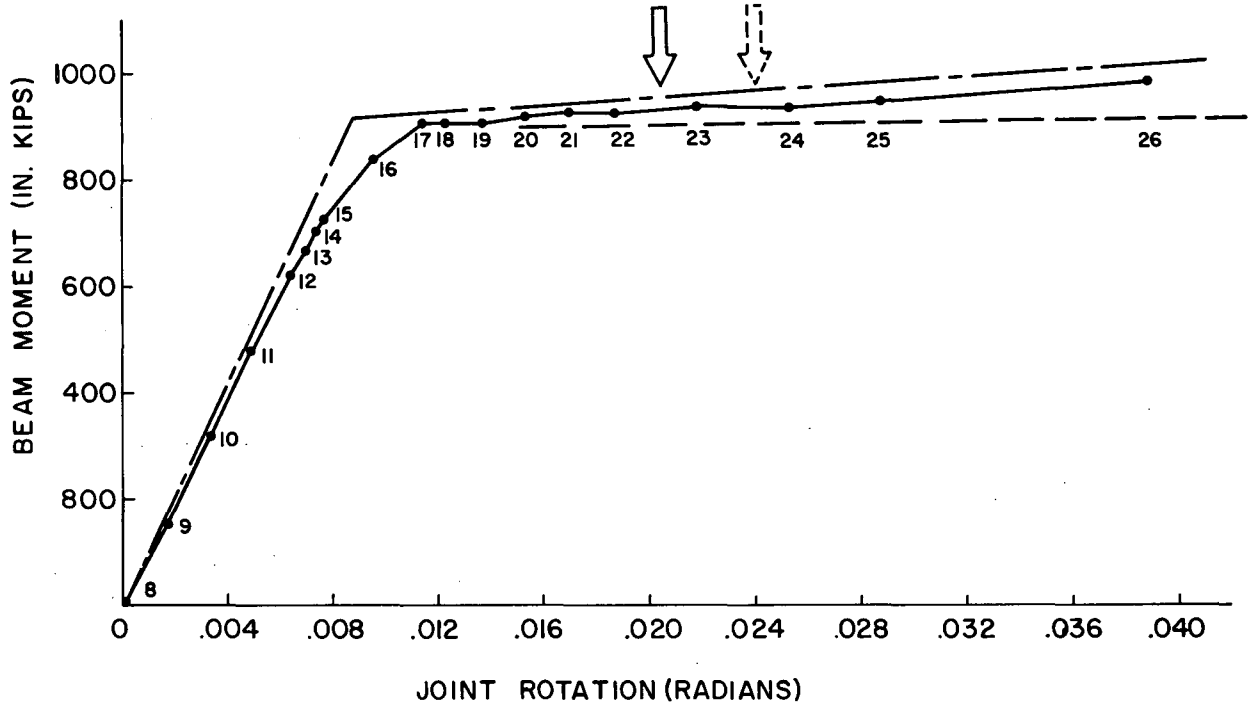

Fig. 5.4 Beam Moment-Rotation Curve

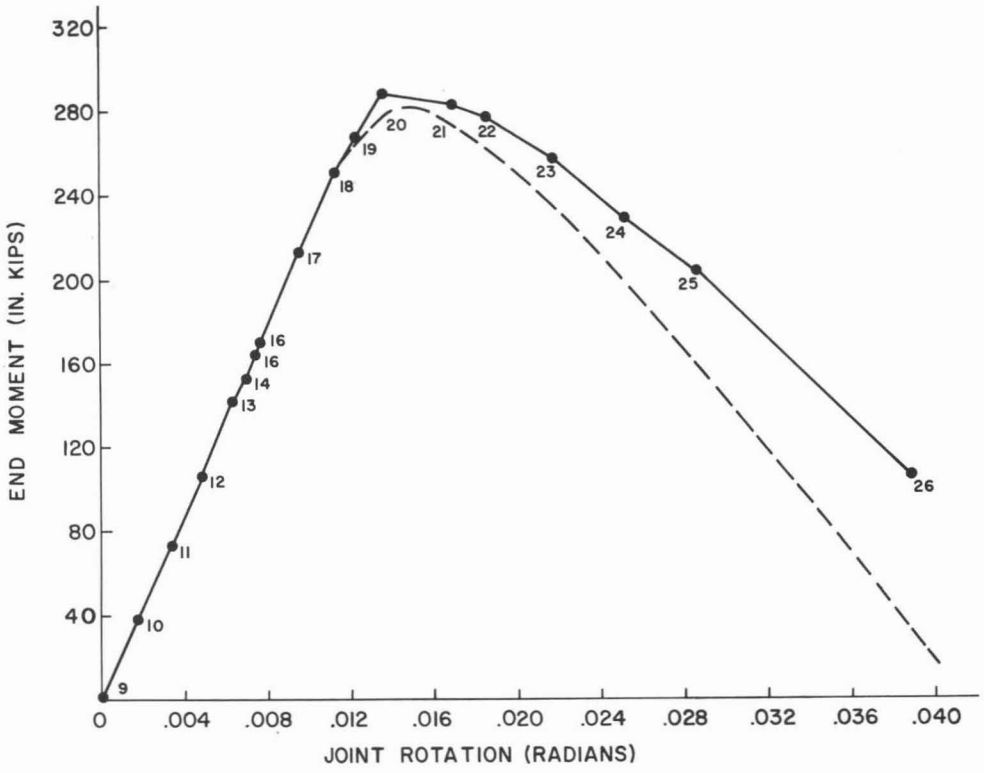

Fig. 5.5 Column Moment-Rotation Curve

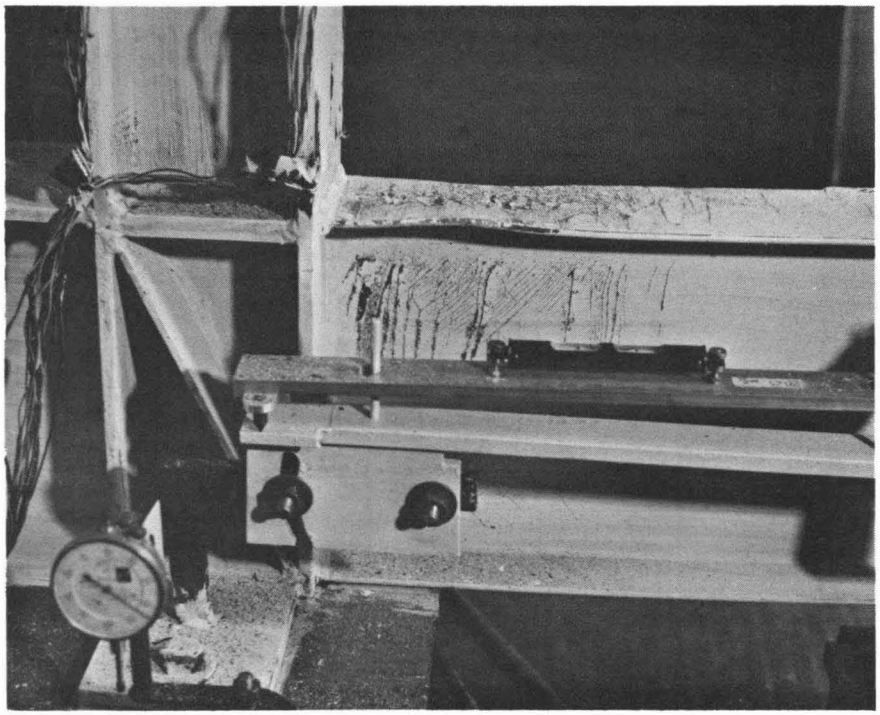

Fig. 5.6 Lower Connection Area After Testing

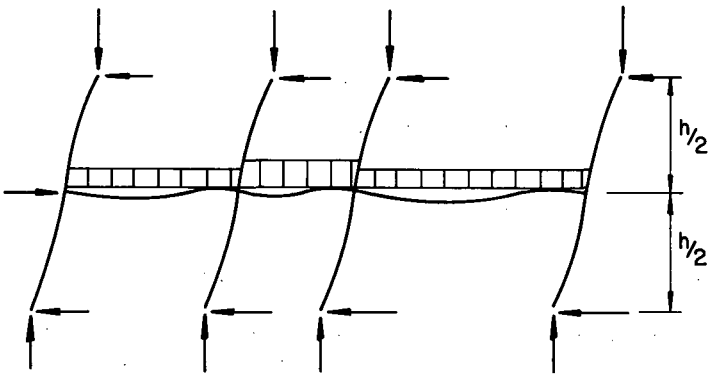

Fig. 5.7 Subassemblage for Design of Unbraced Frames

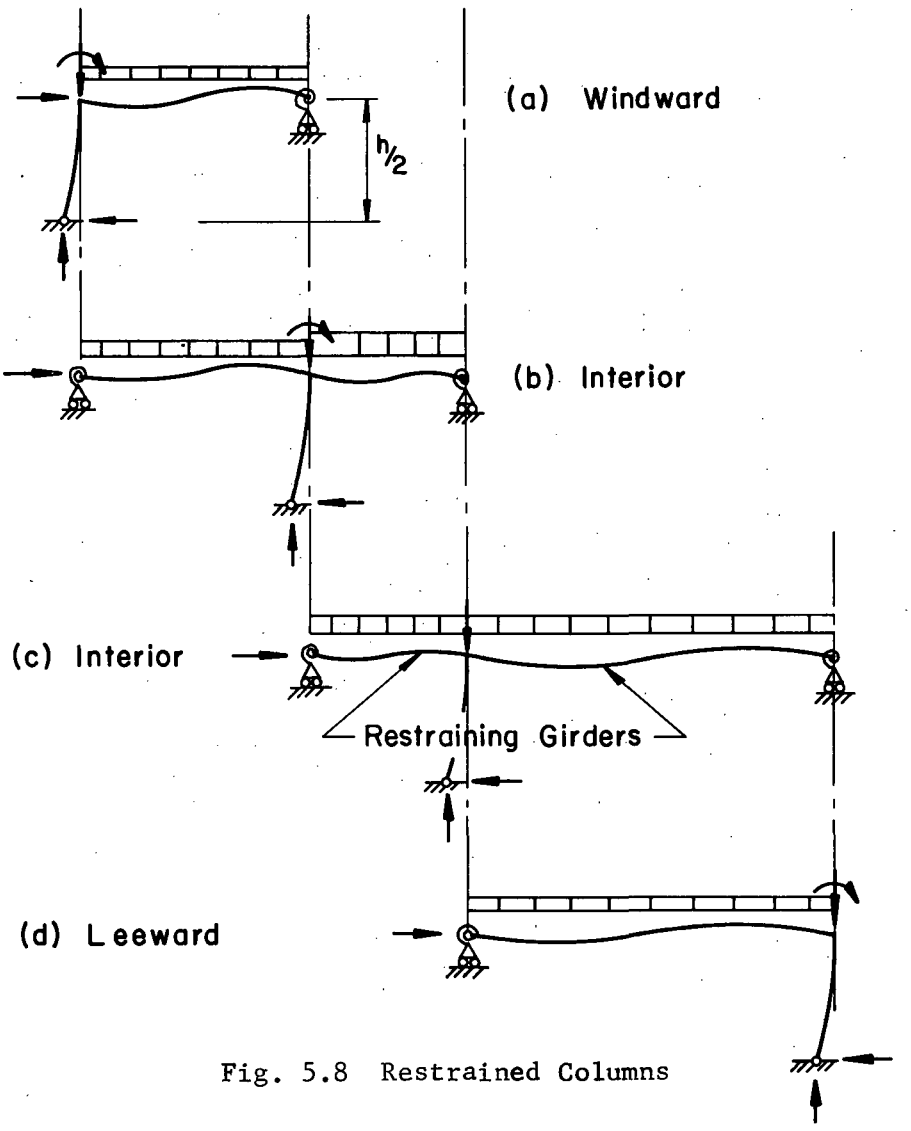

Fig. 5.8 Restrained Columns

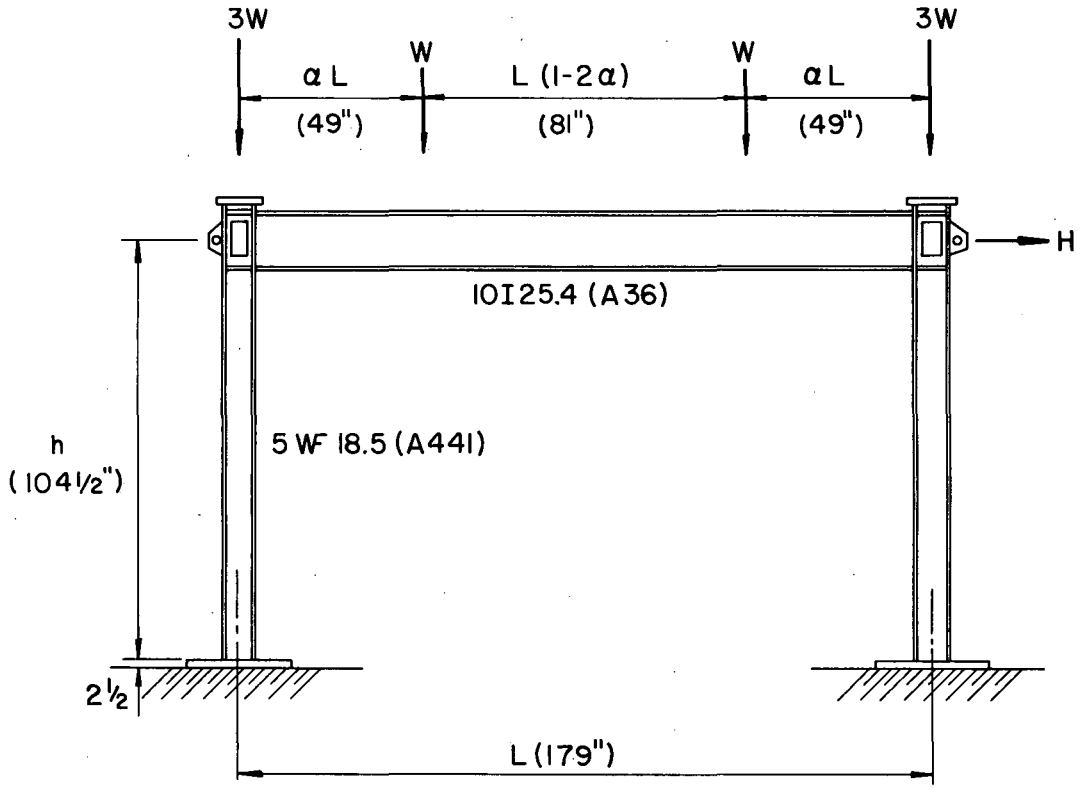

Fig. 5.9 Unbraced Subassemblage Test

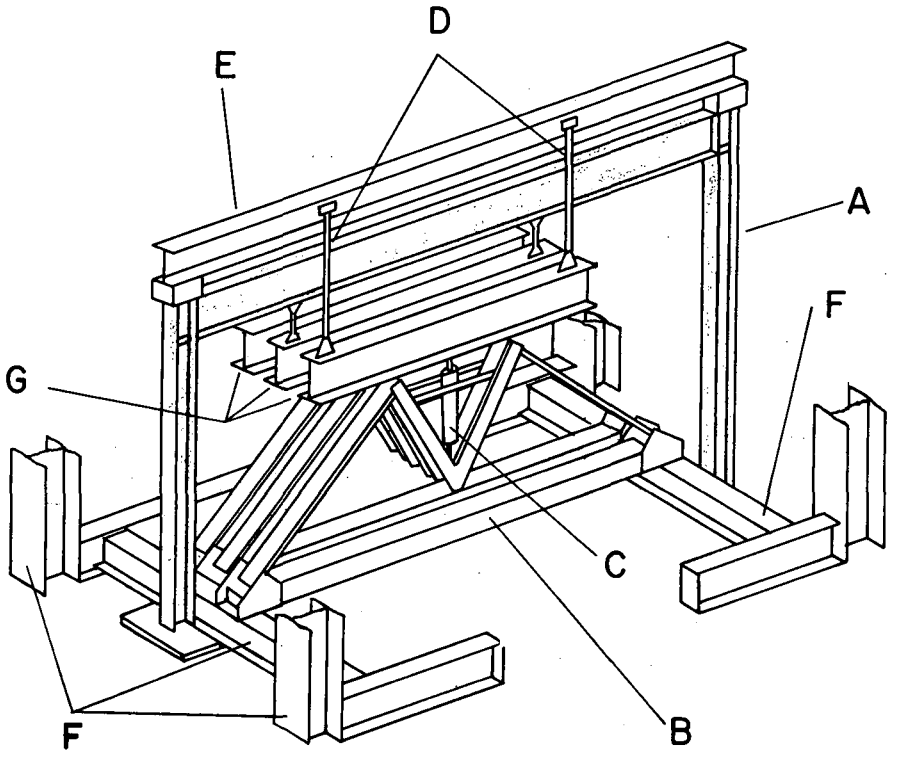

Fig. 5.10 Vertical Loading System

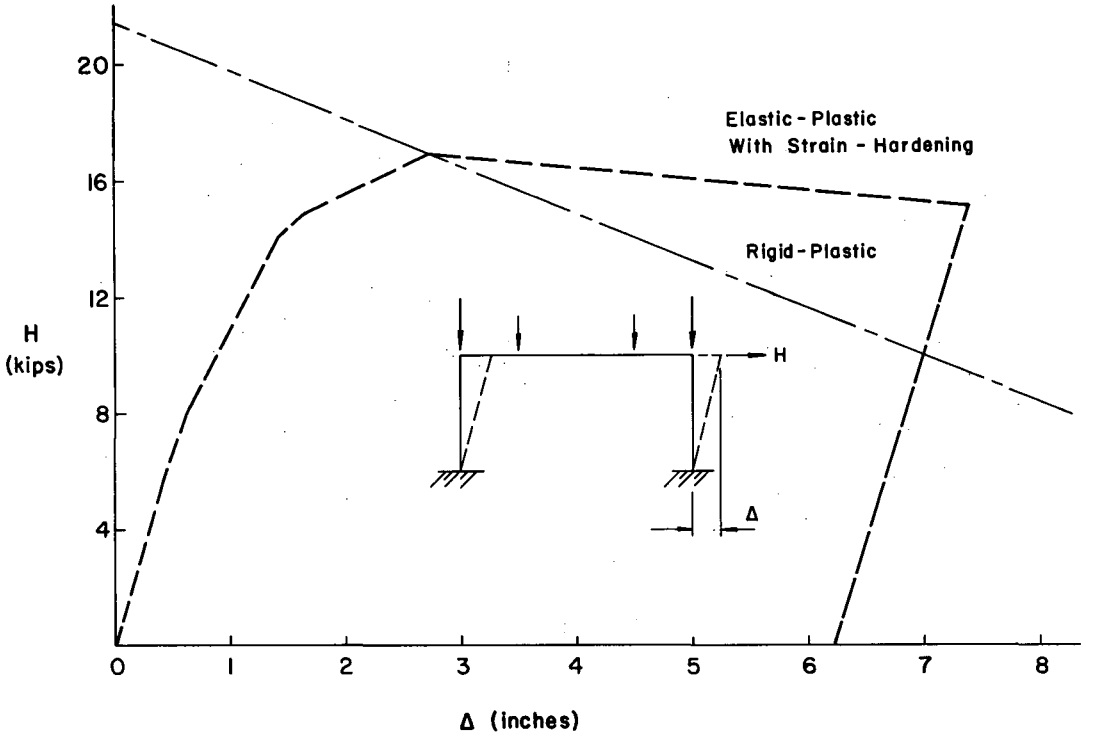

Fig. 5.11 Predicted Load-Deformation Response

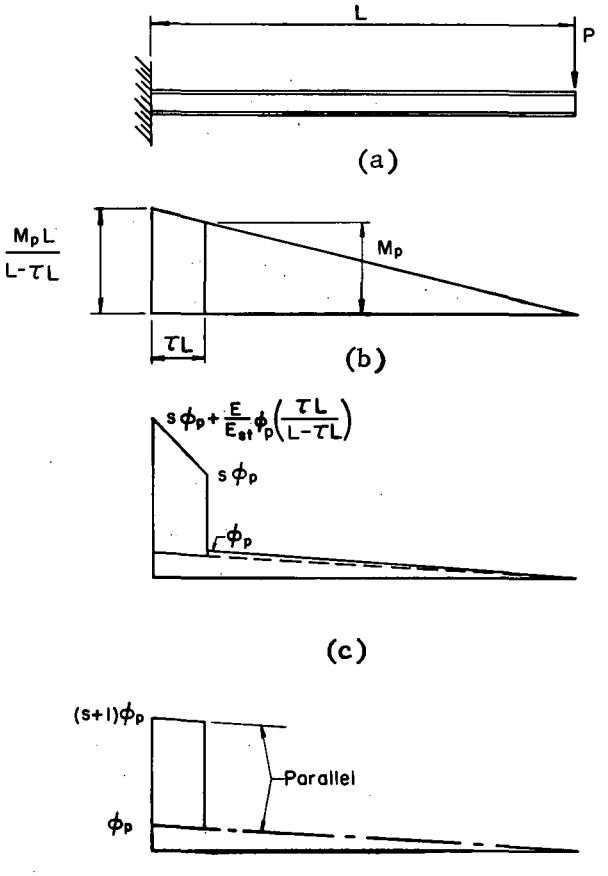

Fig. 5.12 Cantilever Beam

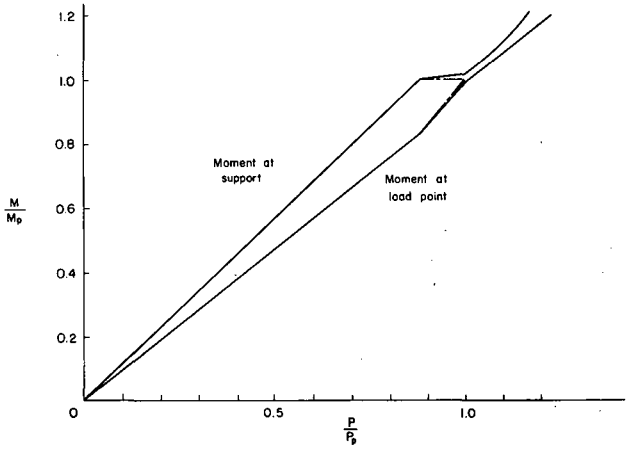

Fig. 5.13 Load-Moment Curves for Propped Cantilever

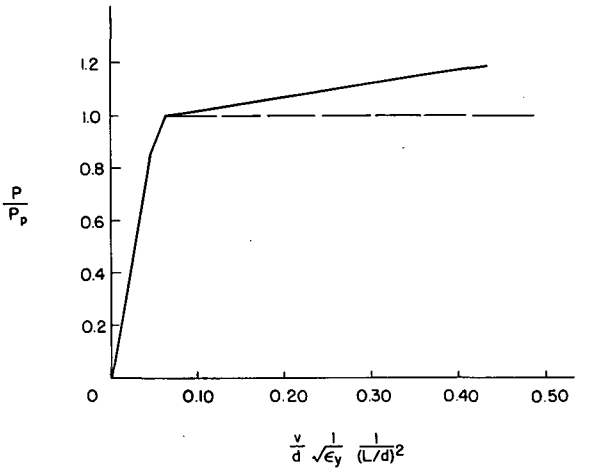

Fig. 5.14 Load-Deflection Curve for Propped Cantilever

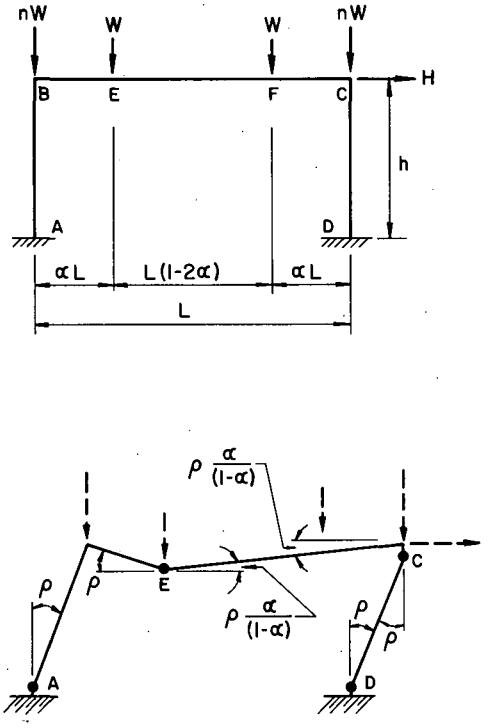

Fig. 5.15 Failure Mechanism

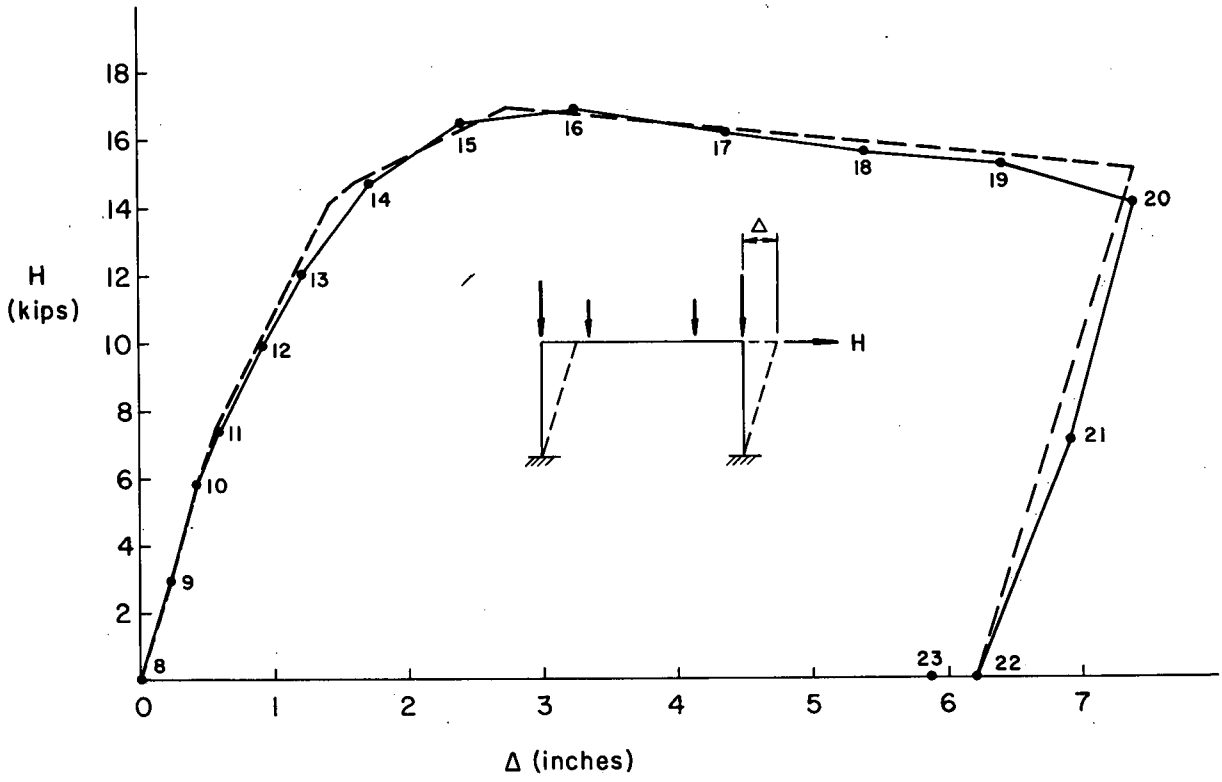

Fig. 5.16 Experimental Response

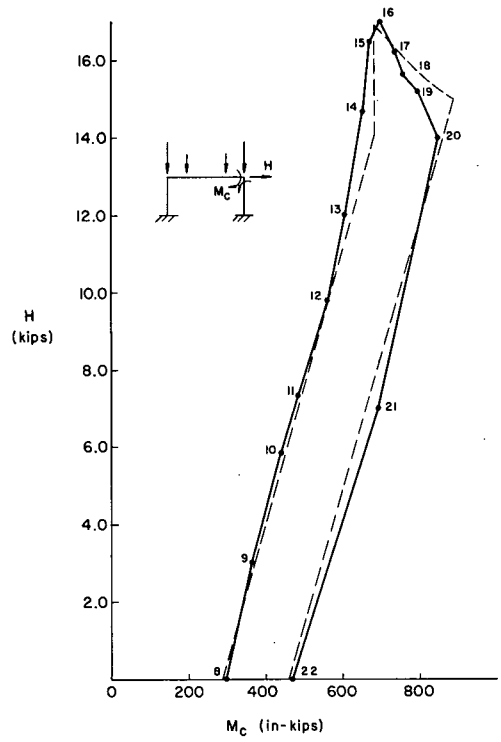

Fig. 5.17 Load-Moment Curve

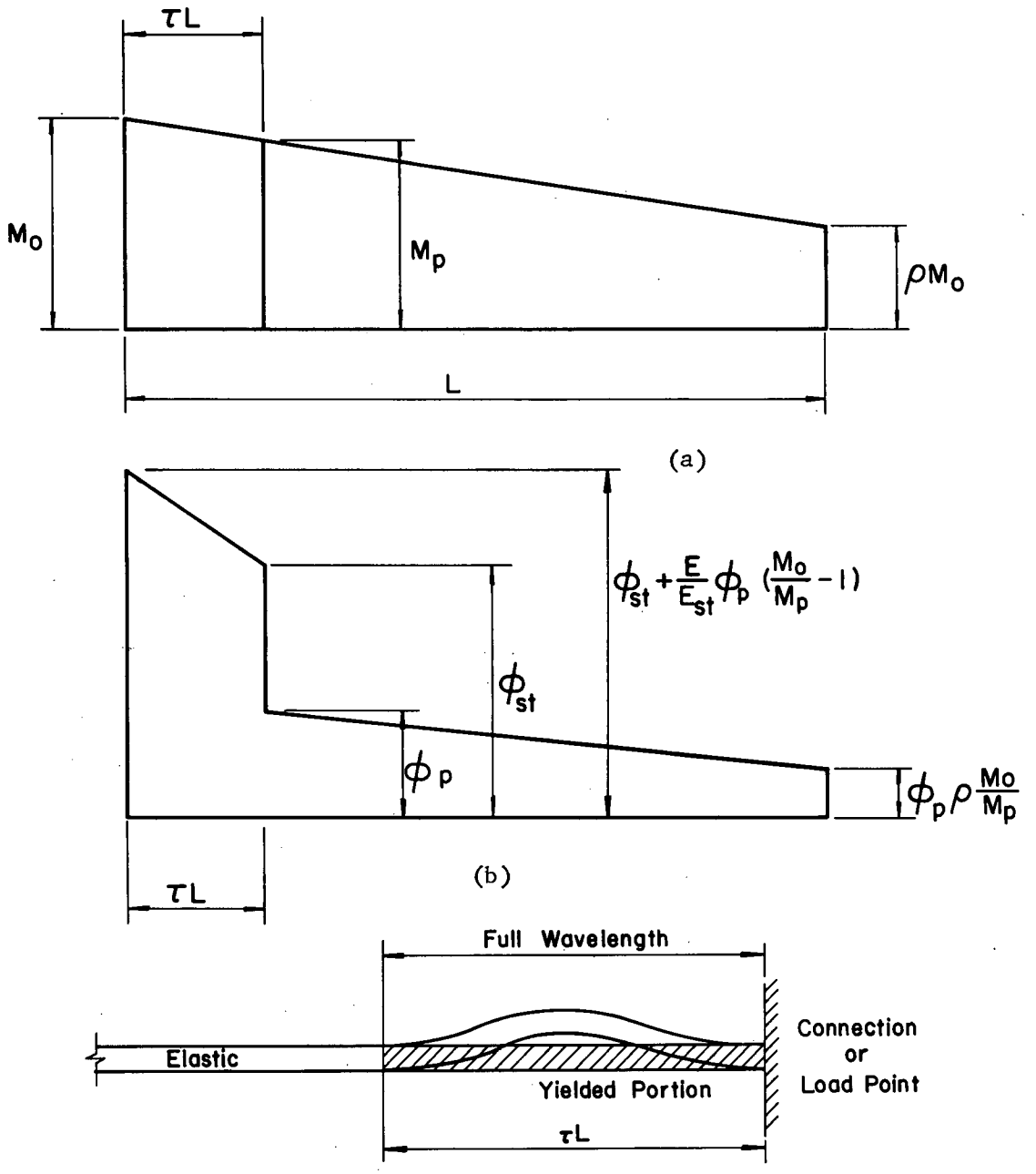

A.1 Member Segment Under Moment Gradient

11. REFERENCES

1. ASCE and WRC
   COMMENTARY ON PLASTIC DESIGN IN STEEL, ASCE Manual No. 41, 1961

2. Beedle, L.S.
   PLASTIC DESIGN OF STEEL FRAMES, John Wiley & Sons, Inc., New York, 1958

3. Beedle, L.S.
   BASIC CONCEPTS IN PLASTIC DESIGN, LECTURE 2, LECTURE NOTES ON PLASTIC DESIGN OF MULTI-STORY FRAMES, Fritz Laboratory Report No. 273.20, Lehigh University, 1965

4. Horne, M.R.
   INSTABILITY AND THE PLASTIC THEORY OF STRUCTURES, Transactions of the Engineering Institute of Canada, Vol. 4, No. 2, 1960

5. Bleich, F.
   BUCKLING STRENGTH OF METAL STRUCTURES, McGraw-Hill Book Company, Inc., New York, 1952

6. Lu, Le-Wu
   STABILITY OF FRAMES UNDER PRIMARY BENDING MOMENTS, Proc. ASCE, Vol. 89, ST3, June 1963

7. Mazur, E.F., Chang, I.C., and Donnel, L.H.
   STABILITY OF FRAMES IN THE PRESENCE OF PRIMARY BENDING MOMENTS, Proc. ASCE EM4, August 1961

8. Adams, P.F.
   LOAD-DEFORMATION RELATIONSHIPS FOR SIMPLE FRAMES, Fritz Laboratory Report No. 273.21, December 1964

9. Moses, F.
   INELASTIC FRAME BUCKLING, Proc. ASCE, Vol. 90, ST6, December 1964

10. Yang, C.H., Beedle, L.S., and Johnston, B.G.
    PLASTIC DESIGN AND THE DEFORMATION OF STRUCTURES, The Welding Journal, 30(7), 348-S, July 1951

11. Roderick, J.W.
    THE ELASTO-PLASTIC ANALYSIS OF TWO EXPERIMENTAL PORTAL FRAMES, The Structural Engineer, August 1960

12. Haaijer, G.
    ECONOMY OF HIGH STRENGTH STEEL STRUCTURAL MEMBERS, Proc. ASCE, Vol. 87, ST8, December 1961

13. NEW BETHLEHEM V STEELS, Bethlehem Steel Company, Bethlehem, Pennsylvania

14. Dieter,Jr.,.G. E.
MECHANICAL METALLURGY, McGraw-Hill Book Company, Inc., New York, 1961

15. Horne, M.R.
THE EFFECT OF STRAIN-HARDENING ON THE EQUILIZATION OF MOMENTS IN THE SIMPLE PLASTIC THEORY, British Welding Research Association FE.1 - Committee on Load Carrying Capacity of Frame Structures, September 1949

16. Lay, M.G.
THE EXPERIMENTAL BASES FOR PLASTIC DESIGN, Bulletin No. 99, Welding Research Council, September 1964

17. Yang, C.H.
THE PLASTIC BEHAVIOR OF CONTINUOUS BEAMS, Thesis presented to Lehigh University, Bethlehem, Pa. in 1951, in partial fulfillment of the requirements for the degree of Doctor of Philosophy

18. Hrennikoff, A.P.
THEORY OF INELASTIC BENDING WITH REFERENCE TO LIMIT DESIGN, Trans., ASCE, Vol. 113, p. 213, 1948

19. Massonnet, C., Anslijn, R. and Mas, E.
PLASTIC BENDING TESTS ON CONTINUOUS BEAMS OF STEEL A37 AND A52, Steel, No. 12, December 1963

20. Yang, C.H., Beedle, L.S., and Johnston, B.G.
RESIDUAL STRESS AND THE YIELD STRENGTH OF STEEL BEAMS, Proceedings, Welding Journal Research Supplement, April 1952

21. Hrennikoff, A.P.
IMPORTANCE OF STRAIN-HARDENING IN PLASTIC DESIGN, Proc. ASCE, Vol. 91, ST4, August 1965

22. Adams, P.F. and Galambos, T.V.
Discussion of IMPORTANCE OF STRAIN-HARDENING IN PLASTIC DESIGN, Proc. ASCE, Vol. 92, ST2, April 1966

23. Kerfoot, R.P.
ROTATION CAPACITY OF BEAMS, Fritz Laboratory Report No. 297.14, March 1965

24. Lay, M.G. and Smith, P.D.
ROLE OF STRAIN-HARDENING IN PLASTIC DESIGN, Proc. ASCE, Vol. 91, ST3, June 1965

25. Lay, M.G. and Galambos, T.V.
THE INELASTIC BEHAVIOR OF BEAMS UNDER MOMENT GRADIENT, Fritz Laboratory Report No. 297.12, July 1964

26. Lay, M.G. and Galambos, T.V.
INELASTIC STEEL BEAMS UNDER UNIFORM MOMENT, Proc. ASCE, Vol. 91, ST6, December 1965

27. Lay, M.G.
FLANGE LOCAL BUCKLING IN WIDE-FLANGE SHAPES, Proc. ASCE, Vol. 91, ST6, December 1965

28. Haaijer, G. and Thurlimann, B.
LOCAL BUCKLING OF WIDE-FLANGE SHAPES, Fritz Laboratory Report No. 205E5, December 1954

29. Adams, P.F., Lay, M.G., and Galambos, T.V.
EXPERIMENTS ON HIGH STRENGTH STEEL MEMBERS, Welding Research Council Bulletin No. 110, November 1965

30. Yura, J.A.
THE STRENGTH OF BRACED MULTI-STORY STEEL FRAMES, Fritz Laboratory Report No. 273.28, September 1965

31. Richards, C.W.
ENGINEERING MATERIALS SCIENCE, Wadsworth Publishing Co., Inc., Belmont, California, 1961

32. Beedle, L.S. and Tall, L.
BASIC COLUMN STRENGTH, Proc. ASCE, Vol. 86, ST7, July 1960

33. Ketter, R.L., Kaminsky, E.L., and Beedle, L.S.
PLASTIC DEFORMATION OF WIDE-FLANGE BEAM-COLUMNS, Trans. ASCE, Vol. 120, 1955, p.1028

34. Yang, C.H., Beedle, L.S., and Johnston, B.G.
RESIDUAL STRESS AND THE YIELD STRENGTH OF STEEL BEAMS, Progress Report No. 5, Research Supplement, The Welding Journal, Vol. 31, 1952, pps. 205s-229s

35. Nitta, A. and Thurlimann, B.
EFFECT OF COLD BENDING ON COLUMN STRENGTH, Fritz Laboratory Report No. 272.2, July 1960

36. Johnston, B. and Opila, F.
COMPRESSION AND TENSION TESTS OF STRUCTURAL ALLOYS, Proc. ASTM, 41, 1941, pps. 552-570

37. Freudenthal, A.
THE INELASTIC BEHAVIOR OF ENGINEERING MATERIALS AND STRUCTURES, John Wiley & Sons, Inc., New York, N.Y., 1950

38. Chajes, A., Britvec, S.J., and Winter, G.
EFFECT OF COLD-STRAIGHTENING ON STRUCTURAL SHEET STEELS, Proc. ASCE, Vol. 89, ST2, April 1963

39. Lay, M.G.
Discussion of EFFECT OF LARGE ALTERNATING STRAINS ON STEEL BEAMS, Proc. ASCE, Vol. 91, ST4, August 1965

40. Arnold, P., Adams, P.F., and Lu, L.W.
BEHAVIOR OF A HYBRID PORTAL FRAME, Fritz Laboratory Report No. 297.18, (in preparation)

41. Galambos, T.V.
BEAMS, LECTURE NOTES ON PLASTIC DESIGN OF MULTI-STORY FRAMES, Chapter 3, Fritz Laboratory Report 273.20, Lehigh University, 1965

42. Tamaro, Jr., G.J.
COLUMN CURVE FOR LOW SLENDERNESS RATIOS, M.S. Thesis, Lehigh University, 1961

43. Adams, P.F.
DETERMINATION OF THE STATIC YIELD LEVEL AND THE STRAIN-HARDENING MODULUS, Fritz Laboratory Report No. 297.7, March 1964

44. Shanley, F.R.
STRENGTH OF MATERIALS, McGraw-Hill Book Company, Inc., New York, N.Y., 1957

45. Lay, M.G.
YIELDING OF UNIFORMLY LOADED STEEL MEMBERS, Proc. ASCE, Vol. 91, ST6, December, 1965

46. Ostapenko, A.
LOCAL BUCKLING, STRUCTURAL STEEL DESIGN, edited by L. Tall, Ronald Press, New York, N.Y., 1964

47. Haaijer, G.
PLATE BUCKLING IN THE STRAIN-HARDENING RANGE, Proc. ASCE, Vol. 83, EM2, April 1957

48. Timoshenko, S.P. and Woinowsky-Krieger, S.
THEORY OF PLATES AND SHELLS, McGraw-Hill Book Company, New York, 2nd Edition, 1959

49. Haaijer, G. and Thurlimann, B.
INELASTIC BUCKLING IN STEEL, Trans. ASCE, Vol. 125, Part 1, 1960

50. Bijlaard, P.P.
Discussion of INELASTIC BUCKLING IN STEEL, Trans. ASCE, Vol. 125, Part 1, 1960

51. Fisher, J.W., Lee, G.C., Yura, J.A., and Driscoll,Jr., G.C. PLASTIC ANALYSIS AND TESTS OF HAUNCHED CORNER CONNECTIONS, Bulletin No. 91, Welding Research Council, October 1963

52. GUIDE TO DESIGN CRITERIA FOR METAL COMPRESSION MEMBERS, Column Research Council, Ann Arbor, Michigan, 1960

53. Nagaraja Rao, N.R. STRENGTH OF HYBRID STEEL COLUMNS, Ph.D. Dissertation, Lehigh University, 1965, University Microfilm Inc., Ann Arbor, Michigan

54. Kato, B. BUCKLING STRENGTH OF PLATES IN PLASTIC RANGE, Communication with L. S. Beedle, February 1965

55. Wood, R.H. PLASTIC AND ELASTIC DESIGN OF SLABS AND PLATES, Ronald Press Company, New York, N.Y., 1961

56. Lay, M.G. and Gimsing, N. EXPERIMENTAL STUDIES OF THE MOMENT-THRUST-CURVATURE RELATIONSHIP, Welding Journal, Vol. 30, No. 2, Research Supplement p. 86s, February 1965

57. Ueda, Y. ELASTIC, ELASTIC-PLASTIC AND PLASTIC BUCKLING OF PLATES WITH RESIDUAL STRESSES, Ph.D. Dissertation, Lehigh University, 1962, University Microfilms, Inc., Ann Arbor, Michigan

58. MANUAL OF STEEL CONSTRUCTION, American Institute of Steel Construction, 6th Edition, 1963

59. Handelman, G.H. and Prager, W. PLASTIC BUCKLING OF A RECTANGULAR PLATE UNDER EDGE THRUSTS, Technical Note No. 1530, National Advisory Committee for Aeronautics, Washington, D.C., August 1948

60. Lu, L.W. DESIGN OF BRACED FRAMES - COLUMNS, LECTURE NOTES ON PLASTIC DESIGN OF MULTI-STORY FRAMES, Chapter 11, Fritz Laboratory Report No. 273.20, Lehigh University, 1965

61. Lu, L.W. DESIGN OF COLUMNS IN UNBRACED FRAMES, LECTURE NOTES ON PLASTIC DESIGN OF MULTI-STORY FRAMES, Chapter 18, Fritz Laboratory Report No. 273.20, Lehigh University, 1965

62. Parikh, B.P.
THE ELASTIC-PLASTIC ANALYSIS AND DESIGN OF UNBRACED MULTI-STORY FRAMES, Ph.D. Dissertation, Lehigh University, (in preparation)

63. Driscoll, Jr., G.C.
GENERAL DESIGN PROBLEMS, LECTURE NOTES ON PLASTIC DESIGN OF MULTI-STORY FRAMES, Chapter 1, Fritz Laboratory Report No. 273.20, Lehigh University, 1965

64. Galambos, T.V. and Ketter, R.L.
COLUMNS UNDER COMBINED BENDING AND THRUST, Trans. ASCE, Vol. 126, 1961

65. Lay, M.G.
MECHANICS OF COLUMN DEFLECTION CURVES, Fritz Laboratory Report No. 278.12, July 1964

66. Yen, B.T.
BEAMS, CHAPTER 7 of "STRUCTURAL STEEL DESIGN", Edited by L. Tall, Ronald Press Company, New York, N.Y., 1964

67. Driscoll, Jr., G.C.
ROTATION CAPACITY OF A THREE SPAN CONTINUOUS BEAM, Fritz Laboratory Report No. 268.1, October 1956

68. Driscoll, Jr., G.C.
ROTATION CAPACITY REQUIREMENTS FOR SINGLE SPAN FRAMES, Fritz Laboratory Report No. 268.5, September 1958

69. Kerfoot, R.P.
ROTATION CAPACITY OF BEAMS, Fritz Laboratory Report No. 297.14, March 1965

70. Kusuda, T., Sarubbi, R.G., and Thurlimann, B.
THE SPACING OF LATERAL BRACING IN PLASTIC DESIGN, Fritz Laboratory Report No. 205E.11, June 1960

71. Lee, G.C. and Galambos, T.V.
POST BUCKLING STRENGTH OF WIDE-FLANGE BEAMS, Proc. ASCE, Vol. 88, EM1, February 1962

72. Lay, M.G.
THE STATIC LOAD-DEFORMATION BEHAVIOR OF PLANAR STEEL STRUCTURES, Ph.D. Dissertation, Lehigh University, 1964 University Microfilms, Inc., Ann Arbor, Michigan

73. Fukumoto, Y.
MOMENT-CURVATURE-THRUST PROGRAM FOR WIDE-FLANGE SHAPES, Fritz Laboratory Report No. 205A.37, August 1963

74. Ojalvo, M.
RESTRAINED COLUMNS, Proc. ASCE, Vol.86, EM5, October 1960

75. Parikh, B.P., Daniels, J.H., and Lu, L.W.
DESIGN AIDS BOOKLET, Fritz Laboratory Report No. 273.23, 1965

76. Aglietti, R.A., Lay, M.G., and Galambos, T.V.
TEST ON A36 AND A441 STEEL BEAM COLUMNS, Fritz Laboratory Report No. 278.14, June 1964

77. Galambos, T.V. and Fukumoto, Y.
INELASTIC LATERAL-TORSIONAL BUCKLING OF BEAM-COLUMNS, Fritz Laboratory Report No. 205A.34, August 1963

78. Miranda, C. and Ojalvo, M.
INELASTIC LATERAL TORSIONAL BUCKLING OF BEAM-COLUMNS, Proc. ASCE, Vol. 91, EM6, December 1965

79. Galambos, T.V., Adams, P.F. and Fukumoto, Y.
FURTHER STUDIES ON THE LATERAL TORSIONAL BUCKLING OF STEEL BEAM-COLUMNS, Fritz Laboratory Report No. 205A.36, February 1965

80. Galambos, T.V. and Lay, M.G.
END-MOMENT END-ROTATION CHARACTERISTICS FOR BEAM-COLUMNS, Fritz Laboratory Report No. 205A.35, May 1962

81. Tall, L.
COMPRESSION MEMBERS, CHAPTER 9, STRUCTURAL STEEL DESIGN, Edited by L. Tall, Ronald Press, New York, N.Y., 1964

82. Fisher, J.W.
DESIGN OF CONNECTIONS, LECTURE NOTES ON PLASTIC DESIGN OF MULTI-STORY FRAMES, Chapter 5, Fritz Laboratory Report No. 273.20, Lehigh University, 1965

83. Graham, J.D., Sherborne, A.N., Kabbaz, R.N. and Jensen, C.D.
WELDED INTERIOR BEAM-TO-COLUMN CONNECTIONS, AISC, New York, 1959

84. Lu, L.W.
INELASTIC BUCKLING OF STEEL FRAMES, Proc. ASCE, Vol.91, ST6, December 1965

85. Lu, L.W.
FRAME BUCKLING, LECTURE NOTES ON PLASTIC DESIGN OF MULTI-STORY FRAMES, Chapter 15, Fritz Laboratory Report No. 273.20, Lehigh University, 1965

86. Levi, V., Driscoll,Jr., G.C., and Lu, L.W.
ANALYSIS OF BEAM AND COLUMN SUBASSEMBLAGES IN PLANAR MULTI-STORY FRAMES, Fritz Laboratory Report No. 273.11, 1964

87. Levi, V. and Driscoll,Jr., G.C.
PLASTIC DESIGN OF BRACED MULTI-STORY FRAMES, Fritz Laboratory Report No. 273.3, 1961

88. Lay, M.G. and Galambos, T.V.
THE EXPERIMENTAL BEHAVIOR OF RESTRAINED COLUMNS, Welding Research Council Bulletin, No. 110, November 1965

89. Daniels, J.H., and Lu, L.W.
THE SUBASSEMBLAGE METHOD OF DESIGNING UNBRACED MULTI-STORY FRAMES, Fritz Laboratory Report No. 273.37, March 1966

90. Lay, M.G., Aglietti, R.A., and Galambos, T.V.
TESTING TECHNIQUES FOR RESTRAINED BEAM-COLUMNS, Fritz Laboratory Report No. 278.7, October 1963

91. Yarimci, E., Parikh, B.P., Lu, L.W. and Driscoll,Jr., G.C.
PROPOSAL FOR UNBRACED MULTI-STORY FRAME TESTS, Fritz Laboratory Report No. 273.25, March 1965

92. Wakabayashi, M.
THE RESTORING FORCE CHARACTERISTICS OF MULTI-STORY FRAMES, Bulletin of the Disaster Prevention Research Institute (Japan), Vol. 14, Part 2, February 1965

93. Roderick, J.W.
THE ELASTO-PLASTIC ANALYSIS OF TWO EXPERIMENTAL PORTAL FRAMES, The Structural Engineer, August 1960

94. Vickery, B.J.
INFLUENCE OF DEFORMATION AND STRAIN-HARDENING ON THE COLLAPSE OF RIGID FRAME STRUCTURES, Institution of Civil Engineers, Australia, Civil Engrg. Transactions, Vol. CE3, No. 2, September 1961

12. ACKNOWLEDGEMENTS

This study is part of a general investigation "Plastic Design in High Strength Steel" currently being carried out at Fritz Engineering Laboratory, Department of Civil Engineering. Professor L. S. Beedle is Director of the Laboratory and Professor L. W. Lu is the Project Director. The investigation is sponsored jointly by the Welding Research Council, and the Department of the Navy, with funds furnished by the American Institute of Steel Construction, the American Iron and Steel Institute, Lehigh University Institute of Research, the Bureau of Ships and the Bureau of Yards and Docks. The Column Research Council acts in an advisory capacity.

Professor T. V. Galambos supervised the dissertation which forms the basis of this report. His continuing encouragement and guidance is acknowledged gratefully.

The assistance and contributions of Messrs. B. P. Parikh, P. Arnold, R. P. Kerfoot and M. G. Lay are acknowledged. Mr. S. L. Phillips of the Bethlehem Steel Company provided information on the rotarizing process.

The report was typed by Miss Grace Mann and the drawings were made by Mr. J. Gera.